JAERI-M
83-065

EVALUATION REPORT ON CCTF CORE-I PEFLOOD TESTS C1-16 (RUN 25), C1-21 (RUN 40) and C1-22 (RUN 41) ——COMPARISON OF RESULTS BETWEEN FLECHT COUPLING TESTS AND FLECHT-SET TESTS——

May 1983

Yoshio MURAO, Takashi SUDOH* and
Tadashi IGUCHI

日本原子力研究所
Japan Atomic Energy Research Institute

JAERI-M レポートは，日本原子力研究所が不定期に公刊している研究報告書です。

入手の問合わせは，日本原子力研究所技術情報部情報資料課（〒319—11 茨城県那珂郡東海村）あて，お申しこしください。なお，このほかに財団法人原子力弘済会資料センター（〒319—11 茨城県那珂郡東海村日本原子力研究所内）で複写による実費頒布をおこなっております。

JAERI-M reports are issued irregularly.

Inquiries about availability of the reports should be addressed to Information Section, Division of Technical Information, Japan Atomic Energy Research Institute, Tokai-mura, Naka-gun, Ibaraki-ken 319—11, Japan.

編集兼発行　日本原子力研究所
印　　刷　日立高速印刷株式会社

JAERI-M 83-065

Evaluation Report on CCTF Core-I Reflood Tests C1-16 (Run 25), C1-21 (Run 40) and C1-22 (Run 41)

—— Comparison of results between FLECHT coupling tests and FLECHT-SET tests ——

Yoshio MURAO, Takashi SUDOH* and Tadashi IGUCHI
Division of Nuclear Safety Research,
Tokai Research Establishment, JAERI

(Received March 23, 1983)

In order to confirm that the phenomena in the CCTF are consistent with and analogous to those in the other test facilities, three CCTF tests with the experimental conditions simulated the FLECHT-SET TESTS, 3105B, 2714B and 3420B were performed. The downcomer and the upper plenum water accumulations and the pressure drops in the intact loops of the CCTF and the FLECHT-SET were the same, however, the pressure drops in the broken loop and resultant hydrodynamic oscillation in the system and the core thermo-hydrodynamic behaviors were different from each other.

It was found that the differences were mainly introduced from the pressure drops at the broken cold leg nozzle in the CCTF, while the pressure drops did not appear in the FLECHT-SET tests because of the different design and operation of the facility.

Accordingly, under the consideration of the defferences of the designs and operation methods of the facilities, the phenomena observed in both facilities can be concluded to be analogous with each other.

Keywords: Reactor Safety, Reflood Experiment, Loss-of-coolant Accident, FLECHT Test, Two-phase Flow, Heat Transfer

---

The work was performed under contract with the Atomic Energy Bureau of Science and Technology Agency of Japan.

* Nuclear Data Center

大型再冠水円筒第一次炉心試験C1－16（RUN25），C1－21（RUN40），C1－22（RUN41）評価報告書 －FLECHT－SET試験結果とその結合試験結果との比較－

日本原子力研究所東海研究所安全工学部
村尾　良夫・須藤　高史*・井口　正

（1983年3月23日受理）

円筒炉心試験装置（CCTF）内の現象が他の試験装置内の現象と類似のものであることを確証するため，FLECHT－SET実験3105B，2714B，3420Bを模擬した試験条件で3回のCCTF試験を行った。ダウンカマおよび上部プレナムの蓄水，健全ループの圧力損失は，CCTFとFLECHT－SETで同じであったが，破断ループの圧力損失，及びそれによって生じたシステム内の水力学的振動，ならびに炉心内の熱水力挙動は両者で異なっていた。

これらの違いは，主としてCCTFにおける破断コールドレグでの圧力損失によってもたらされたことがわかった。FLECHT－SET実験においては，構造の違い，装置の運転法の違いによりこの圧力損失は現われなかった。

従って，両試験装置の構造，運転法の違いを考慮に入れれば，両試験装置で観測された現象は互に類似なものであると結論できる。

本報告書は，電源開発促進対策特別会計法に基づき，科学技術庁からの受託によって行った研究の成果である。

＊　原子力データセンター

Contents

1. Introduction 1

2. Experiment 3

1. Apparatus 3
2. Test procedure 5

3. Results and Discussion 9

1. System behaviors 9
2. Core thermo-hydrodynamic behaviors 13
3. Analogy of the phenomena observed in the both test results 14

4. Conclusions 15

Nomenclature 16

Acknowledgement 17

References 17

Appendix A 28

Appendix B 35

Appendix C 58

Appendix D 81

Appendix E 104

目　　次

1. 序　　論 …… 1

2. 試　　験 …… 3

1. 試験装置 …… 3

2. 試験手順 …… 5

3. 試験結果と考察 …… 9

1. システム挙動 …… 9

2. 炉心熱水力挙動 …… 13

3. 試験装置の相似性 …… 14

4. 結　　論 …… 15

記 号 表 …… 16

謝　　辞 …… 17

参考文献 …… 17

付 録 A …… 28

付 録 B …… 35

付 録 C …… 58

付 録 D …… 81

付 録 E …… 104

List of Tables

Table 1 Comparison of dimensions of CCTF with those of FLECHT-SET.
Table 2 Comparison of experimental conditions between CCTF tests and FLECHT-SET tests.

List of Figures

Fig. 1 Axial power distributions of CCTF and FLECHT-SET heated rods.
Fig. 2 Comparison of upper plenum and hot leg of CCTF with those of FLECHT-SET.
Fig. 3 Schematic of CCTF discharge line
Fig. 4 Differential pressures through downcomer, core and lower plenum.
Fig. 5 Comparison of core and downcomer differential pressure of CCTF tests with those of FLECHT-SET tests.
Fig. 6 Comparison of loop differential pressures of CCTF tests with those of FLECHT-SET tests.
Fig. 7 Comparison of core flooding rates of CCTF tests with those of FLECHT-SET tests.
Fig. 8 Comparison of total mass flooded into core of CCTF tests with those of FLECHT-SET tests
Fig. 9 Comparison of upper plenum differential pressures of CCTF tests with those of FLECHT-SET tests.
Fig. 10 Comparison of core inlet fluid temperatures of CCTF tests with those of FLECHT-SET tests.
Fig. 11 Comparison of clad surface temperatures of CCTF tests with those of FLECHT-SET tests.
Fig. 12 Comparison of quench from envelopes of CCTF tests with scattering range of quench times of FLECHT-SET tests.
Fig. 13 Comparison of void fractions at the midplane of CCTF tests with FLECHT-SET tests.
Fig. 14 Comparison of heat transfer coefficients between the measured and the calculated with a film boiling correlation.

1. Introduction

In the reflood phase of the loss-of-coolant accident (LOCA) of a Pressurized Water Reactor (PWR), the water from the emergency core cooling system (ECCS) floods the overheated core and cools it. In this process, the core flooding is accelerated by the difference between the heads of the downcomer and the core, and suppressed by the back-pressure at the upper plenum induced by the vent loss of the steam generated by cooling the core. Such effects are important to evaluate the core flooding rate which governs the core thermo-hydrodynamics and are called "system effects".

In a quasi-steady state, the flooding rate $\dot{m}_F$ can be expressed as,[1]

$$\dot{m}_F = \dot{m}_C + \dot{m}_U + (\sqrt{(1 + \Delta P_{BCN}/\Delta P_I)2\rho_{gB}/k_B} + 3\sqrt{2\rho_{gI}/k_I})S_L \times \sqrt{\Delta P_D - \Delta P_C - \Delta P_U} \quad , \tag{1}$$

where

$$\Delta P_{BCN} = \Delta P_B - \Delta P_I \quad , \tag{2}$$

and $\dot{m}$ and ΔP are mass flow rate or mass accumulation rate and pressure difference, respectively. Subscripts F, D, C, U, I, B and BCN indicate flooding, downcomer, core, upper plenum, intact loop, broken loop and broken cold leg nozzle and connecting pipe, respectively. The broken loop is defined as a flow path from the upper plenum to the break through the broken hot leg. And the broken cold leg nozzle and the connecting pipe is defined as a flow path from the downcomer to the break through the broken cold leg nozzle. Thus the flooding rate depends on the water accumulation and the pressure differences over the system.

The cylindrical core test facility (CCTF) was constructed to study the system effect and a typical test which is named the base case test was analyzed comparing with the so-called evaluation model (EM model) of safety analysis of reactors. The observed phenomena was considerably similar to those assumed in the EM model. The following phenomena indicated more conservatism than EM model: 1) The water accumulation in the upper plenum, 2) Existence of the significantly large pressure drop at the broken cold leg nozzle and the connecting pipe.

In order to know whether the phenomena in CCTF is consistent with and analogous to those in the other test facilities, FLECHT-coupling tests were planned and performed. The tests have nearly same experimental conditions as selected FLECHT-SET phase B tests.[2),(3)]

In this study, the results from the FLECHT-coupling tests of CCTF are compared with those from the corresponding FLECHT-SET tests and the characteristics of CCTF are discussed.

The FLECHT-coupling tests of CCTF are named C1-16 (Run 25), C1-21 (Run 40) and C1-22 (Run 41). Major test results are shown in Appendixes.

2. Experiment

1. Apparatus

The outline of the CCTF facility has been described in the previous report.[1] For the comparison with the FLECHT-SET phase B1 facility, details of the CCTF will be described here.

Since design requirements for CCTF are similar to those for FLECHT-SET, the both facilities should be analogous. The facilities were scaled down in proportion to the core flow area scaling, 1/21.4 for CCTF and 1/370 for FLECHT-SET, respectively. The vertical dimensions of the components are preserved in the scaling.

The major differences of these facilities are compared in Table 1. The following major differences are discussed:

1) The axial peaking factor of the core,
2) The configuration of the downcomer,
3) The configuration of the upper plenum,
4) The configuration of the primary loop, and
5) The broken cold leg nozzle and the connecting line for overflow of water.

Axial peaking factor of the core

An axial peaking factor of the fuel rod is assumed to be 1.55 in the safety analysis of a PWR,[5] however actual value is much less than that. Therefore, 1.49 was adopted in CCTF. This brings the following merit: The allowable maximum temperature of the heated rod is limited to 1173K (900°C) for surviving against thermal shocks due to quenching. In the system effect test, an average linear power of the core is of importance and a lower peaking factor induces a lower maximum temperature in the core at the same power rating. Therefore, a lower peaking factor produces the capability of tests which have more severe condition under the limitation of the maximum core temperature. The axial power distribution of the heated rod is indicated in Fig. 1. That for the FLECHT-SET is also shown in the figure. In the FLECHT-SET, the axial peaking factor is 1.66 and the power levels of the top and bottom portions of the core are relatively higher.

Configuration of downcomer

The most of the reflood test facilities including the FLECHT-SET facility have a pipe downcomer instead of an annular downcomer of a PWR. In the CCTF, the annular downcomer was intended to be equipped. The flow area of the downcomer had to be scaled down in proportion to the scaling factor of the core area, 1/21.4. However, if the same scaling rule was applied, the downcomer annulus would be too narrow, of about 0.03 m gap, to simulate the hydrodynamic behavior in a PWR downcomer having about 0.2 m gap.

In order to solve this problem, the flow area of the core baffle was included in the flow area of the downcomer and the added flow area was scaled down. Thus the CCTF obtained the annular downcomer of 0.0615 m gap. To preserve the ratio of the heat release rate to the unit volume of the downcomer fluid, the inside downcomer wall was designed to be kept at the saturation temperature and the outside wall temperature was designed to be controlled. In the FLECHT-coupling test, the outside wall was kept at the saturation temperature to simulate the FLECHT-SET tests.

In the FLECHT-SET, a pipe downcomer was equipped and the intact loop was connected at the opposite side of the overflow line.

Configuration of upper plenum

The flow area of the upper plenum in the CCTF is about twice of the core flow area, whereas that of FLECHT-SET is 21 times larger than the core flow area. And in FLECHT-SET the extention of the heated rods penetrate the upper plenum and there is no simulator of internals.

The internals of the CCTF simulates those of the previous design for the Westinghouse 17 × 17 array assemblies. The radial dimensions of the structures and the dimensions of the openings and the gap between adjacent guide tubes are scaled down in 8/15 of the actual.

Figure 2 shows the comparison of the upper plenum, the hot leg and the inlet plenum of the steam generator of the CCTF with those of the FLECHT-SET.

Broken cold leg nozzle and connecting line

In the CCTF, as shown in Fig. 3, the broken cold leg of the vessel side is simulated with a 2.8 m long 6 inches pipe of the same size as the intact loop piping and connected to the water separator (Containment tank 1) with a pipe having a flow area of four times of the intact loop piping.

Containment tanks 1 and 2 are connected with 10 inches pipe. On the other hand, in the FLECHT-SET, the downcomer and the overflow tank is connected with a pipe having a flow area of 11.32 times of the broken loop piping. The two overflow tank and the containment tanks of the FLECHT-SET are connected with a 3 inches pipe of which flow area is 3.06 times of that of the broken loop.

When the water in the downcomer overflows to the broken cold leg nozzle with steam flowing from all the intact loops, two-phase mixture flows through the nozzle and pressure drop is induced by the accerelation of liquid with steam. In the CCTF base case test, a big pressure drop was induced as reported in Ref.(1). However in FLECHT-SET tests no significant pressure drop was observed since the facility has relatively larger discharge pipe as a broken cold leg of the vessel side and most of tests were performed with variable flow rate under controlling the downcomer liquid level not to exceed the overflow level.

Primary loop

The CCTF has three intact loops and one broken loop, for studying the parallel channel oscillation. While the FLECHT-SET has one equivalent intact loop and one broken loop.

In the broken loop and three intact loops of the CCTF, the elevation, the flow path length and the slope angle of the steam generator riser are preserved as same as those in the reference PWR.[6] However, the average length of heat transfer tubes in the steam generators is 5.3 m shorter than the actual (20.5 m). The flow areas are scaled down by the ratio of about 1/21.4. The total flow resistance of primary loops in CCTF was ajusted to the value referred in FLECHT-SET[2] as shown in Table 1.

The ECC injection ports are at the cold legs. An additional ECC injection port was equipped at the lower plenum. For the FLECHT coupling tests, the lower plenum injection port was used.

The break point was assumed to be near the surface of the biological shield of the pressure vessel, which is just downstream of the injection port of ECCS.

2. Test procedure

For coupling tests, the following three FLECHT-SET tests were selected: Run 3104B, Run 2714B and Run 3420B. In the first two of the selected FLECHT-SET tests, the flow rate of the low pressure coolant

injection (LPCI) was controlled for the water in the downcomer not to overflow in order to avoid the hydrodynamic oscillation induced by condensation of steam with the subcooled water. In 3420B, the saturated water was used to avoid such a condensation effect. In the CCTF, satureated water was filled in nearly the half of the lower plenum and then subcooled water was scheduled to push the saturated water upwards in order to produce gradual temperature falling down for preventing condensation. In these coupling tests, the water of ECCS was injected to only the lower plenum injection port.

Other experimental conditions are nearly the same as FLECHT-SET tests as shown in Table 2. The average power is higher in the CCTF tests than in the corresponding FLECHT-SET tests and the peak power is almost identical. The initial clad temperatures of heated rods before heating initiation are nearly the saturation temperature and the peak clad temperature of the heated rods at the initiation of reflood are almost identical. Accordingly, the stored energy of the core at the initiation of reflood is higher in the CCTF tests than in the corresponding FLECHT-SET tests.

Table 1 Comparison of dimensions of CCTF with those of FLECHT-SET

Item	CCTF	FLECHT-SET
Scaling factor of core flow area	1/21.4	1/370
Core		
Axial peaking factor	1.49	1.66
Ratio of unheated rod	0.109	0.09
Downcomer		
Configuration	Annulus	Pipe
Upper plenum		
Scaling factor of cross section	∿ 1/10	∿ 1/18
Internals	Simulated with 8/15 scaled internals	Extention of heated rod
Primary loops		
Quantity of loops	3 Intact+1 Broken loops	1 Intact+1 Broken loops
K factor of pump	∿ 15	∿ 14.7[1)]
of other portion	∿ 10	8.9[2)]
Scaling of broken cold leg nozzle	1/21.4	1/32.7

1) Includes COld leg flow resistance (Original value, 20.53, was devided by 1.4)

2) Excludes Inlet plenum cross over

Table 2 Comparison of experimental conditions between CCTF tests and FLECHT-SET tests.

RUN No. / COMMENTS	CCTF C1-16	FLECHT 3105B	CCTF C1-21	FLECHT 2714B	CCTF C-122	FLECHT 3420B
Containment pressure (MPa)	0.415	0.407	0.152	0.145	0.152	0.138
Peak Power (kW/m)	2.78	2.76	2.82	2.76	2.82	2.76
Averaged Power (kW/m)	1.47	1.37	1.49	1.37	1.49	1.37
Acc flow rate (m^3/s)	0.1002	0.1044*	0.1002	0.1014*	0.1005	0.0981*
LPCI flow rate (m^3/s)	0.01113	variable	0.01108	variable	0.01108	0.01122
Acc injection time (s)	17	14	15	11	15	15
ECC water temperature (K)	340	339.7	340	340.2	384	387
SG secondary water level (m)	7.4	7.3	7.4	7.5	7.4	7.2
SG secondary temperature (K)	536	540	537	539	538	540
Initial clad temperature (K)	866	866	867	866	870	866

* Equivalent value based on core flow area

3. Results and Discussion

The main results are indicated in Appendix B, C and D. And the notation of the tag identifications of data in these results are explained in Appendix A.

1. System behaviors

Figures 4(a), (b) and (c) indicate the differential pressures through the downcomer, the core and the lower plenum for the three FLECHT coupling tests. The data have more or less time-averaged, i.e. they are the average of 0.5 seconds, while the sampling time for the differential pressure measurement was 0.2 seconds. The figures show big oscillations in the differential pressures. It is found that the oscillations appeare at the time when the downcomer water level reachs the overflow level of the downcomer, i.e. the level of the broken cold leg nozzle. Since the oscillation occurs even in the test with the injection of the almost saturated water, i.e. 3420B coupled test, the effect of condensation at the downcomer or the broken cold leg nozzle on the oscillation seems to be weak. In the base case test, in which the ECC water was injected from the cold leg ECC ports during the LPCI injection period, it was observed that the injected water was dispersed by the steam flowing in the intact loop[(1)] and it was inferred that the dispersed water was entrained into the downcomer by the steam. The fact that the ECC bypass occured even before the downcomer water level reached the overflow level in the base case test, shows that a fraction of the entrained water bypassed through the downcomer and flowed through the broken cold leg nozzle. At the nozzle, a relatively large pressure drop occured due to the acceleration of the water to the velocity of the steam. The pressure drop at the broken cold leg and the connecting pipe, ΔP_{BCN}, was found to be weakly dependent on the downcomer water level in the base case test. This is common in the cold leg injection tests. However, ΔP_{BCN} for the lower plenum injection tests is inferred to be strongly dependent on the downcomer water level, since the water entrained into the broken cold leg nozzle is almost negligible before the downcomer water level reaches the overflow level.

In the FLECHT coupling tests, i.e. lower plenum injection tests, it is reasonable that the big ΔP_{BCN} appears when the downcomer water level reaches the overflow level and it disappeared when the downcomer water level goes down below the overflow level. When the downcomer water level reaches the

overflow level and the water initiates to overflow through the broken cold leg nozzle, the pressures in the pressure vessel and the loops increase due to the increase of ΔP_{BCN}. This causes the increase of the core flooding rate as estimated from Eq. (1) and the decrease of the injection flow rate into the lower plenum, resulting in the decrease of the downcomer water mass. Hence, the downcomer water level initiated to fall down. And when the downcomer water level falls down below the overflow level, ΔP_{BCN} becomes small and the situation is reversed. Thus the oscillation is inferred to be sustained in the lower plenum injection test. Though the response of the lower plenum injection rate depends on the softness of the injection system, specially on the existence of the gas volume, at least, the increase of the pressure at the injection point cause the reduction of the injection flow rate.

In the later section, the time averaged differential pressures will be used for convenience, since the tendency of the transients are hidden behind the oscillatory responses.

Figure 5 indicates the core and downcomer differential pressures, ΔP_C and ΔP_D, respectively, of the three FLECHT coupling tests in the CCTF and the counterpart FLECHT-SET tests. ΔP_Ds of the three CCTF tests rapidly increases to the value corresponding to the overflow level and then stay at the almost constant value. ΔP_Ds of the FLECHT-SET tests show the similar trends, however, the saturated values are slightly smaller. This is attributed to the unique operation of the tests, i.e. the water level of the downcomer was regulated not to exceed the overflow level during the test of Run 3105B and 2714B, and the steam void was generated by injecting superheated liquid in the test of Run 3420B. In the CCTF tests, the downcomer wall was not superheated and the ECC water was injected directly into the lower plenum.

In the CCTF base case test[1] the gradual increase of ΔP_D was observed. The downcomer wall was superheated and the ECC water which was injected at lower flow rate to the cold leg ECC ports was heated with the steam flowing through the intact loops. During the Accumulator (Acc) injection period, the injected water could not fill the downcomer completely due to the lower flow rate. During the LPCI injection period, the injected water was dispersed by the steam flow, resulting in the partial bypass of the ECC water and the reduction of the water accumulation rate in the downcomer. That is the reason why the gradual increase of ΔP_D, i.e. the gradual water accumulation in the downcomer, appeared in the CCTF base case test, was

not observed in the present CCTF tests.

The responses of ΔP_C for the present tests and the corresponding FLECHT-SET tests qualitatively agreed with each other, however, quantitatively not for the low pressure tests, i.e. 2714B and 3420B coupled tests. This might be caused by the lower flooding rate as explained later.

Figure 6 shows the differential pressures across the broken loop and the intacts loops, ΔP_B and ΔP_Is, respectively. In the CCTF, the curves of the three ΔP_Is in each test are overlapped with each other, therefore, one of the curves is indicated for the three intact loops. ΔP_Is of the CCTF tests and the FLECHT-SET tests are nealry identical. On the contrary, ΔP_Bs of the both tests are remarkably different from each other. ΔP_B of the CCTF tests are much higher than that of the FLECHT-SET tests and ΔP_B of the FLECHT-SET tests are almost same as ΔP_I. From Eq.(2), this big difference between ΔP_B and ΔP_Is in the CCTF tests indicates the existence of the significantly large pressure drop at the broken cold leg nozzle, ΔP_{BCN}, due to the acceleration of the two-phase mixture flow of the steam from the intact loops and the water overflowed through the broken cold leg nozzle. In Run 3105B and 2714B of the FLECHT-SET tests, the water did not overflow and the steam velocity was not high since the pipe of the overflow line was relatively large as previously mentioned. However, in Run 3420B the superheated water was injected and the water was allowed to overflow with the steam flowing from the intact loop, resulting in a slight difference between ΔP_B and ΔP_I.

As indicated in Eq.(1), the existence of ΔP_{BCN} introduces the higher core flooding rate, $\dot{m}_F$. ΔP_{BCN} induces higher pressure in the pressure vessel, since the pressure at the foot of the cold leg nozzle of the pressure vessel was $P + \Delta P_{BCN}$, where P is the pressure of the containment tank and which was kept the pre-set value. In addition, the pressure in the intact loops increase by ΔP_{BCN} and the pressure in the broken loop also increases due to the increase of the upper plenum pressure. The increase of the loop pressures causes the increase of the density of the steam flowing in the loops, resulting in the higher core flooding rate as shown in Eq. (1). The heat transfer in the core is generally thought to be enhanced by increases of the flooding rate, the core inlet subcooling and the pressure in the pressure vessel. Accordingly, the higher ΔP_{BCN} enhances the heat transfer in the core and introduces bigger safety margine. In the CCTF, the length of cold leg connected to the broken cold leg nozzle was determined to be about 2.8 m based on the assumption of the break at

the outside of the biological shield of the reactor vessel. When the break at the nozzle is assumed, the length of the broken cold leg is shorter. The differential pressure measured across the foot of the nozzle and the location of 0.4 m deep in the nozzle was about a half of ΔP_{BCN}. Hence, even in the case of short nozzle, the significant influence of ΔP_{BCN} on the core heat transfer can be expected.

The core flooding rates of the CCTF and the FLECHT-SET tests are compared in Fig. 7. They are calculated from the mass balance of the mass flow rates and the mass accumulations measured in the system. Usually, the core flooding mass flow rates calculated from the data of the downstream and the upstream of the core inlet, $\dot{m}_{Fd}$ and $\dot{m}_{Fu}$, respectively, did not agree with each other during the LPCI injection period[1]. In the these FLECHT coupling tests, however, the good agreement was obtained. In the other tests, the disagreement was attributed to the leakage of steam or water from the upper plenum to the downcomer or the containment tank. In the FLECHT coupling tests, the leakage pass might be sealed with the water filled in the downcomer, since the more water was accumulated in the downcomer in the cases of the lower plenum injection tests than in the cold leg injection tests. Further investigation is necessary to idensify the reason of the disagreement between $\dot{m}_{Fd}$ and $\dot{m}_{Fu}$.

Figure 8 shows the comparison of the total masses flooded into the core for the FLECHT-SET Run 2714B and the coupled CCTF test. Initially the total masses for both tests are almost the same, however, as ΔP_{BCN} grows up, the discrepancy of the total masses became significanly large. The average core flooding velocities after 150 seconds are 1.93 cm/s and 1.47 cm/s for the CCTF test and the FLECHT-SET test, respectively. This discrepancy can be explained by Eq. (1) if it is assumed that $\Delta P_{BCN} = 2 \cdot \Delta P_I$, the pressure increase by ΔP_{BCN} is 0.05 MPa and $\dot{m}_C = \dot{m}_U = 0$.

Figure 9 shows the comparison of the differential pressures of the upper plenum, ΔP_Us for the CCTF and the FLECHT-SET tests. It is found that the water accumulation behaviors for both tests in the upper plenum are qualitatively same with each other. Generally the upper plenum water accumulation rate is dependent on the liquid and steam mass flow rate. Though the discrepancy seems to be reasonable under the consideration of the large ΔP_{BCN}, the quantitative interpretation can not be obtained due to the lack of the proved correlation for these phenomena.

Figure 10 shows the fluid temperatures measured at the core inlet for the CCTF tests and the nominal values for the corresponding FLECHT-SET tests.

The discrepancy between the fluid temperatures was caused by the difference of temperature of the coolant filled in the lower plenum and the ECC injection line before each experiment was initiated, i.e. the saturated water was filled in hearly half of the lower plenum for the CCTF tests but not for the FLECHT-SET tests.

2. Core thermo-hydrodynamic behaviors

Figure 11(a), (b) and (c) show the comparison of the clad surface temperatures measured in the CCTF tests and the corresponding FLECHT-SET tests. The temperatures were measured at the midplane of peak power rods. The turnaround temperature and turnaround time of the CCTF and the FLECHT-SET are different from each other. The core cooling rates are much different. In the 3105B coupled test, the CCTF test shows lower core cooling rate than the FLECHT-SET test. While, in the other two tests, the situations are the reverse.

And Figure 12(a), (b) and (c) show the quench envelopes which indicate the quench front propagation in the CCTF core. In the figures, the scattering range of the quench times measured in the FLECHT-SET tests are also indicated. The quench front propagations of the CCTF are nearly the same as those of the FLECHT-SET, however, in the CCTF 3105B coupled test which was conducted at the pressure of 0.4 MPa, the quench times appears to be slightly earlier than those of the corresponding FLECHT-SET test.

The void tractions at the midplane of the core of the FLECHT-SET 2714B and its coupling test of CCTF are compared in Fig. 13. Just after the reflood initiated, the void fraction in the FLECHT-SET test decreases to a certain value, $\alpha = 0.88$, and then gradually decreases. Judging from the value of the void fraction, the flow above quench front is inferred to be a slug flow in both tests. In the CCTF test, the voil fraction is lower than that of the FLECHT-SET test. This might be mainly induced by the difference of the core flooding rates, since the Murao-Iguchi's correlation[4] for the slug flow void fraction shows that the local liquid mass flux is a very sensitive parameter for the void fraction in such low flooding rate cases. As shown in Fig. 8, the total masses flooded into the core for the 2714B coupled test and the FLECHT 2714B test are almost identical in the early period of the transient and, as explained in the test procedure, the initial stored energy for the CCTF 2714B coupled test was higher than that for the corresponding FLECHT-SET test. However, the initial water accumulation, which is recognized as the rapid reduction of

the void fraction just after the initiation of reflood, for the FLECHT-SET test is lower than that for the CCTF test. Accordingly, it is surmised that the characteristics of core water accumulation for the CCTF is different from that for the ELECHT-SET. This is attributed to the differences of the structure at the top of the core, i.e. the FLECHT facility has no tie plate above the heated portion of the core. However more discussions are necessary in order to identify the mechanism.

Figure 14 shows the measured heat transfer coefficients for the CCTF 2714B coupled test and the corresponding FLECHT-SET test. Two calculated heat transfer coefficients are also plotted on the figure for each test by assuming that the flow at the midplane is slug flow and the Murao & Sugimoto correlation[5] of saturated film boiling is applicable. In those calculations, the measured void fractions were used. These calculations qualitatively explained that the higher void fraction induced the lower heat transfer coefficient in the core, however, the quantitative explanation could not be obtained.

In the case of the FLECHT-SET test, the measured roughly agrees with the calculated. On the other hand, in the CCTF, the measured does not agree with the calculated. In this calculation, the convective heat transfer coefficient was proportional to a function of the void fraction, i.e. $(1-\alpha)^{1/4}$ where is void fraction. As an extreme case, the heat transfer coefficient was calculated with $\alpha = 0$ and it is also indicated in Fig. 12. In the CCTF, the measured curve is almost in the range between the calculated with α = measured value and $\alpha = 0$. Judging from the FLECHT-SET test,[2] the enhancement of the heat transfer in the CCTF tests are attributed to the existence of the oscillation in the core.

3. Analogy of the phenomena observed in the both test results

On the analogy between the phenomena observed in the CCTF and the FLECHT-SET facility, the followings can be stated: The quantitative differences in the core and system thermo-hydrodynamic behavior were introduced from the differences of the system design and operation methods of both facilities. The phenomena observed in both facilities, however, are qualitatively analogous, since most of the observed phenomena were about the same and most of the differences was explained by the consideration of the significantly high pressure drop at the broken cold leg nozzle and the resultant big oscillation.

4. Conclusions

In order to examine the phenomena in the CCTF are consistent with and analogous to those in the other test facilities, three CCTF tests coupling with the FLECHT-SET tests, 3105B, 2714B and 3420B were performed and the results were compared with the data of the corresponding FLECHT-SET tests. The following conclusions were obtained:

1. The downcomer differential pressures of the CCTF and the FLECHT tests were nearly the same. They rapidly increased to the overflow level and then kept almost constant.
2. The core differential pressures, Δp_Cs, of the both 3105B related tests were nearly the same as each other, however, those of the CCTF low pressure tests, i.e. 2714B and 3420B coupled tests were higher than the corresponding FLECHT-SET tests.
3. The differential pressures of the intact loops, ΔP_Is, of the CCTF and the FLECHT-SET tests were nearly identical, however, as observed in the previous tests, for example, C1-5 (Run 14),[1] the differential pressures of the broken loop, ΔP_B, were significantly different between two tests. Significantly large pressure difference between ΔP_B and ΔP_I appeared in CCTF and not in the FLECHT-SET.
4. The difference between ΔP_B and ΔP_I was caused by the existence of the pressure drop at the broken cold leg nozzle, ΔP_{BCN}, which was induced by the acceleration of the overflowed water by the steam flowing from the intact loops. The pressure drop, ΔP_{BCN}, caused big hydrodynamic oscilliations in the three CCTF tests coupling with the FLECHT-SET tests. Such oscillations have not been observed in the other CCTF tests. In the FLECHT-SET, the downcomer water level was controlled not to exceed the bottom of the broken cold leg nozzle whose size was much larger than the CCTF, resulting in low ΔP_{BCN}.
5. The core flooding rates estimated from the measured data of the CCTF test was higher than those of the FLECHT-SET test. This is attributed to the significantly large ΔP_{BCN}, while the higher density of the fluid passing through the orifice of the pump was also attributed to the higher flooding rate in the CCTF 2714B coupled test.
6. The upper plenum water accumulation was observed in the CCTF and FLECHT-SET tests as observed in the previous CCTF test.[1]
7. It was inferred that the higher flooding rates observed in the CCTF tests introduced more water accumulation, i.e. higher ΔP_C, and probably

higher heat transfer. And the big oscillation was inferred to enhance the core heat transfer. However the quantitative interpretation could not be obtained and further studies are necessary for the core thermo-hydrodynamics.

8. It can be concluded that the differences of the system designs and operation methods of CCTF and FLECHT-SET facility introduced the quantitative differences in the core and system thermo-hydrodynamic behavior, however, the phenomena in both facilities are qualitatively analogous, since the differences can be qualitatively interpreted and most of the observed phenomena are about the same.

[Nomenclature]

i	:	Enthalpy (J/kg)
K	:	Factor of flow resistance of a primary loop ($\equiv \Delta P / \frac{1}{2} \rho v^2$)
$\dot{m}$	:	Mass flow rate or mass accumulation rate (kg/s)
S_L	:	Flow area of each primary loop piping (m^2)
ΔP	:	Pressure drop (Pa)
ρ_g	:	Density of steam (kg/m^3)

Subscripts

B	Broken loop
BCN	Broken cold leg nozzle and connected pipe
C	Core
d	downstream
D	Downcomer
DL	Liquid through a cold leg into downcomer
DV	Steam through a cold leg into downcomer
ECC	ECC water injected into cold legs
ECC/LP	ECC water injected into a lower plenum
F	Flooded into a core
I	Intact loop
L	Primary loops
U	Upper plenum
u	upstream

higher heat transfer. And the big oscillation was inferred to enhance the core heat transfer. However the quantitative interpretation could not be obtained and further studies are necessary for the core thermo-hydrodynamics.

8. It can be concluded that the differences of the system designs and operation methods of CCTF and FLECHT-SET facility introduced the quantitative differences in the core and system thermo-hydrodynamic behavior, however, the phenomena in both facilities are qualitatively analogous, since the differences can be qualitatively interpreted and most of the observed phenomena are about the same.

[Nomenclature]

i	:	Enthalpy (J/kg)
K	:	Factor of flow resistance of a primary loop ($\equiv \Delta P / \frac{1}{2} \rho v^2$)
$\dot{m}$	:	Mass flow rate or mass accumulation rate (kg/s)
S_L	:	Flow area of each primary loop piping (m^2)
ΔP	:	Pressure drop (Pa)
ρ_g	:	Density of steam (kg/m^3)

Subscripts

B	Broken loop
BCN	Broken cold leg nozzle and connected pipe
C	Core
d	downstream
D	Downcomer
DL	Liquid through a cold leg into downcomer
DV	Steam through a cold leg into downcomer
ECC	ECC water injected into cold legs
ECC/LP	ECC water injected into a lower plenum
F	Flooded into a core
I	Intact loop
L	Primary loops
U	Upper plenum
u	upstream

Acknowledgement

The authors are much indebted to Mr. T. Iguchi, Dr. H. Akimoto and Messrs. J. Sugimoto and T. Okubo for their technical supports. We would like to express our thanks to Dr. M. Nozawa, Director of Nuclear Safety Research Center and Drs. S. Katsuragi, M. Ishikawa and K. Hirano of Division of Nuclear Safety Research, respectively, JAERI, for their guidance and encouragement for this program. We also would like to express our appreciation to the 2D/3D project members of USA and FRG, especially Dr. L.S. Tong of USNRC and Prof. Dr. F. Mayinger of T.U. München for valuable discussions.

References

(1) Murao, Y. et al.: Evaluation report on CCTF Core-I Reflood tests C1-5 (Run 14) —— Over-all system thermohydrodynamic behaviors observed in the base case test —— , JAERI-M 83-027 (1983).

(2) Waring, J.P. and Hochreiter L.E.: PWR FLECHT-SET phase B1 evaluation report, WCAP-8583, (1973).

(3) Waring, J.P. et al.: PWR FLECHT-SET phase B1 data report, WCAP-8431, (1974)

(4) Murao, Y. and Iguchi, T.: Experimental modeling of core hydrodynamics during reflood phase of LOCA, J. Nucl. Sci. Technol, 19[8], pp.613∿627,(1982).

(5) Murao, Y. and Sugimoto, J.: Correlation of heat transfer coefficient for saturated film boiling during reflood phase prior to quenching, J. Nucl. Sci. Technol., 18[4], pp.275∿284, (1981).

(6) Trojan nuclear plant, Final safety analysis report Vols.1 9, DOCKET-50344-38∿46, (1973).

Acknowledgement

The authors are much indebted to Mr. T. Iguchi, Dr. H. Akimoto and Messrs. J. Sugimoto and T. Okubo for their technical supports. We would like to express our thanks to Dr. M. Nozawa, Director of Nuclear Safety Research Center and Drs. S. Katsuragi, M. Ishikawa and K. Hirano of Division of Nuclear Safety Research, respectively, JAERI, for their guidance and encouragement for this program. We also would like to express our appreciation to the 2D/3D project members of USA and FRG, especially Dr. L.S. Tong of USNRC and Prof. Dr. F. Mayinger of T.U. München for valuable discussions.

References

(1) Murao, Y. et al.: Evaluation report on CCTF Core-I Reflood tests C1-5 (Run 14) —— Over-all system thermohydrodynamic behaviors observed in the base case test —— , JAERI-M 83-027 (1983).

(2) Waring, J.P. and Hochreiter L.E.: PWR FLECHT-SET phase B1 evaluation report, WCAP-8583, (1973).

(3) Waring, J.P. et al.: PWR FLECHT-SET phase B1 data report, WCAP-8431, (1974)

(4) Murao, Y. and Iguchi, T.: Experimental modeling of core hydrodynamics during reflood phase of LOCA, J. Nucl. Sci. Technol, 19[8], pp.613∿627,(1982).

(5) Murao, Y. and Sugimoto, J.: Correlation of heat transfer coefficient for saturated film boiling during reflood phase prior to quenching, J. Nucl. Sci. Technol., 18[4], pp.275∿284, (1981).

(6) Trojan nuclear plant, Final safety analysis report Vols.1 9, DOCKET-50344-38∿46, (1973).

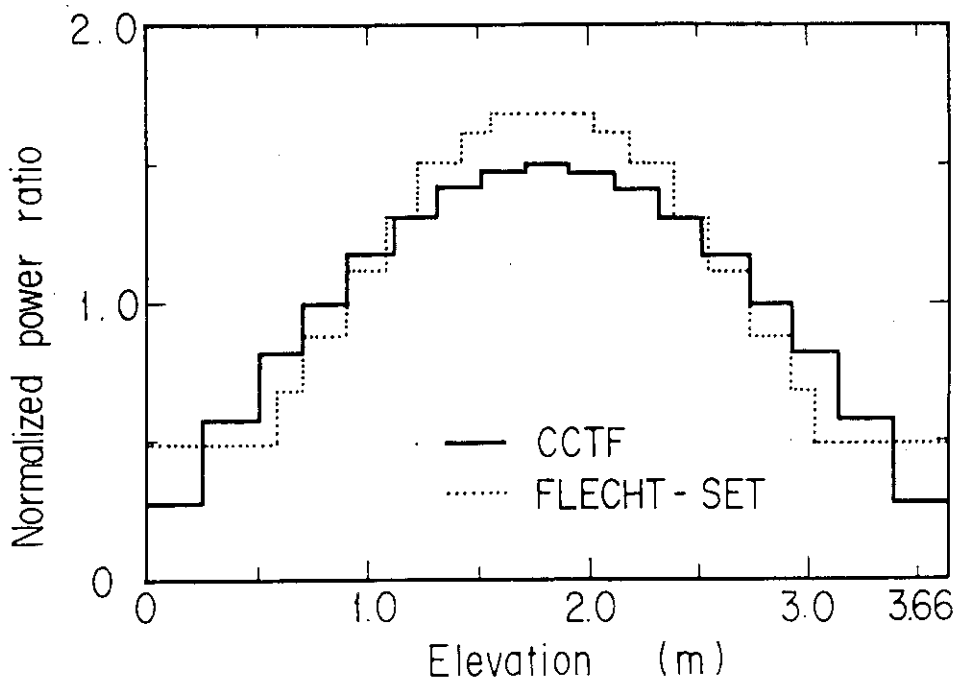

Fig. 1 Axial power distributions of CCTF and FLECHT-SET heated rods.

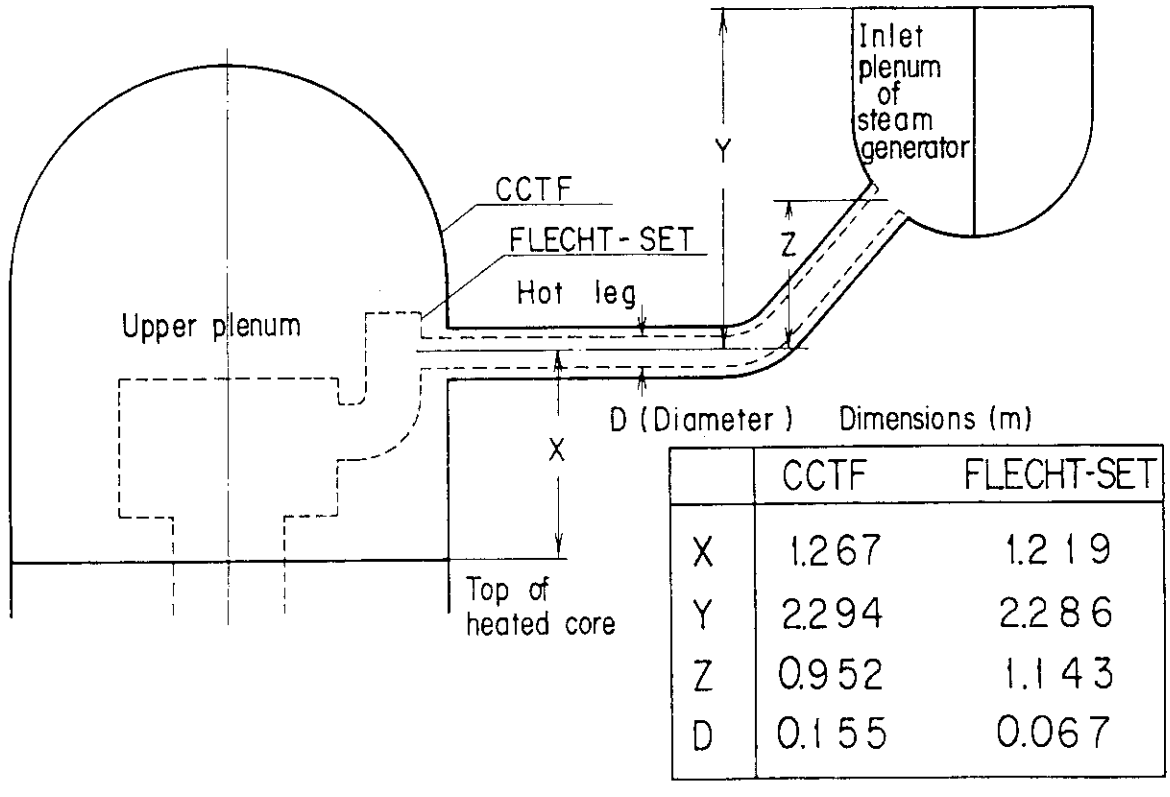

Dimensions (m)

	CCTF	FLECHT-SET
X	1.267	1.219
Y	2.294	2.286
Z	0.952	1.143
D	0.155	0.067

Fig. 2 Comparison of upper plenum and hot leg of CCTF with those of FLECHT-SET.

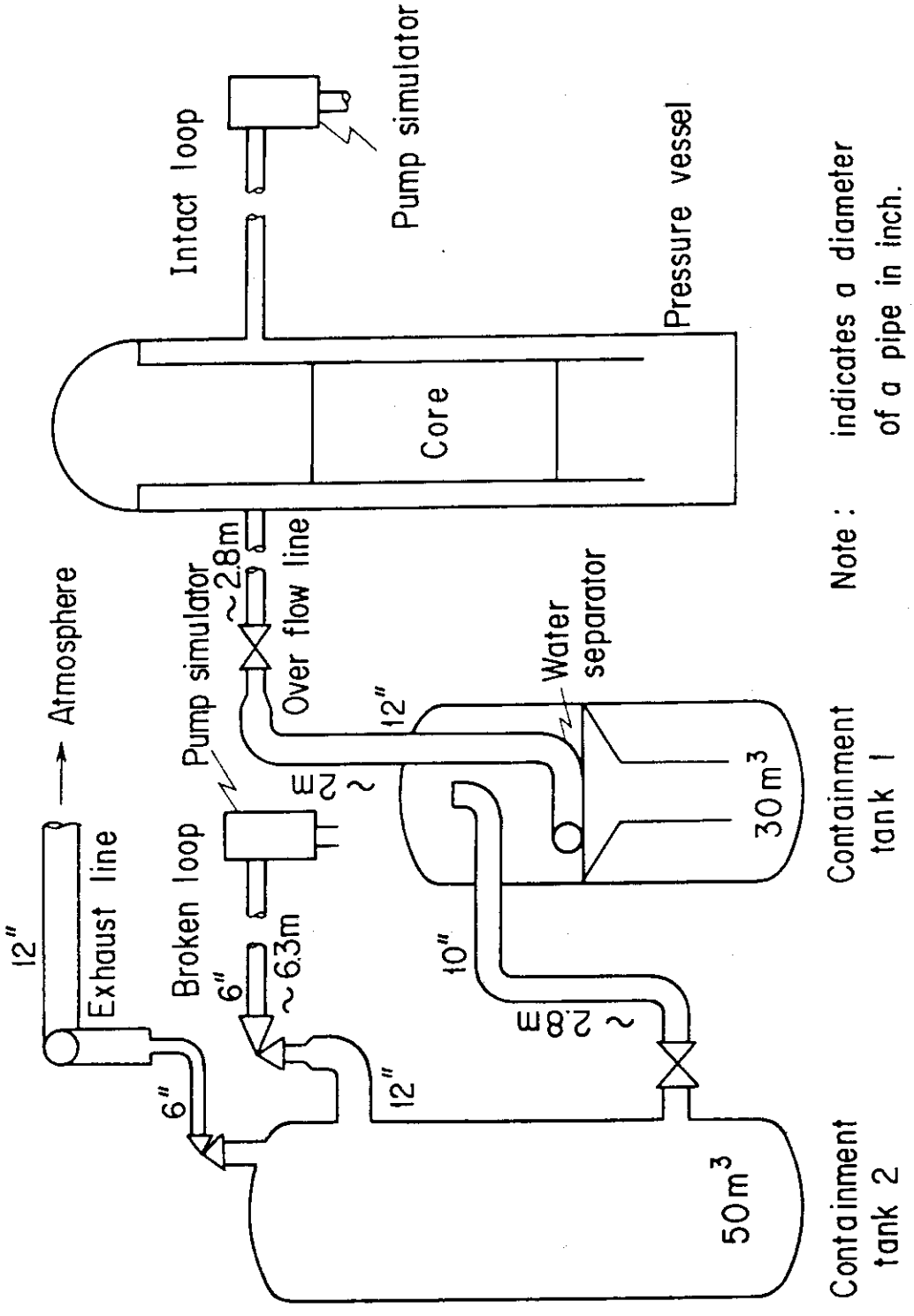

Fig. 3 Schematic of CCTF discharge line

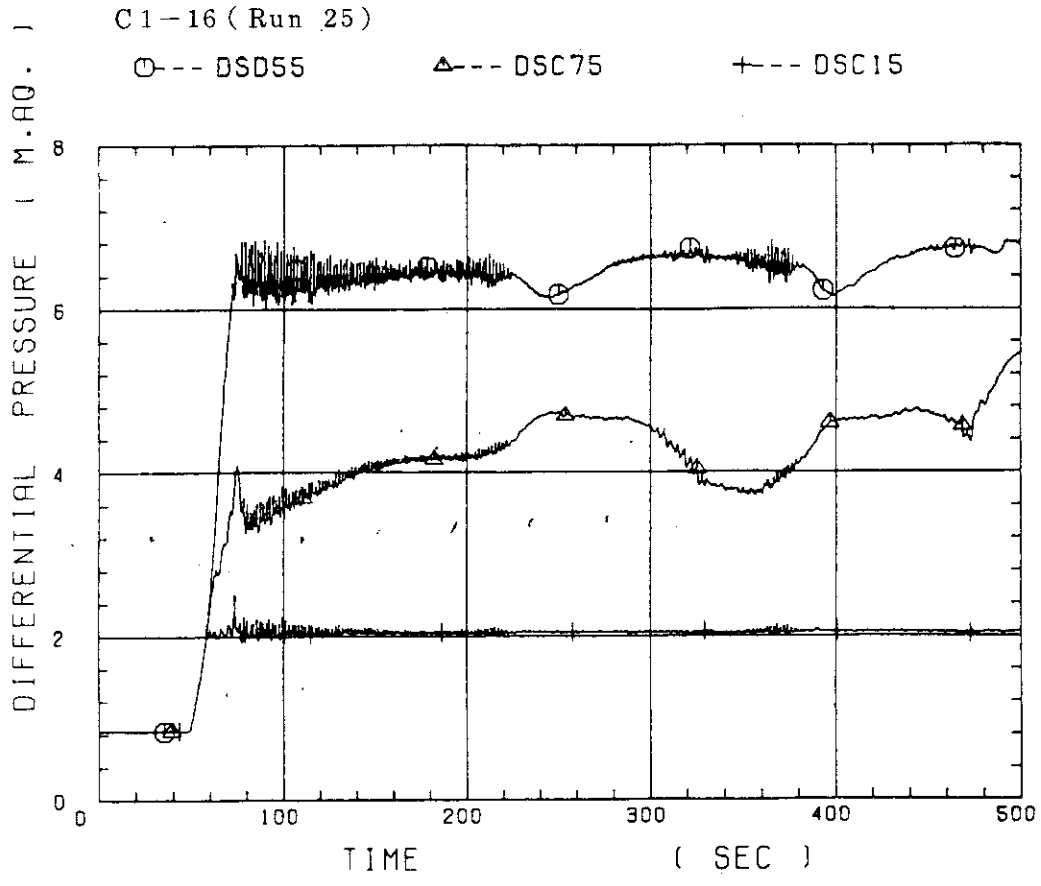

Fig. 4 (a) Differential pressures through downcomer, core and lower plenum.

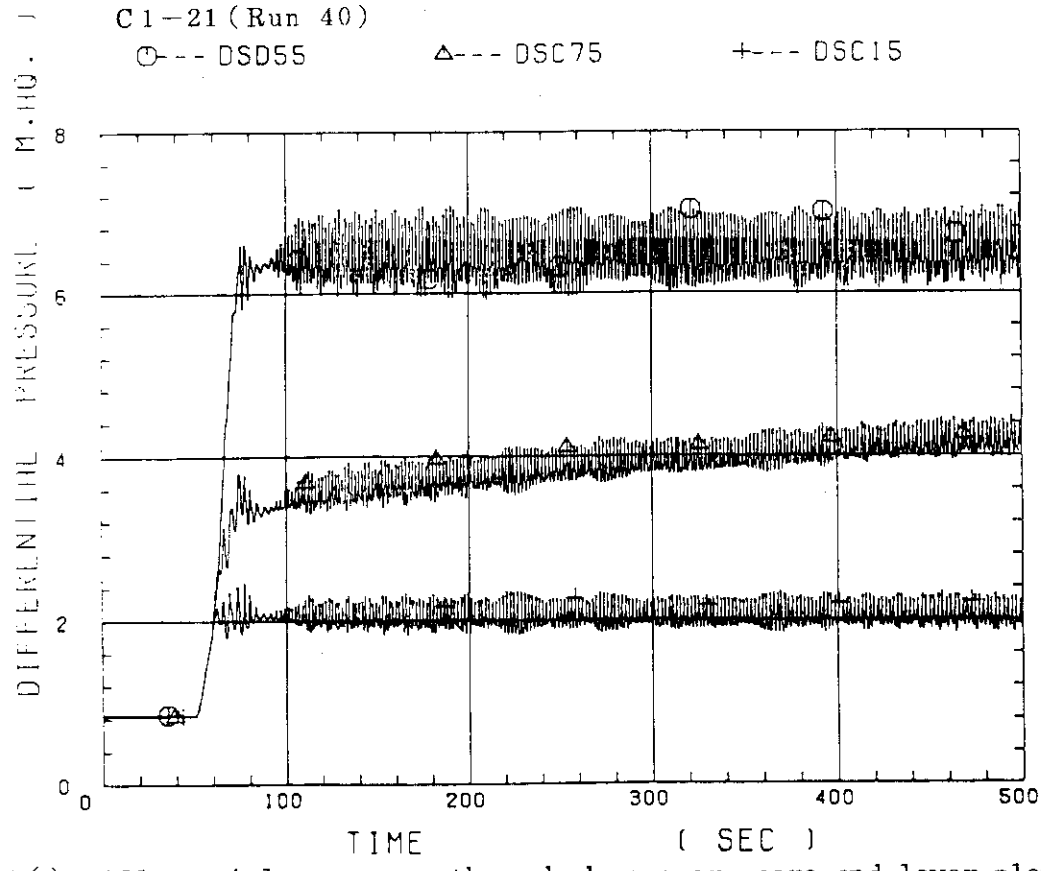

Fig. 4 (b) Differential pressures through downcomer, core and lower plenum.

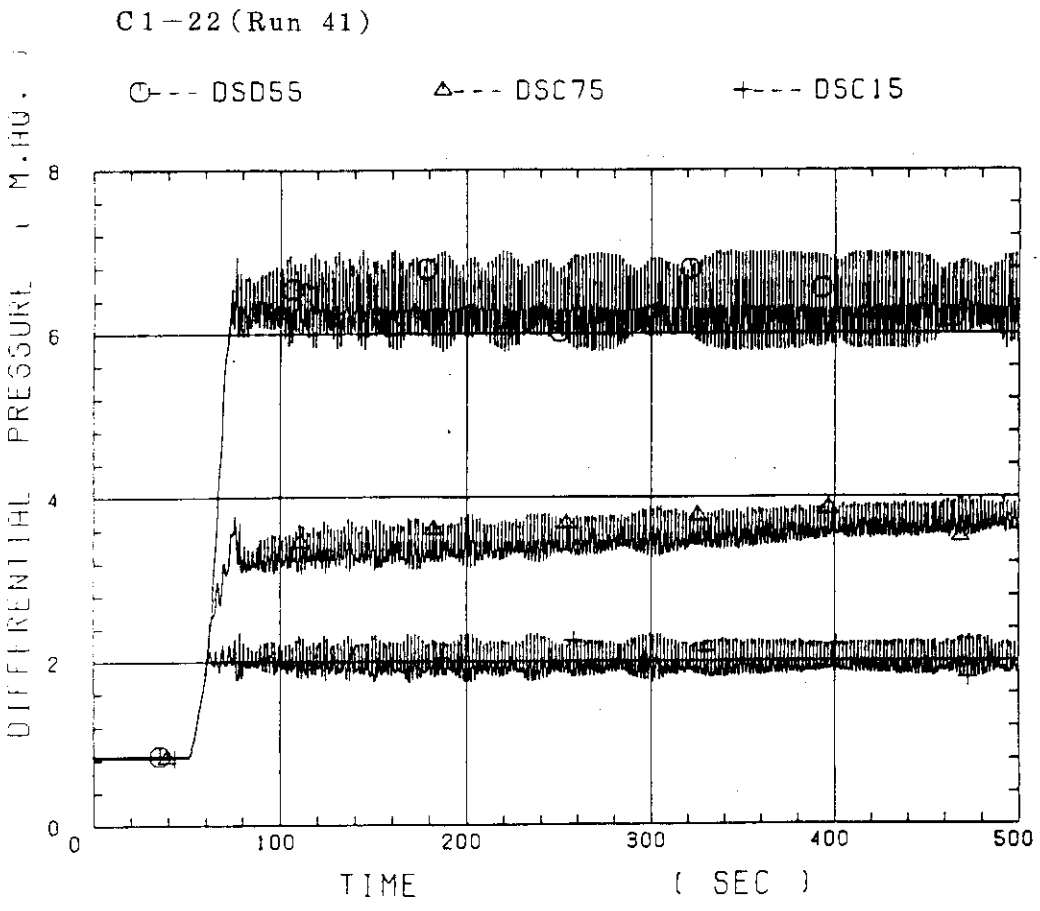

Fig. 4(c) Differential pressures through downcomer, core and lower plenum.

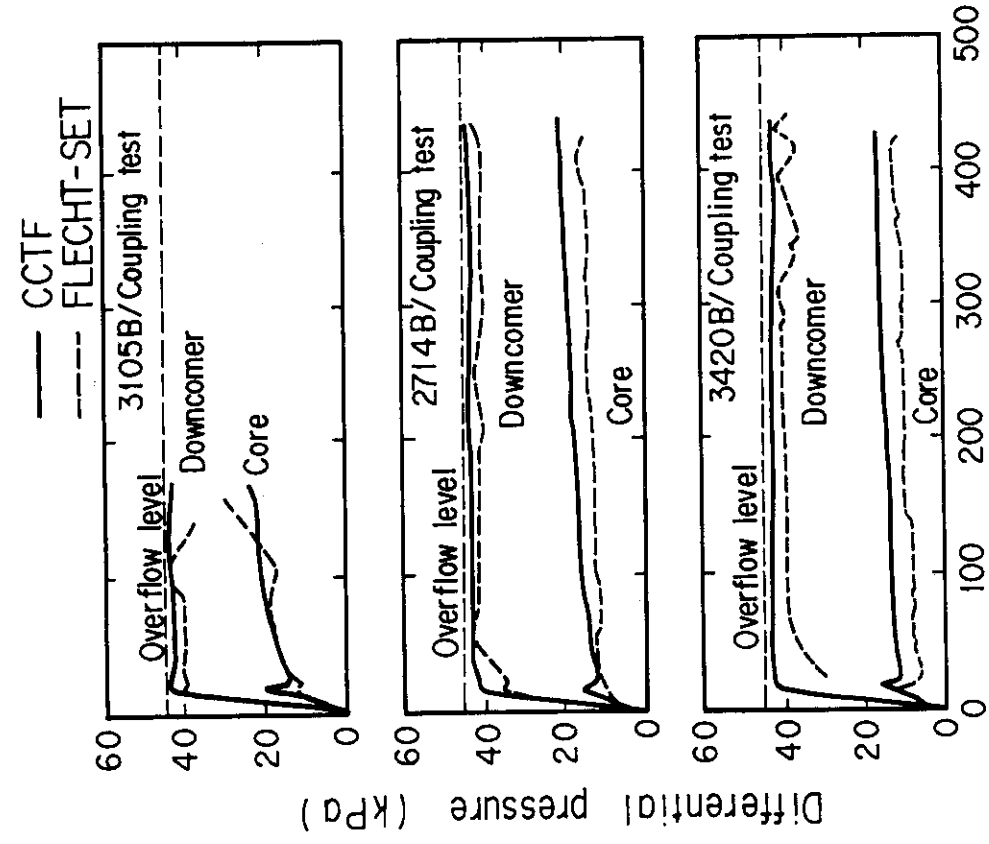

Fig. 5 Comparison of core and downcomer differential pressure of CCTF tests with those of FLECHT-SET tests.

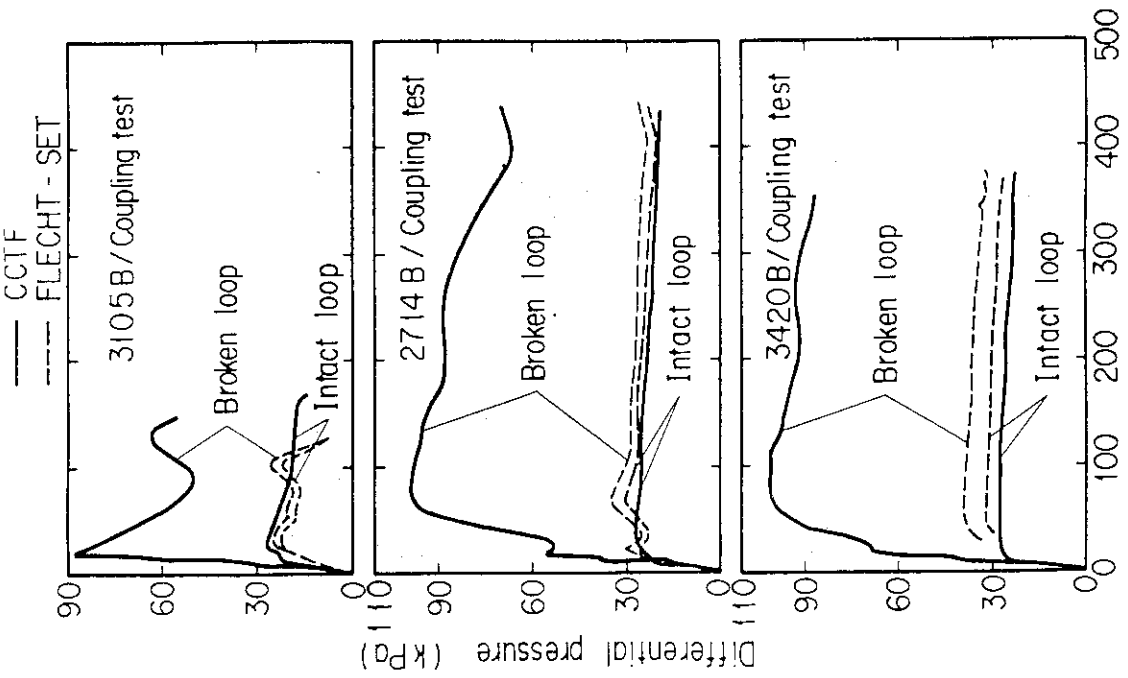

Fig. 6 Comparison of loop differential pressures of CCTF tests with those of FLECHT-SET tests.

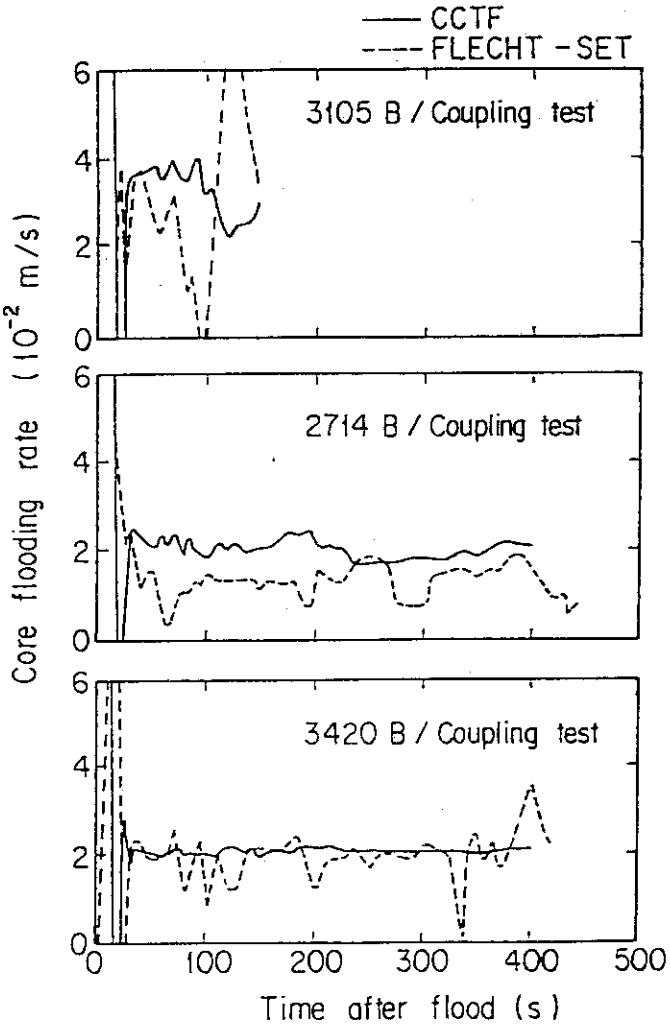

Fig. 7 Comparison of core flooding rates of CCTF tests with those of FLECHT-SET tests.

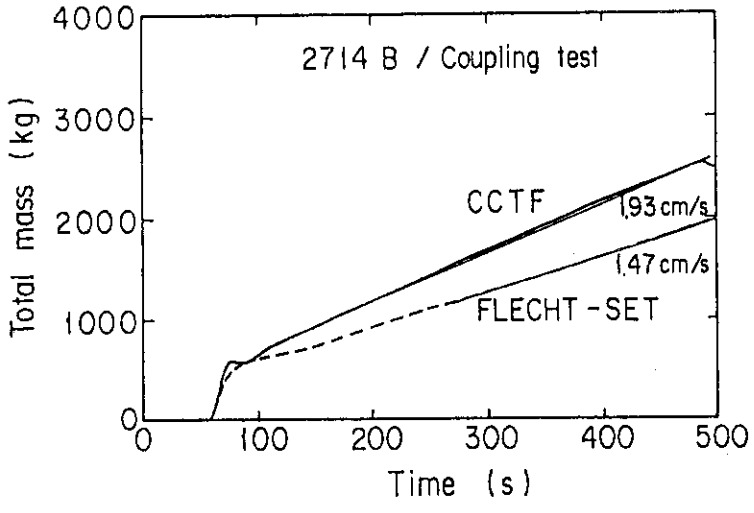

Fig. 8 Comparison of total mass flooded into core of CCTF tests with those of FLECHT-SET tests

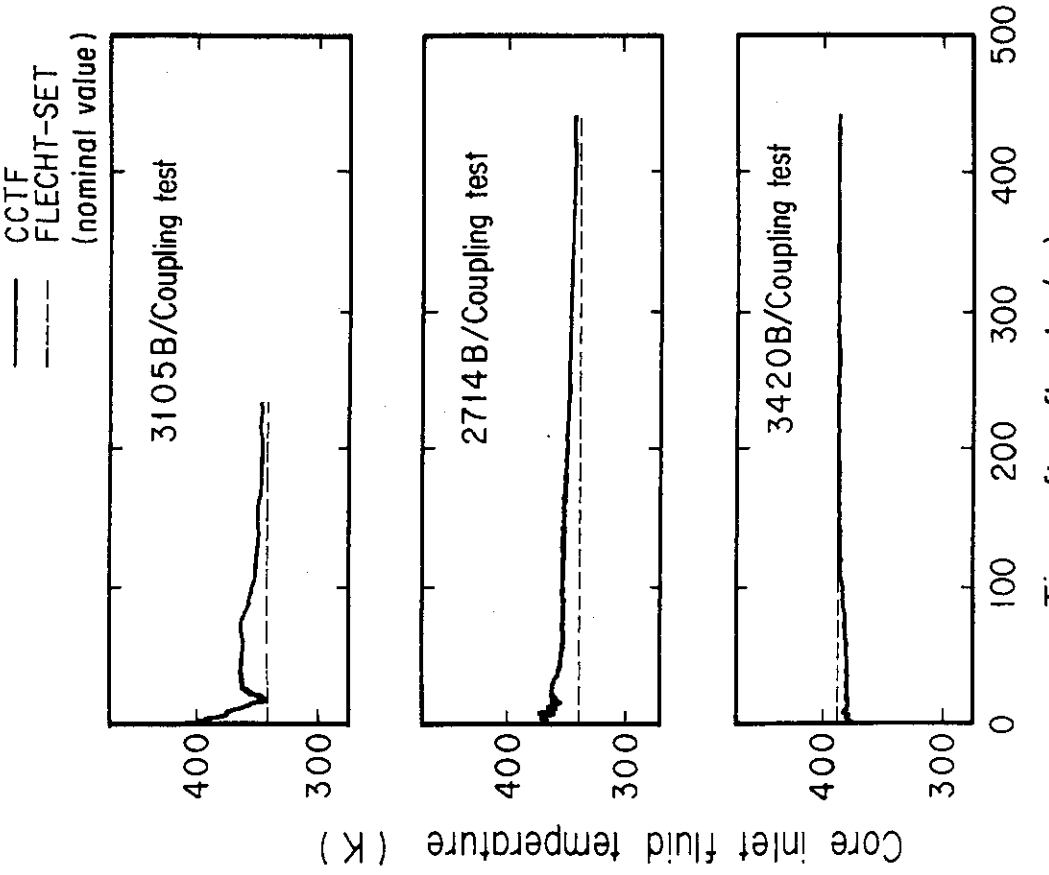

Fig. 10 Comparison of core inlet fluid temperatures of CCTF tests with those of FLECHT-SET tests.

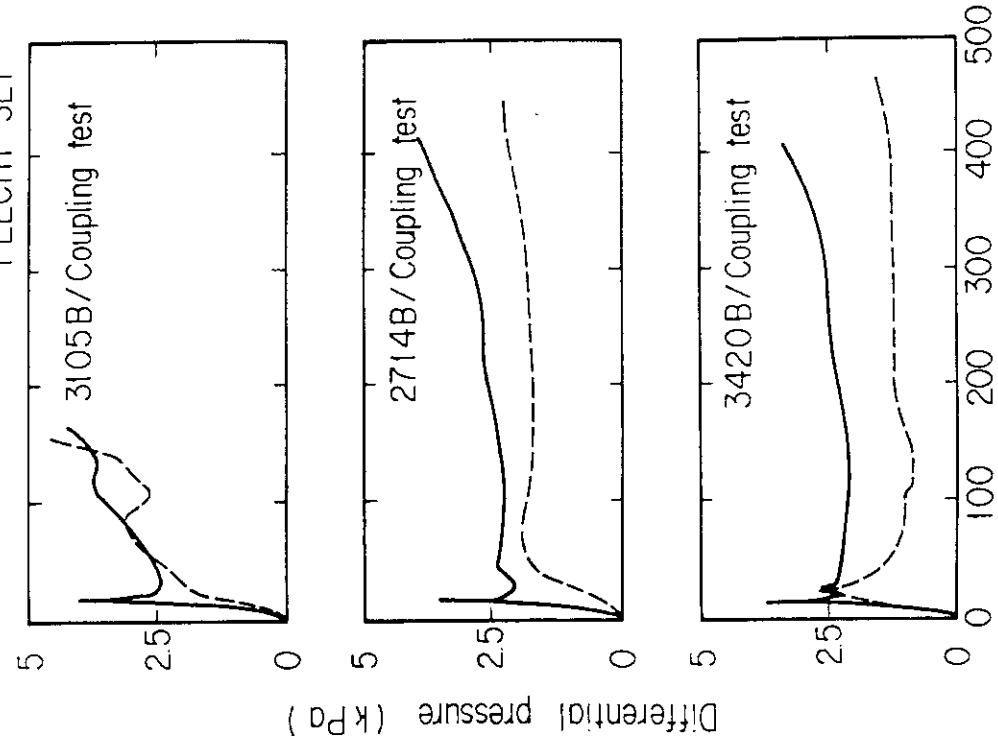

Fig. 9 Comparison of upper plenum differential pressures of CCTF tests with those of FLECHT-SET tests.

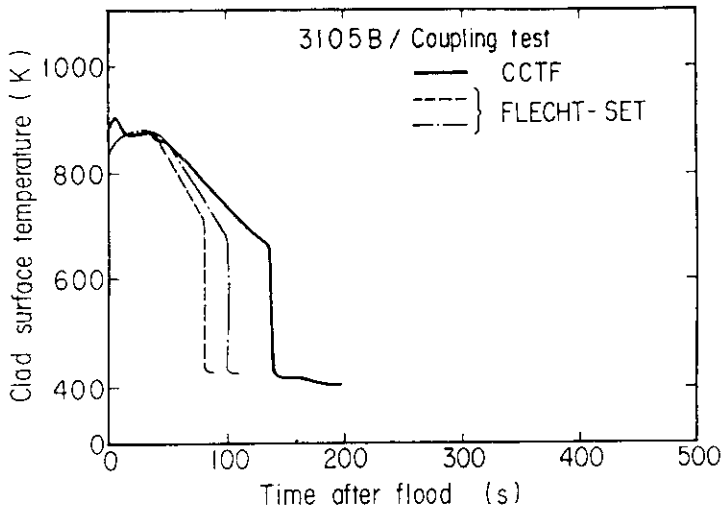

Fig. 11(a) Comparison of clad surface temperatures of CCTF tests with those of FLECHT-SET tests.

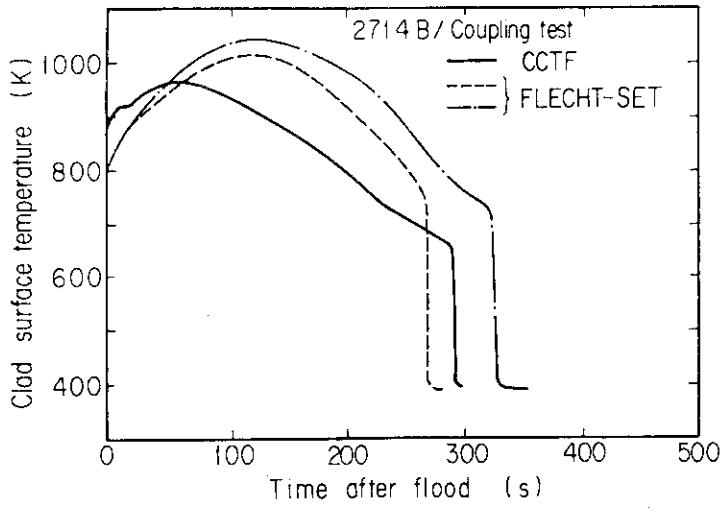

Fig. 11(b) Comparison of clad surface temperatures of CCTF tests with those of FLECHT-SET tests.

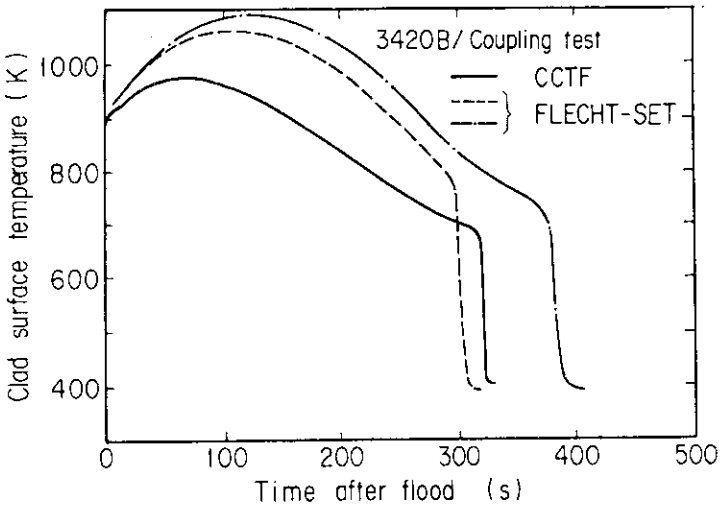

Fig. 11(c) Comparison of clad surface temperatures of CCTF tests with those of FLECHT-SET tests.

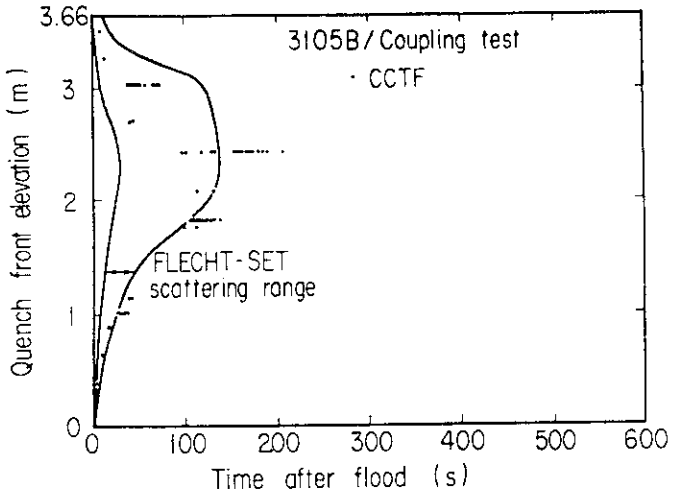

Fig. 12(a) Comparison of quench from envelopes of CCTF tests with scattering range of quench times of FLECHT-SET tests.

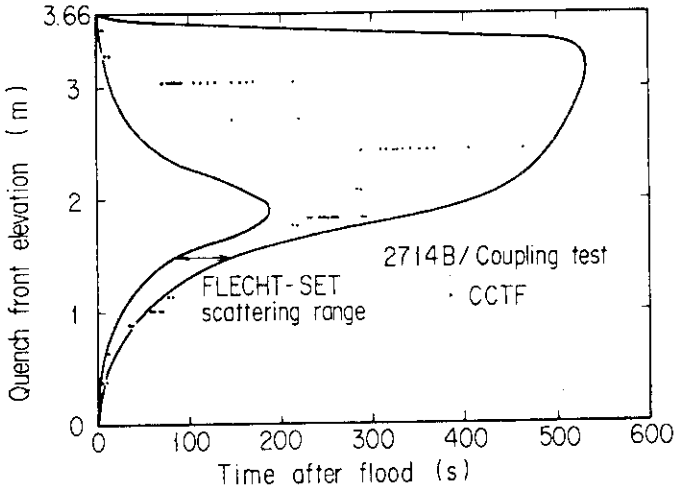

Fig. 12(b) Comparison of quench from envelopes of CCTF tests with scattering range of quench times of FLECHT-SET tests.

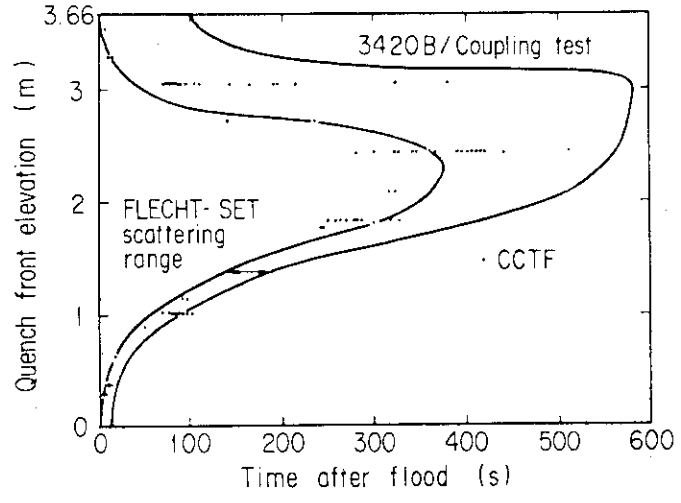

Fig. 12(c) Comparison of quench from envelopes of CCTF tests with scattering range of quench times of FLECHT-SET tests.

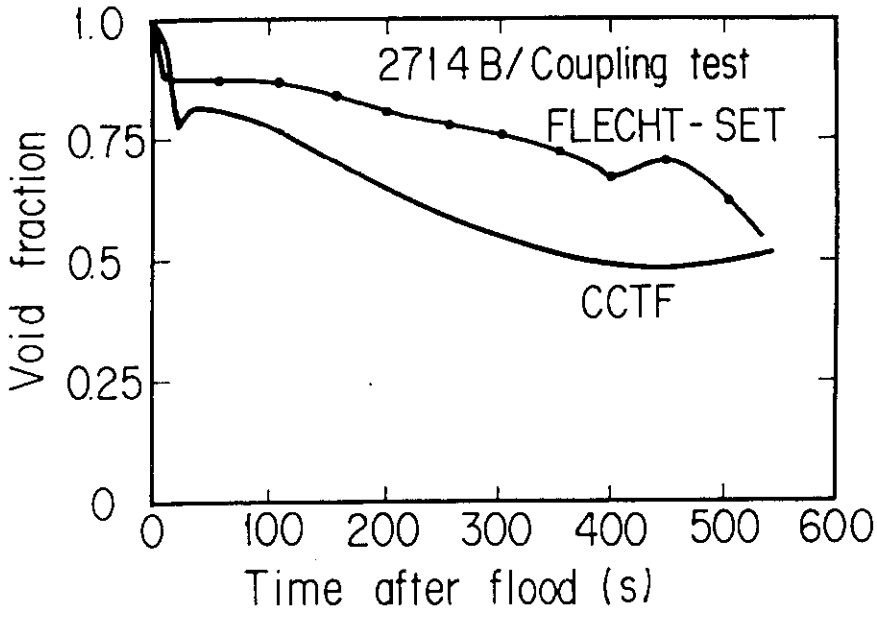

Fig. 13 Comparison of void fractions at the midplane of CCTF tests with FLECHT-SET tests.

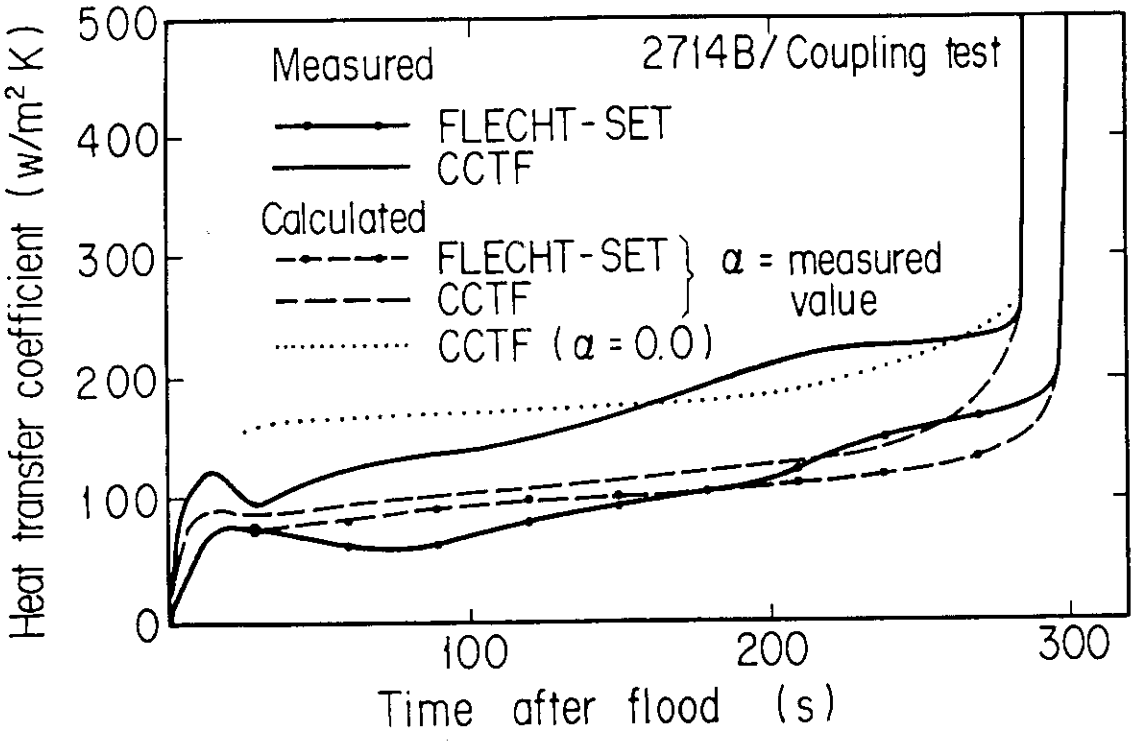

Fig. 14 Comparison of heat transfer coefficients between the measured and the calculated with a film boiling correlation.

Appendix A

Explanation of measuring location of referred data and definition of the evaluated data

Figure list

Fig. A-1 Definition of power zones and bundle numbers
Fig. A-2 Definition of Tag.ID for void fraction (AG(EL.1) ∿ AG(EL.6))
Fig. A-3 Definition of Tag.ID for average linear power of heater rod in each power unit zone (LP01A ∿ LP09A)
Fig. A-4 Definition of Tag.ID for differential pressure through downcomer, upper plenum, core, and lower plenum (DSD55, DT07RT5, DSC75, DSC15)
Fig. A-5 Definition of Tag.ID for differential pressure through intact and broken loop and broken cold leg nozzle (DT23C, DT01B, DPBCN)
Fig. A-6 Definition of Tag.ID for fluid temperature in inlet and outlet plenum and secondary of steam generator (TE□2GW, TE□5GW, TE08G□H)

1. Definition of Tag.ID for clad surface temperatures

Notation : TENNWAM

NN : Bundle number

WA : Power zone

WA = X1, X2 : High power (Local power factor 1.1)

WA = Y1, Y2 : Medium power (Local power factor 1.0)

WA = Z1, Z2 : Low power (Local power factor 0.95)

M : Elevation

	Elevation (m)	Axial power factor
1	0.38	0.568
2	1.015	1.176
3	1.83	1.492
4	2.44	1.312
5	3.05	0.815

2. Definition of power zone and bundle number

See Fig. A-1

3. Definition of Tag.ID for void fraction

See Fig. A-2

4. Definition of Tag.ID for average linear power of heater rod in each power unit zone

See Fig. A-3

5. Definition of carry-over rate fraction (C.R.F)

$$CRF = \frac{\dot{m}_{UP} + \dot{m}_{L}}{\dot{m}_{CR} + \dot{m}_{UP} + \dot{m}_{L}}$$

The calculated data within ±25 s are averaged:

$$(CRF)_i = \frac{1}{101} \sum_{k=i-50}^{i+50} (CRF)_k$$

where

ΔP_{UP} : Average of measured data at four orientations

ΔP_{CR} : Same as above

$$\dot{m}_{UP} = A_{up} \frac{d}{dt} (\Delta P_{UP})$$

$$\dot{m}_{CR} = A_{CR} \frac{d}{dt} (\Delta P_{CR})$$

$$\dot{m}_L = \sum_{k=1}^{4} \dot{m}_{pk}$$

$\dot{m}$: mass flow rate or mass accumulation rate

ΔP: differential pressure

suffix

UP: upper plenum

CR: core

L : loop

p : primary pump

6. Definition of Tag.ID for differential pressure through downcomer, upper plenum, core and lower plenum

   See Fig. A-4

7. Definition of Tag.ID for differential pressure through intact and broken loop and broken cold leg nozzle

   See Fig. A-5

8. Definition of Tag.ID for fluid temperature in inlet and outlet plenum and secondary of steam generator

   See Fig. A-6

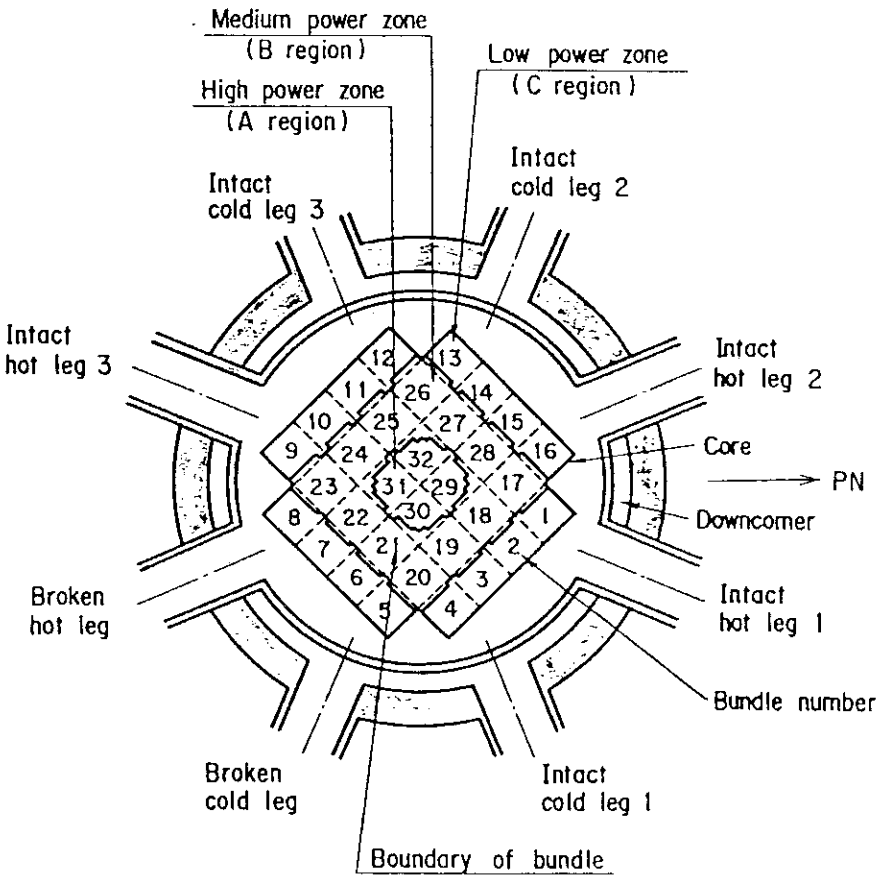

Fig. A-1 Definition of power zones and bundle numbers

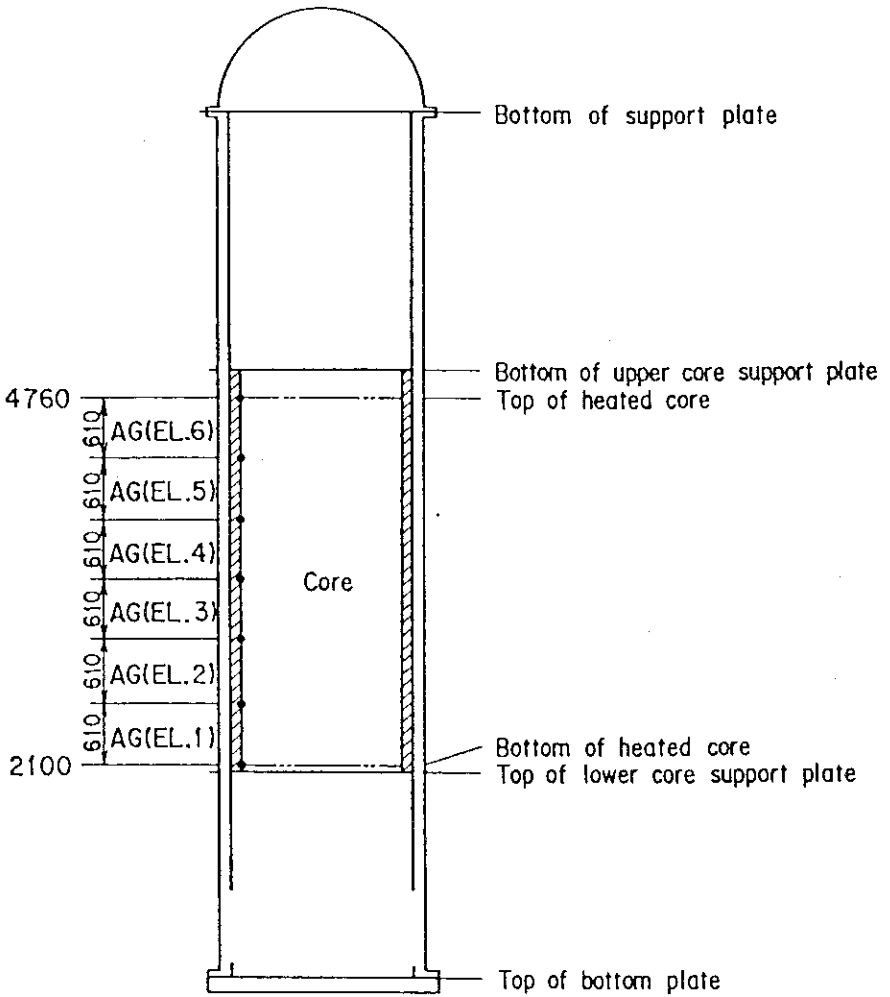

Fig. A-2 Definition of Tag.ID for void fraction
(AG(EL.1) ∿ AG(EL.6))

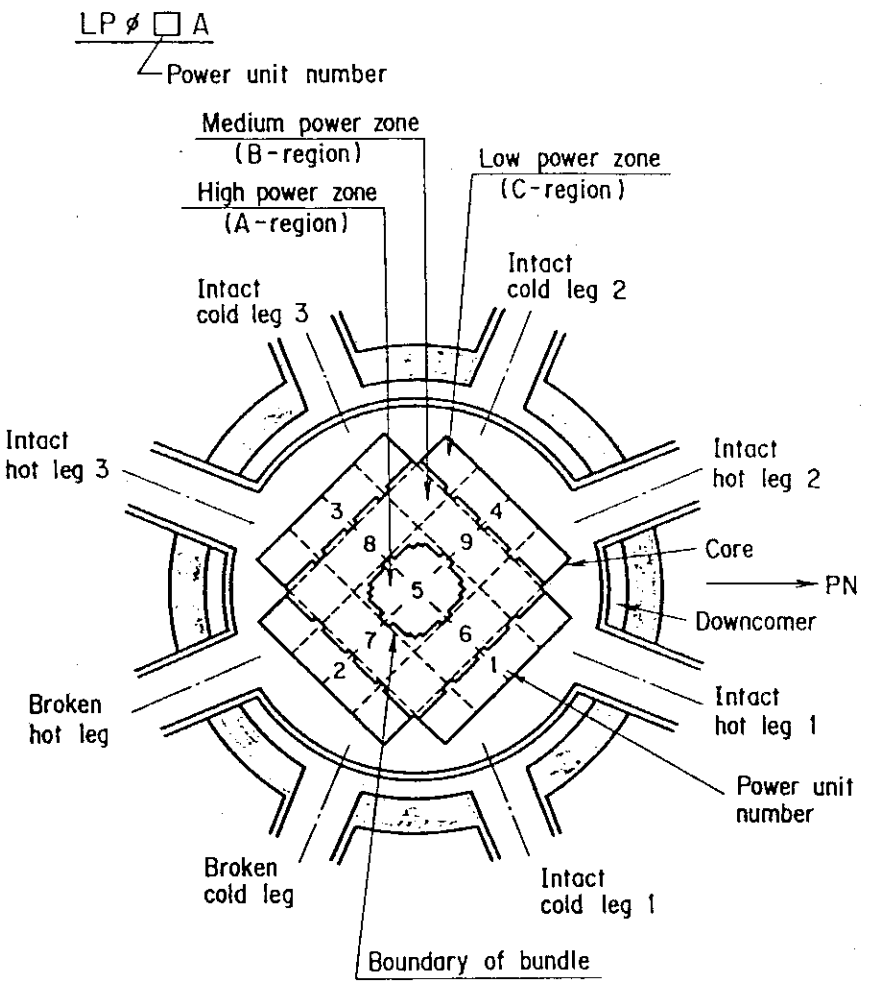

Fig. A-3 Definition of Tag.ID for average linear power of heater rod in each power unit zone (LP01A ∿ LP09A)

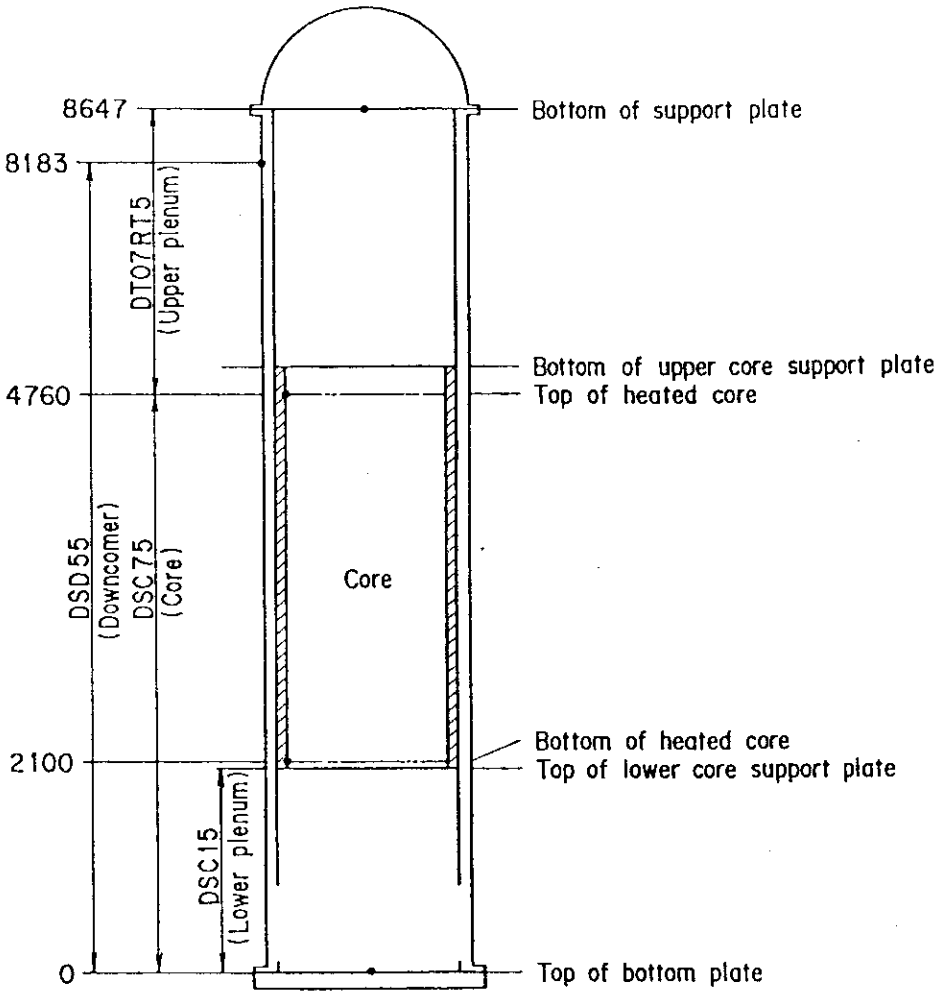

Fig. A-4

Definition of Tag.ID for differential pressure through downcomer, upper plenum, core, and lower plenum (DSD55, DT07RT5, DSC75, DSC15)

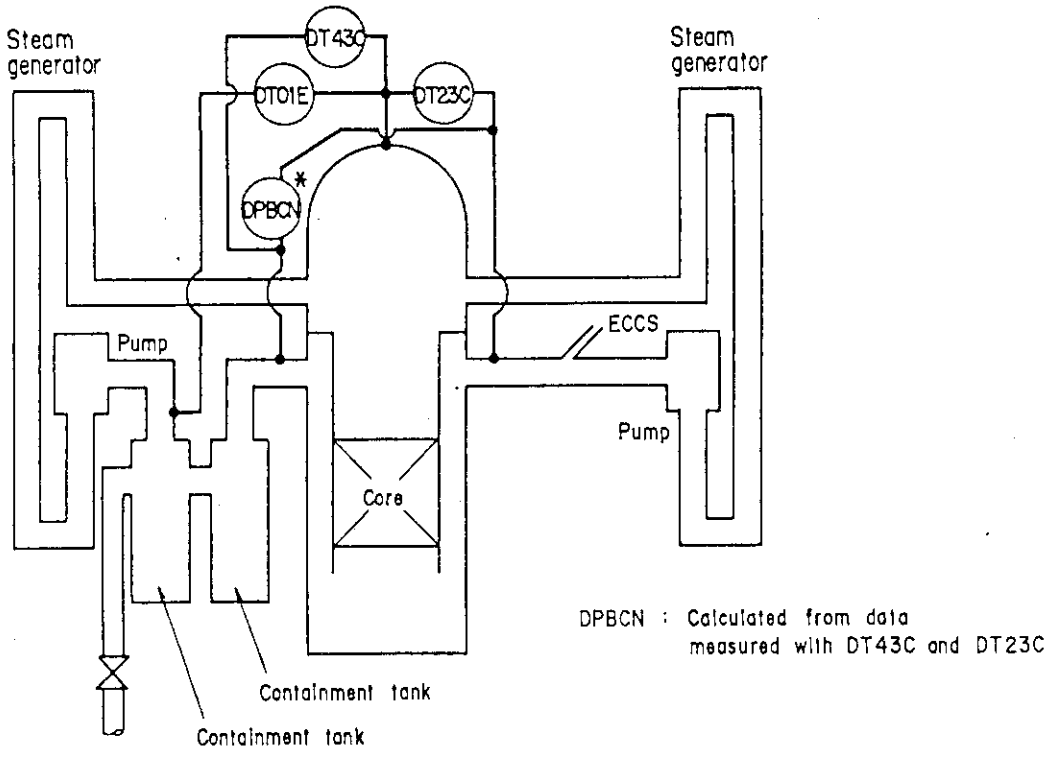

Fig. A-5 Definition of Tag.ID for differential pressure through intact and broken loop and broken cold leg nozzle (DT23C, DT01B, DPBCN)

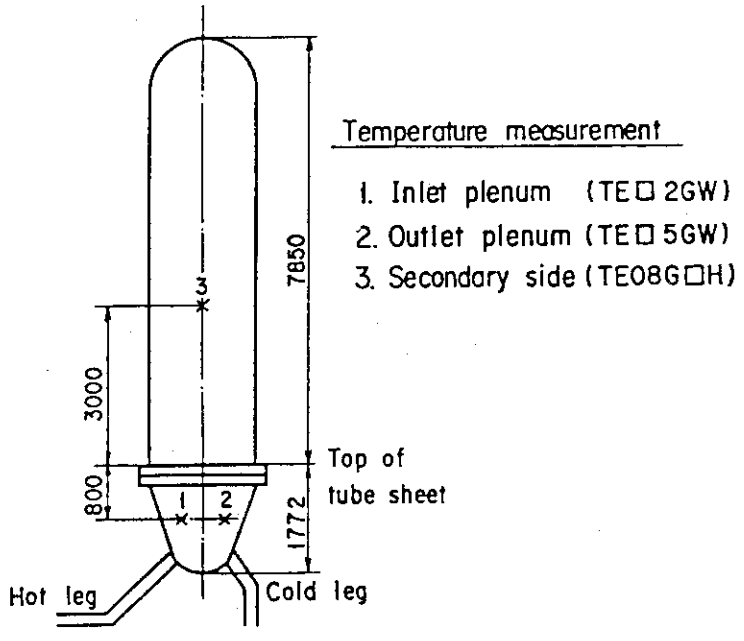

Fig. A-6 Definition of Tag.ID for fluid temperature in inlet and outlet plenum and secondary of steam generator (TE□2GW, TE□5GW, TE08G□H)

Appendix B

Main results of test C1-16 (Run 25)

Table and Figure List

Table B-1 Summary of test conditions

Table B-2 Chronology of events

Fig. B-1 Surface temperature on low power rod (Z-rod) in medium power region (B region) (average power rod)

Fig. B-2 Surface temperature on high power rod (X-rod) in high power region (A region) (peak power rod)

Fig. B-3 Surface temperature on low power rod (Z-rod) in low power region (C region) (lowest power rod)

Fig. B-4 Heat transfer coefficient at midplane of low power rod (Z-rod) in medium power region (B region) (average power rod)

Fig. B-5 Heat transfer coefficient at midplane of high power rod (X-rod) in high power region (A region) (peak power rod)

Fig. B-6 Initial rod surface temperature in high power region (A region)

Fig. B-7 Initial rod surface temperature in medium power region (B region)

Fig. B-8 Inital rod surface temperature in low power region (C region)

Fig. B-9 Turnaround temperature in high power region (A region)

Fig. B-10 Turnaround temperature in medium power region (B region)

Fig. B-11 Turnaround temperature in low power region (C region)

Fig. B-12 Turnaround time in high power region (A region)

Fig. B-13 Turnaround time in medium power region (B region)

Fig. B-14 Turnaround time in low power region (C region)

Fig. B-15 Quench temperature in high power region (A region)

Fig. B-16 Quench temperature in medium power region (B region)

Fig. B-17 Quench temperature in low power region (C region)

Fig. B-18 Quench time in high power region (A region)

Fig. B-19 Quench time in medium power region (B region)

Fig. B-20 Quench time in low power region (C region)

Fig. B-21 Void fraction in core

Fig. B-22 Core inlet mass flow rate

Fig. B-23 Average linear power of heater rod in each power unit zone

Fig. B-24 Carry-over rate fraction

Fig. B-25 Differential pressure through upper plenum

Fig. B-26 Differential pressure through downcomer, core, and lower plenum

Fig. B-27 Differential pressure through intact and broken loops
Fig. B-28 Differential pressure through broken cold leg nozzle
Fig. B-29 Total water mass flow rate from intact loops to downcomer
Fig. B-30 Total steam mass flow rate from intact loops to downcomer
Fig. B-31 Water mass flow rate through broken cold leg nozzle
Fig. B-32 Fluid temperature in inlet plenum, outlet plenum, and secondary of steam generator 1
Fig. B-33 Fluid temperature in inlet plenum, outlet plenum, and secondary of steam generator 2
Fig. B-34 Total accumulator injection rate
Fig. B-35 ECC water injection rates to lower plenum and to cold legs

TABLE B-1 SUMMARY OF TEST CONDITIONS

1. TEST TYPE : FLECHT-SET 3105B COUPLING TEST

2. TEST NUMBER : RUN 025, C1-16; 3. DATE : March 6, 1980

4. POWER : A: TOTAL: 9.82 MW; B:LINEAR: 1.5 KW/M

5. RELATIVE RADIAL POWER SHAPE :

   A: ZONE: A B C

   B: RATIO: 1.06 : 1.0 : 0.79

6. AXIAL POWER SHAPE : CHOPPED COSINE

7. PRESSURE (KG/CM^2A) :

   A: SYSTEM: 4.2, B: CONTAINMENT 4.2,

   C: STEAM GENERATOR SECONDARY: 51

8. TEMPERATURE (DEG.C) :

   A: DOWNCOMER WALL 137, B: VESSEL INTERNALS 135,

   C: PRIMARY PIPING WALL 145, D: LOWER PELNUM LIQUID 127,

   E: ECC LIQUID 67, F: STEAM GENERATOR SECONDARY 263,

   G: CORE TEMPERATURE AT ECC INITIATION 528

9. ECC INJECTION TYPE: 3

   A: COLD LEG, B: LOWER PLENUM, C: LOWER PLENUM + COLD LEG

10. PUMP K-FACTOR : ~ 15

11. ECC FLOW RATES AND DURATION :

   A: ACCUMULATOR 361 M^3/HR FROM 0 TO 26 SECONDS

   B: LPCI 40.1 M^3/HR FROM 26 TO 541 SECONDS

   C: ECC INJECTION TO LOWER PLENUM : FROM 0 TO 541 SECONDS

   (VALVE OPENING AND CLOSING TIMES ARE INCLUDED IN THE INJECTION DURATION)

12. INITIAL WATER LEVEL IN LOWER PLENUM : 0.90 M.

13. POWER CONTROL : ANS x 1.2 + ACTINIDE (30 SEC AFTER SCRAM)

14. EXPECTED BOCREC TIME FROM ECC INITIATION 9 SEC

15. EXPECTED PEAK TEMPERATURE AT BOCREC 600 C

TABLE B-2 CHRONOLOGY OF EVENTS FOR TEST C1-16 (RUN 025)

EVENT	TIME (sec)
Test Initiated (Heater Rods Power on) (Data Recording Initiated)	0.0
Accumulator Injection Initiated (Into lower plenum)	49
Power Decay Initiated (Bottom of Core Recovery)	58
Accumulator Injection Switched from Lower Plenum to Cold Leg	
Accumulator Injection Ended and LPCI Injection Initiated	75
All Heater Rods Quenched	268
Power Off	471
LPCI Injection Ended	590
Test Ended (Data Recording Ended)	817

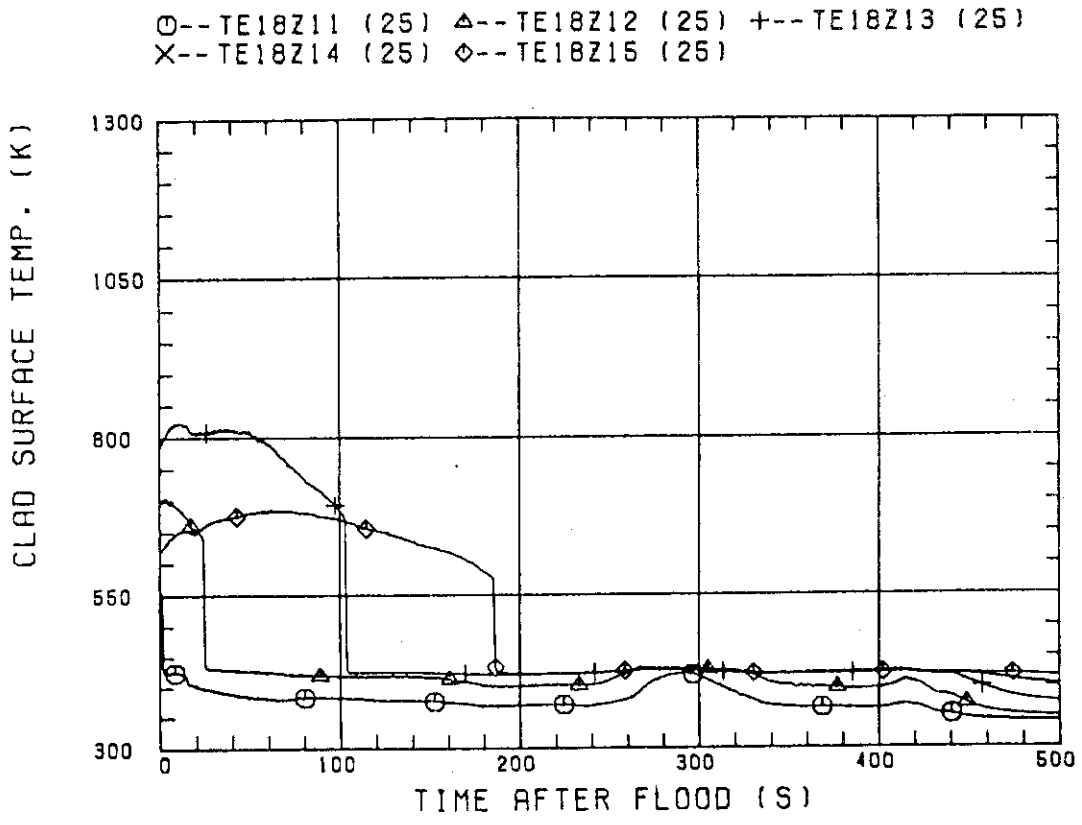

Fig. B-1 Surface temperature on low power rod (Z-rod) in medium power region (B region) (average power rod)

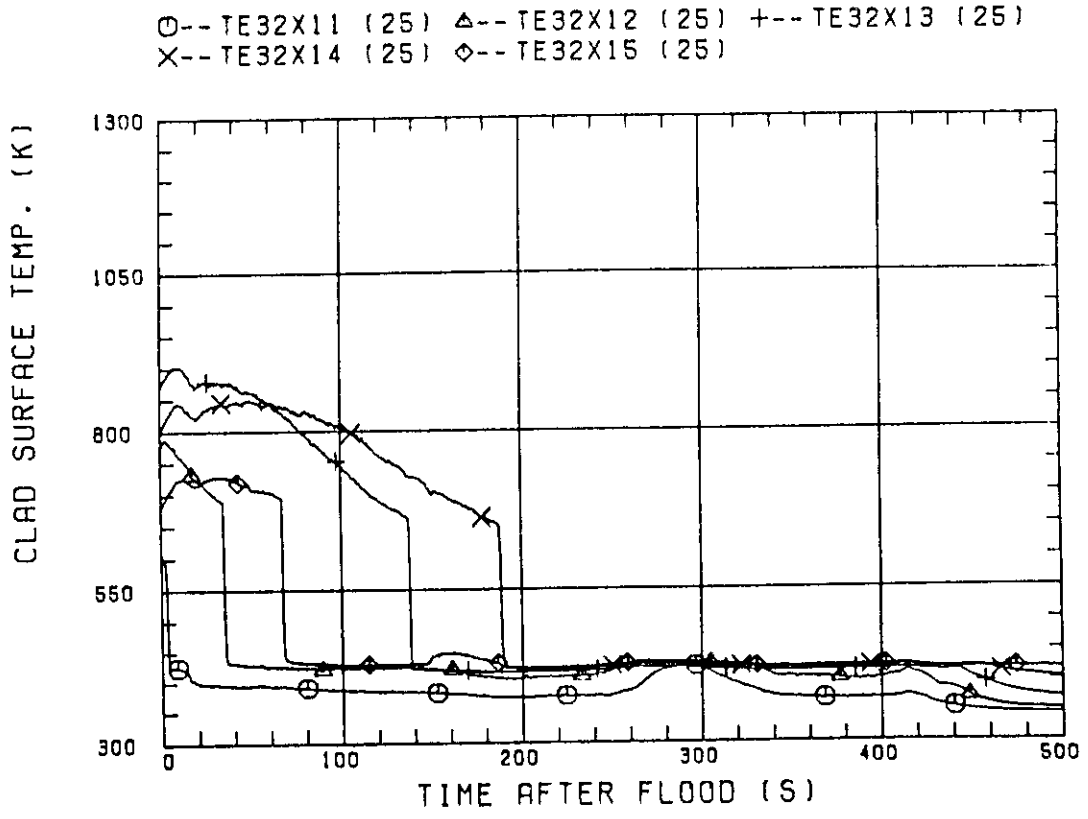

Fig. B-2 Surface temperature on high power rod (X-rod) in high power region (A region) (peak power rod)

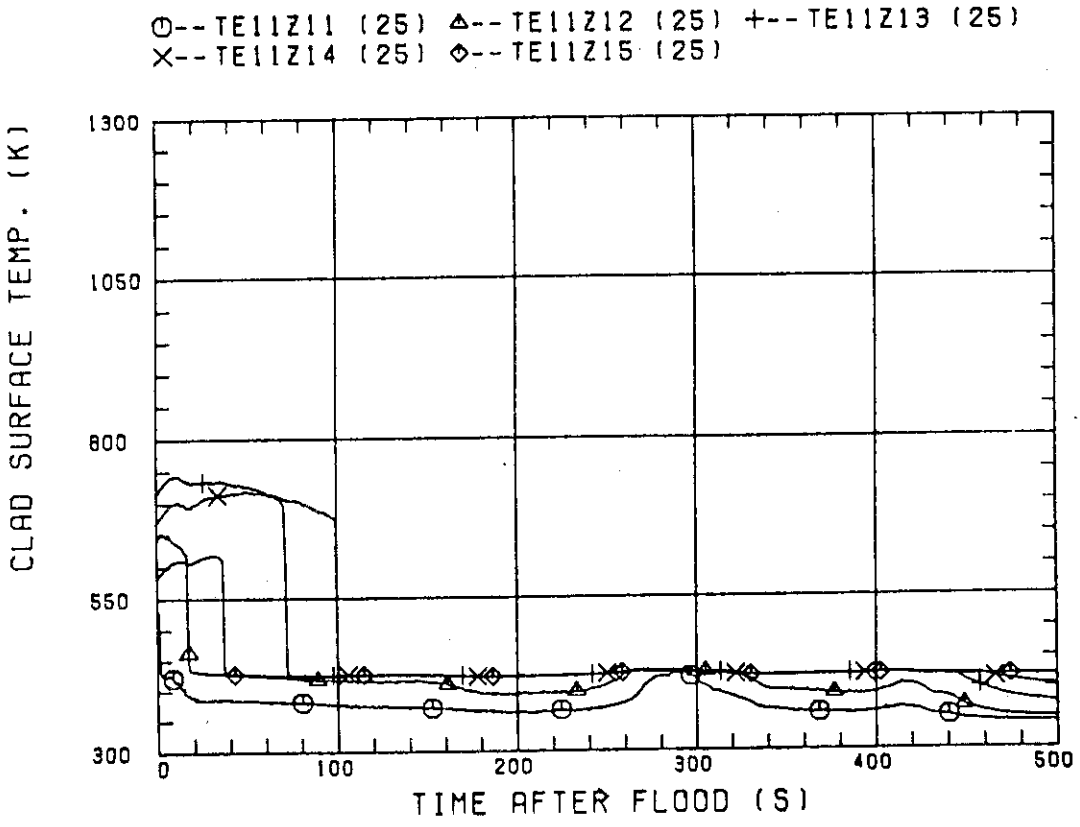

Fig. B-3 Surface temperature on low power rod (Z-rod) in low power region (C region) (lowest power rod)

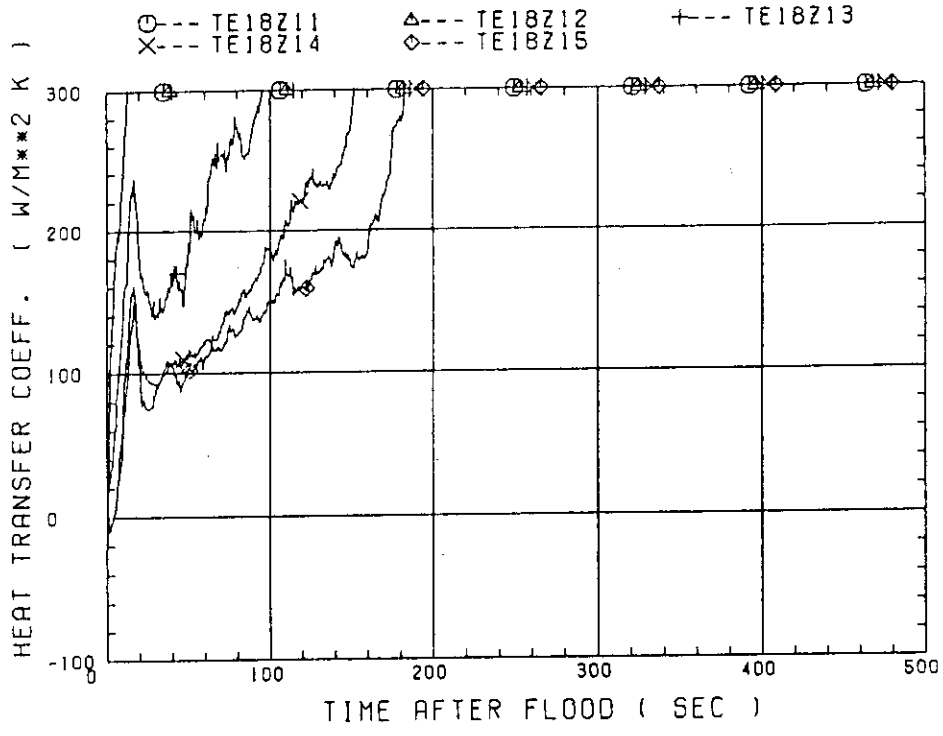

Fig. B-4 Heat transfer coefficient at midplane of low power rod (Z-rod) in medium power region (B region) (average power rod)

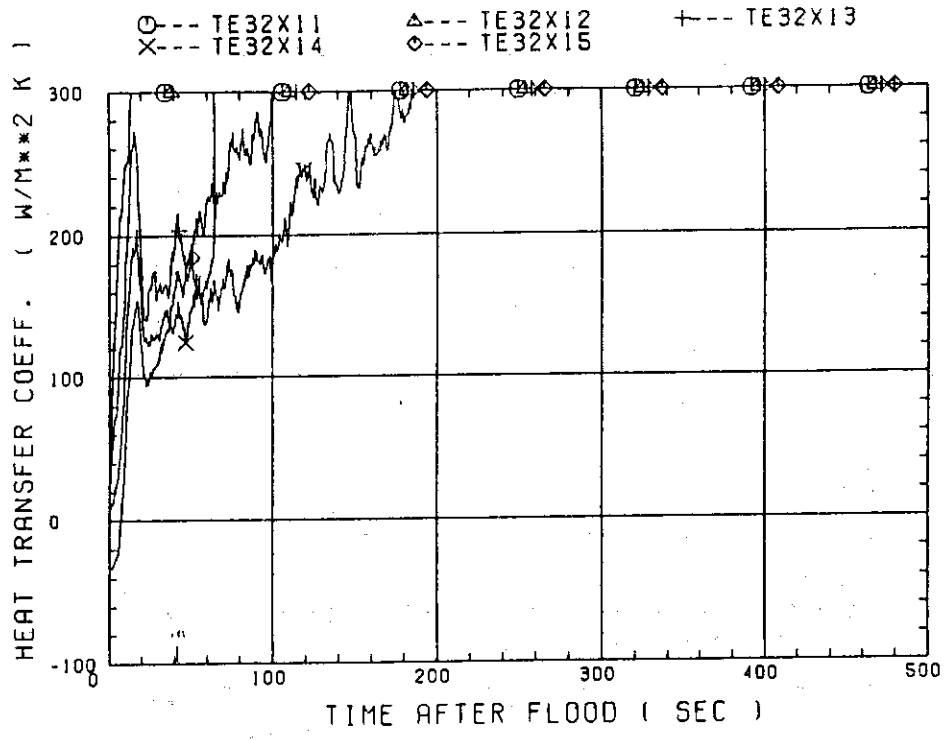

Fig. B-5 Heat transfer coefficient at midplane of high power rod (X-rod) in high power region (A region) (peak power rod)

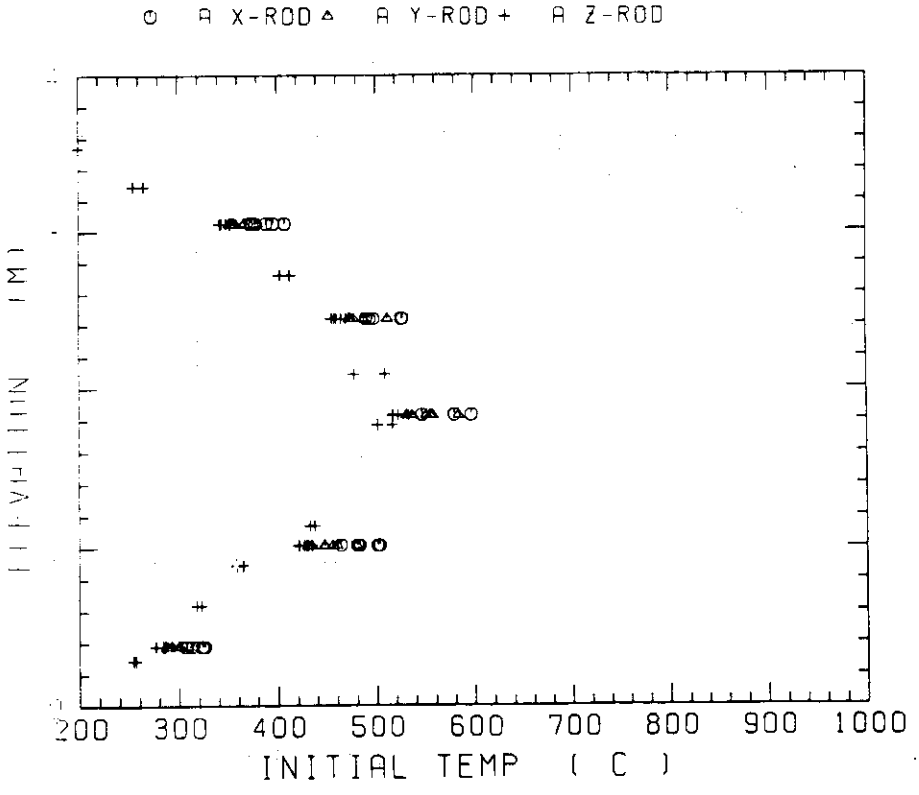

Fig. B-6 Initial rod surface temperature in high power region (A region)

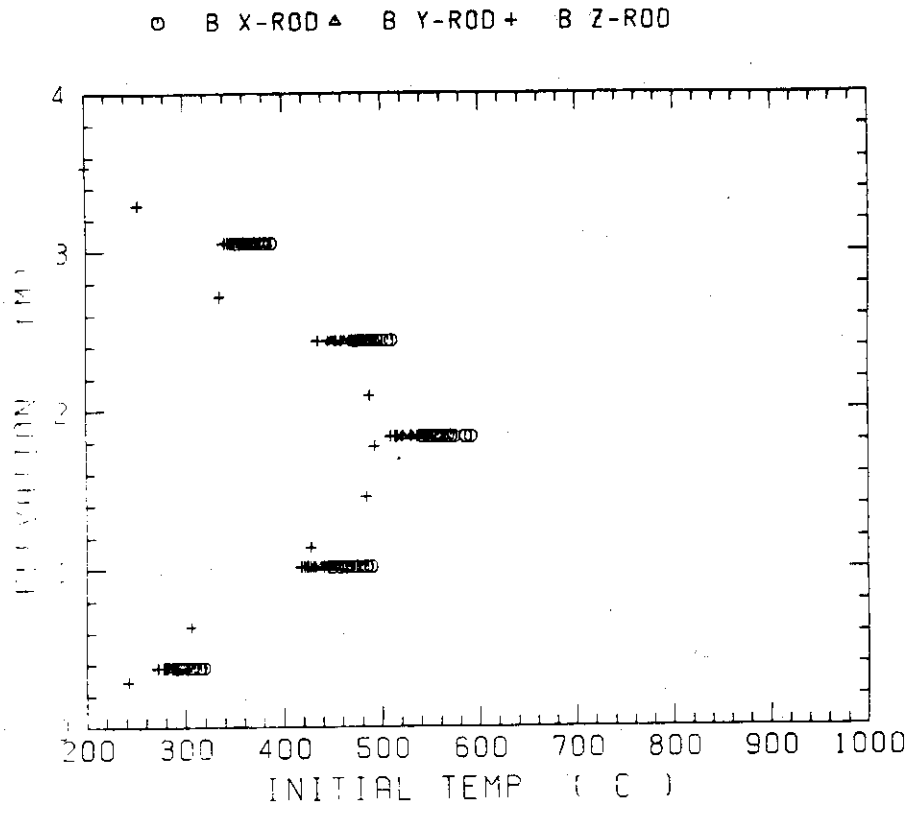

Fig. B-7 Initial rod surface temperature in medium power region (B region)

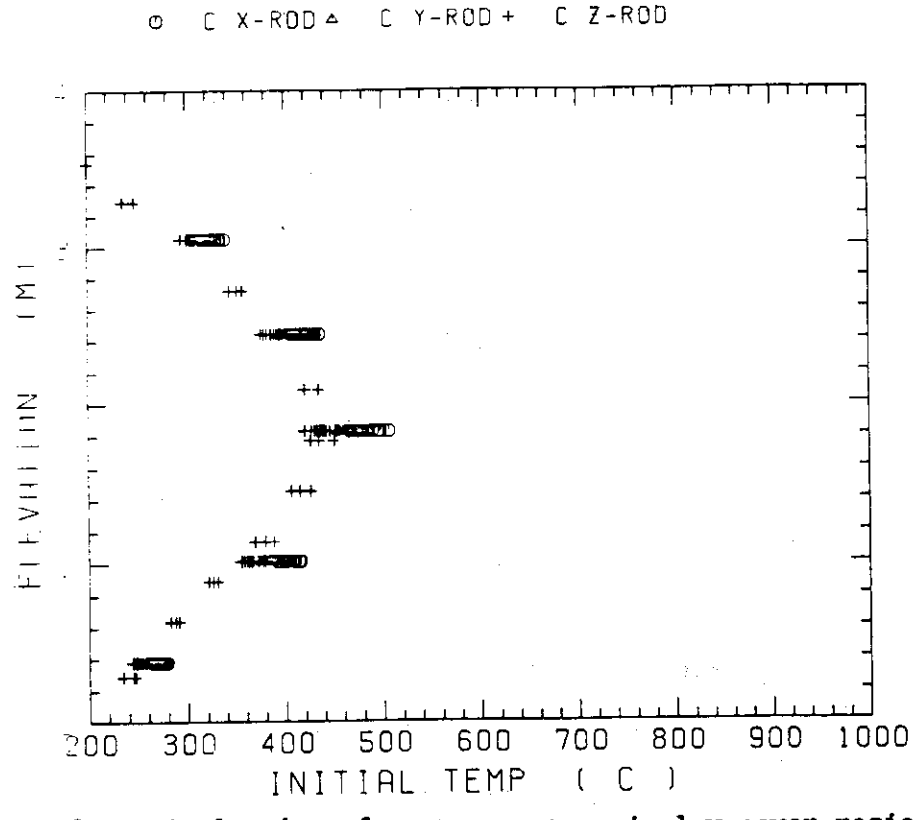

Fig. B-8 Inital rod surface temperature in low power region (C region)

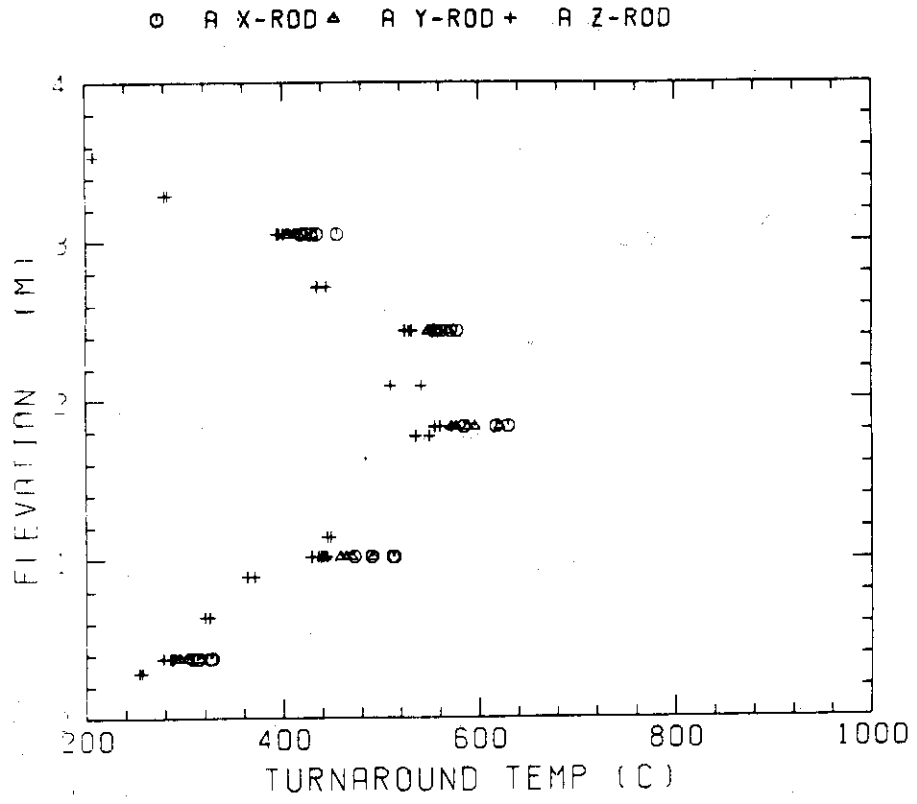

Fig. B-9 Turnaround temperature in high power region (A region)

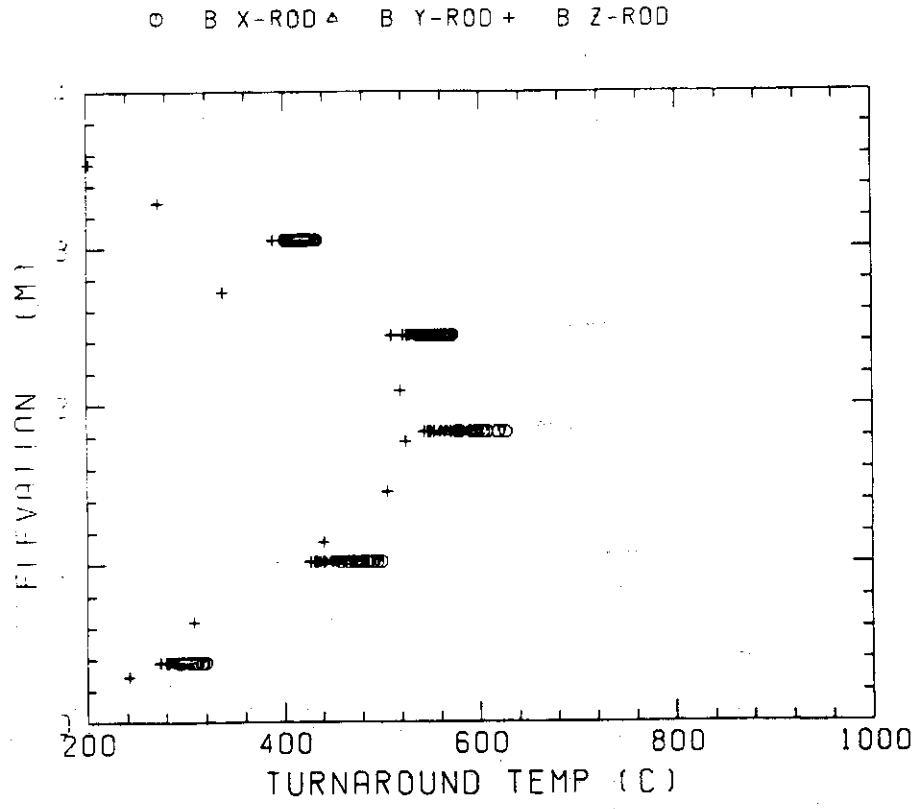

Fig. B-10 Turnaround temperature in medium power region (B region)

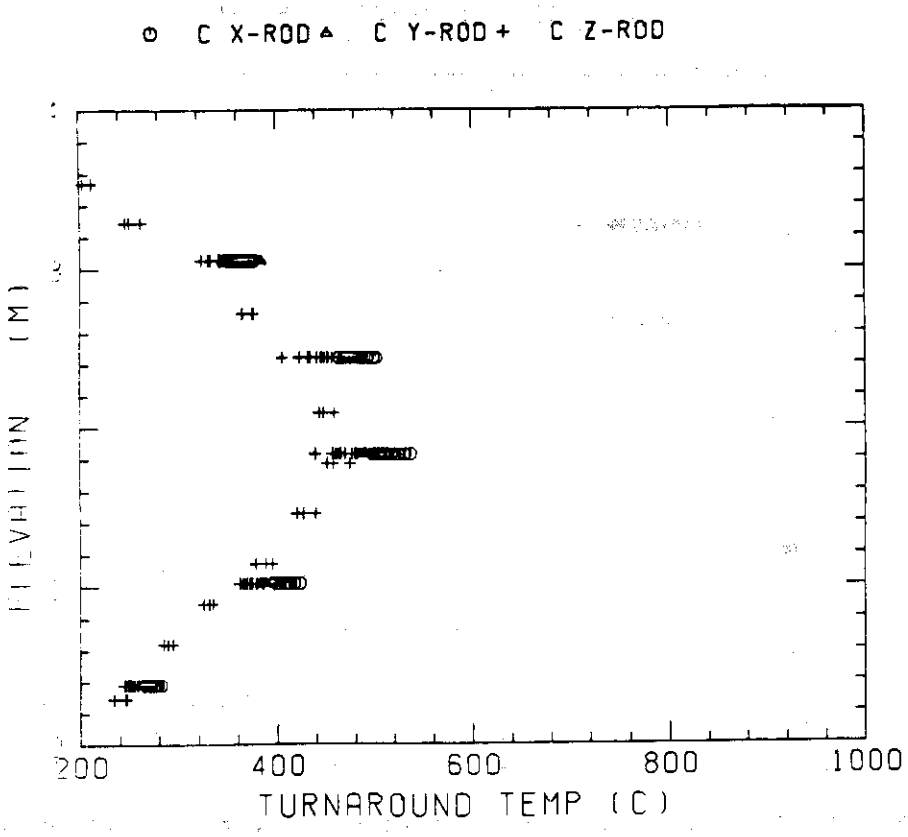

Fig. B-11 Turnaround temperature in low power region (C region)

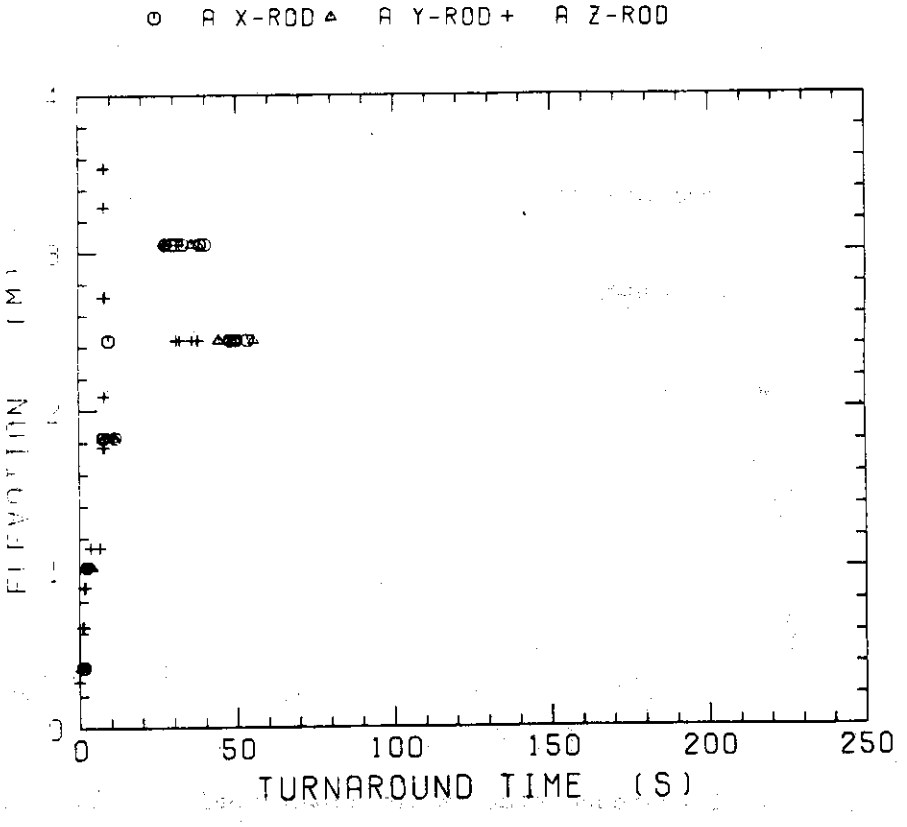

Fig. B-12 Turnaround time in high power region (A region)

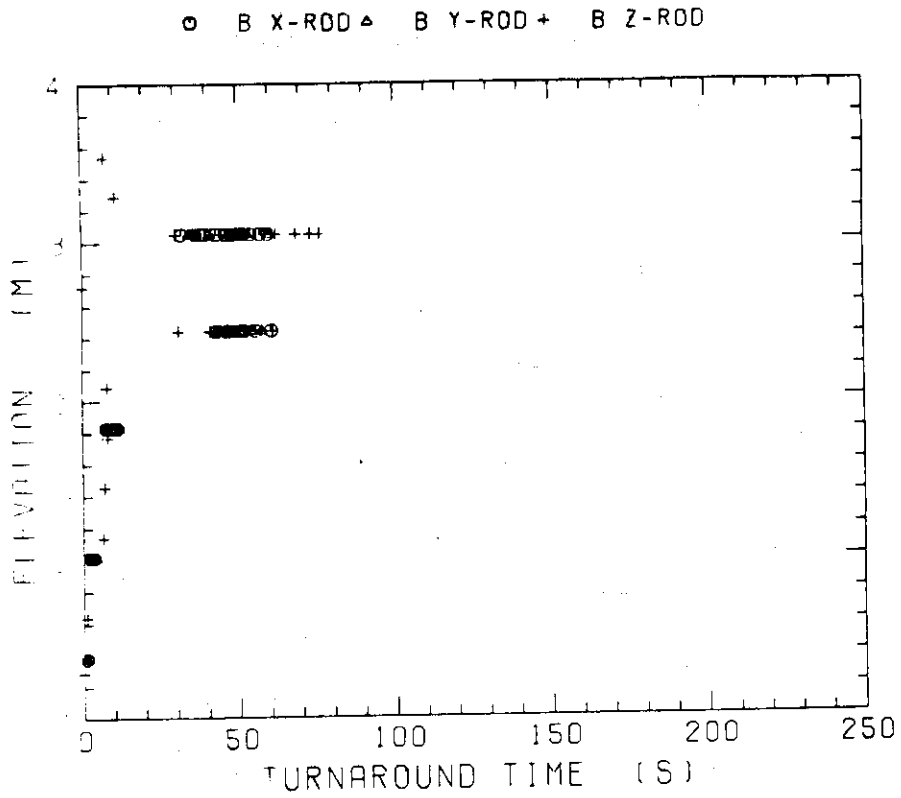

Fig. B-13 Turnaround time in medium power region (B region)

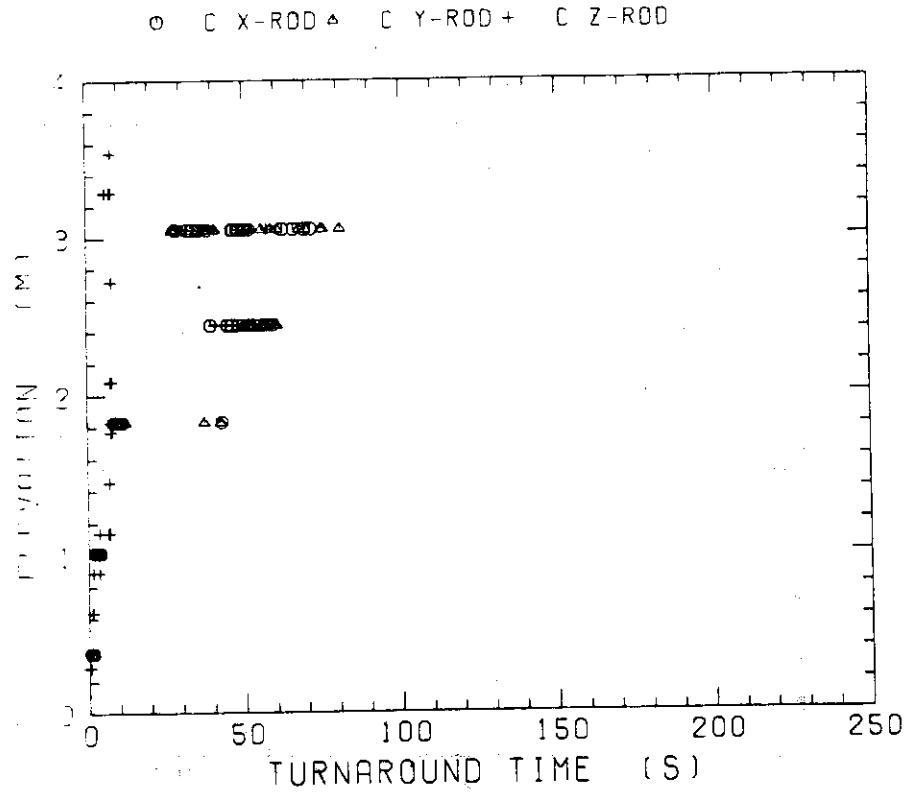

Fig. B-14 Turnaround time in low power region (C region)

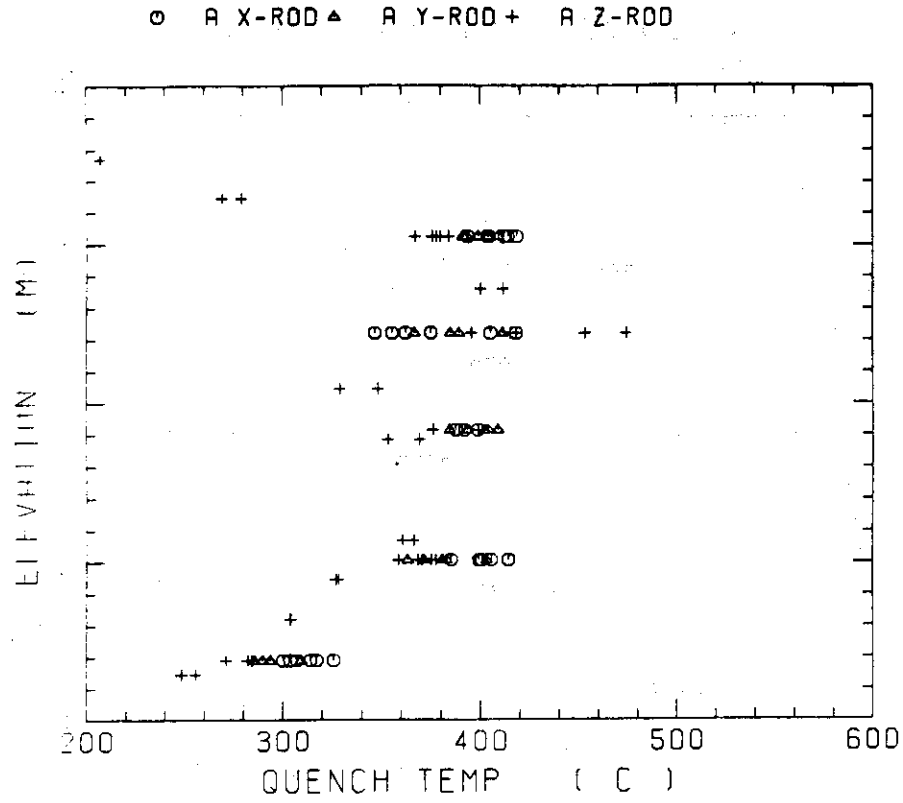

Fig. B-15 Quench temperature in high power region (A region)

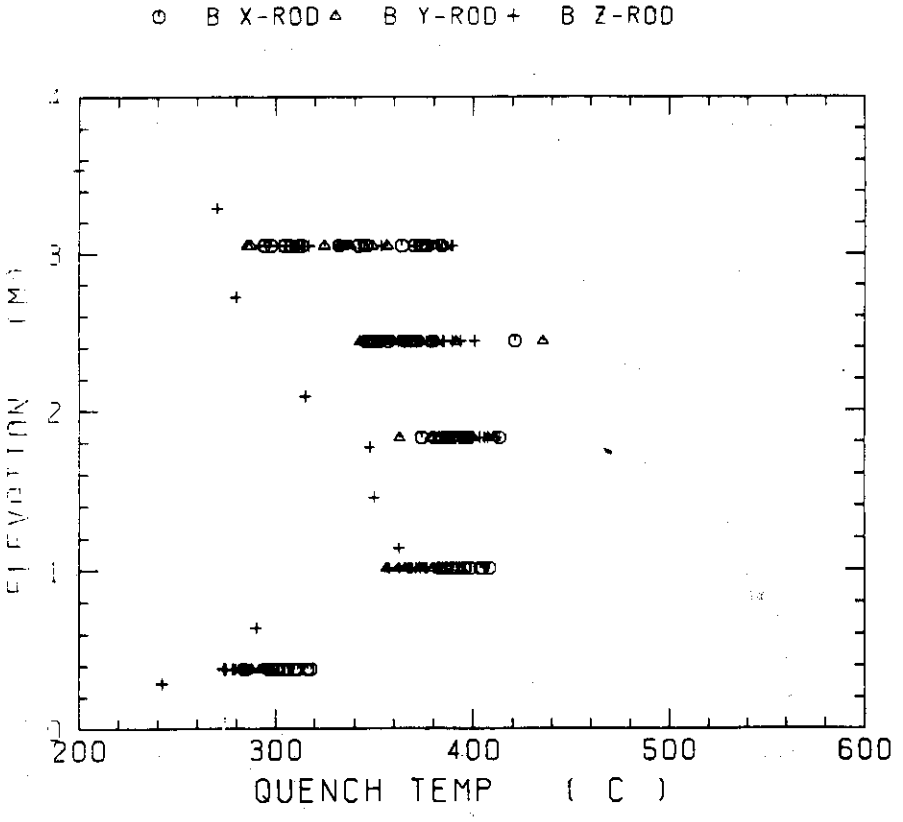

Fig. B-16 Quench temperature in medium power region (B region)

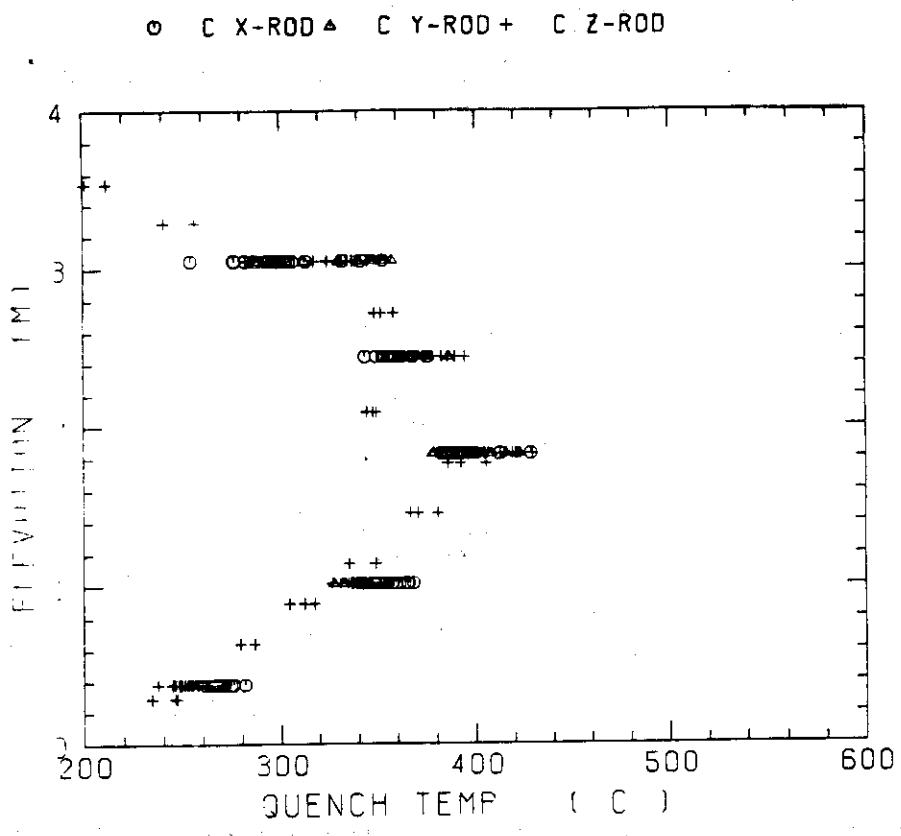

Fig. B-17 Quench temperature in low power region (C region)

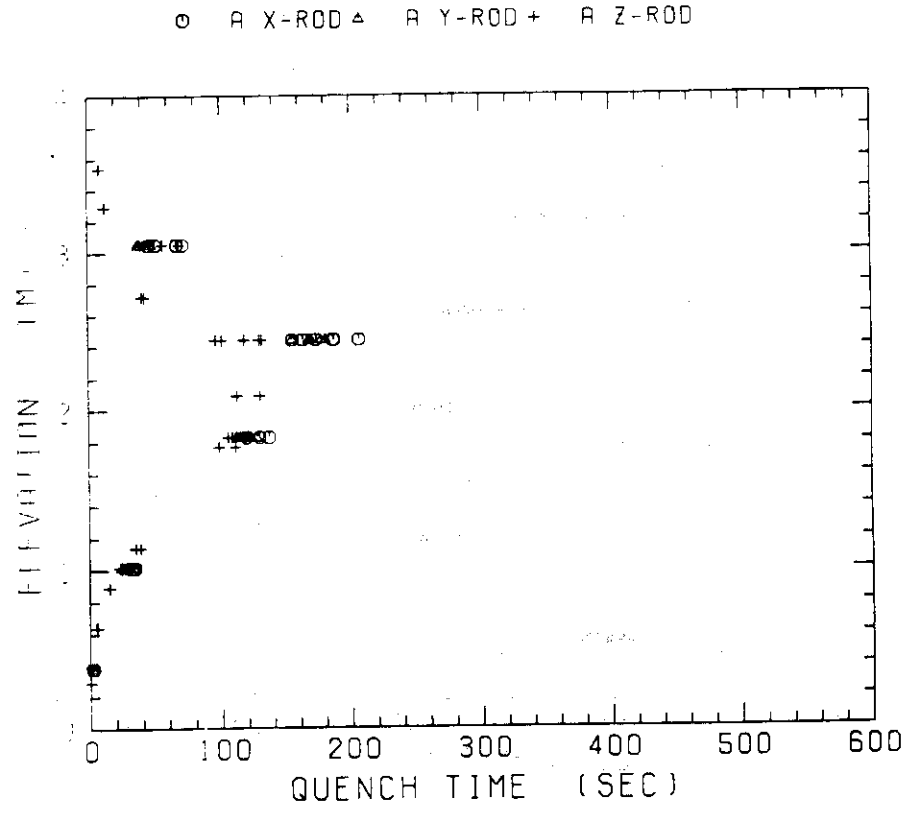

Fig. B-18 Quench time in high power region (A region)

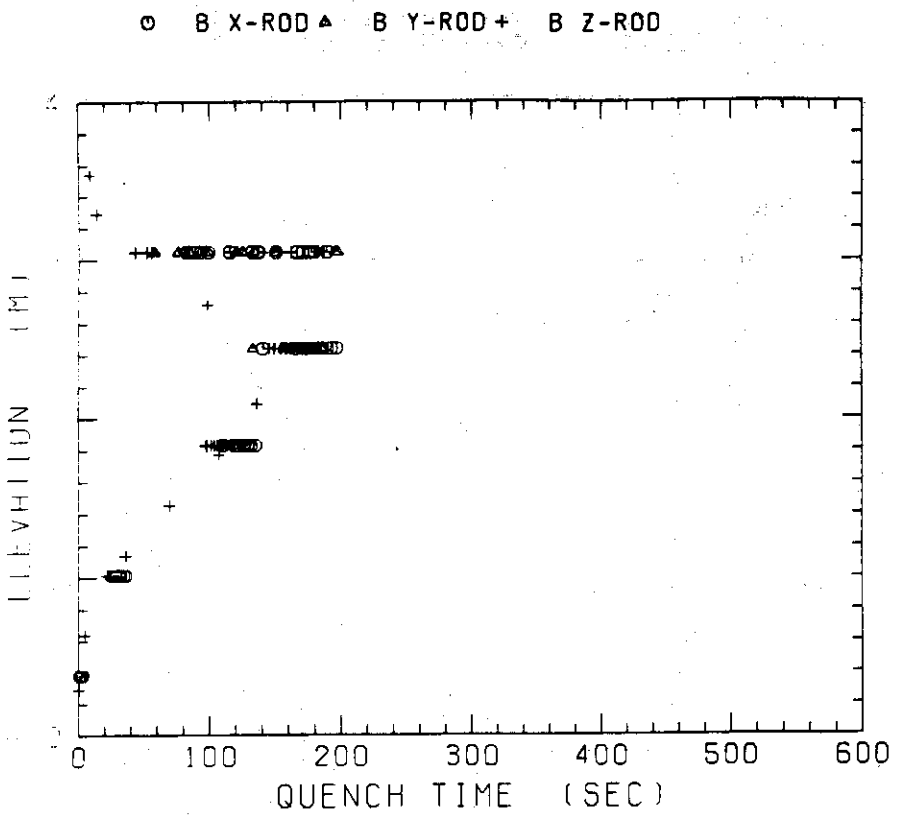

Fig. B-19 Quench time in medium power region (B region)

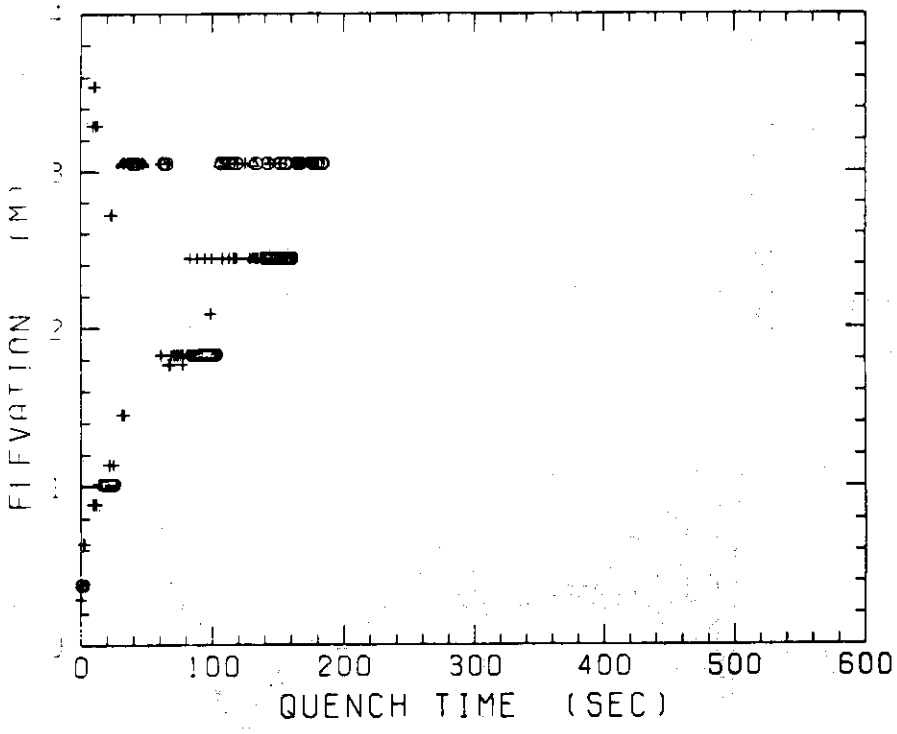

Fig. B-20 Quench time in low power region (C region)

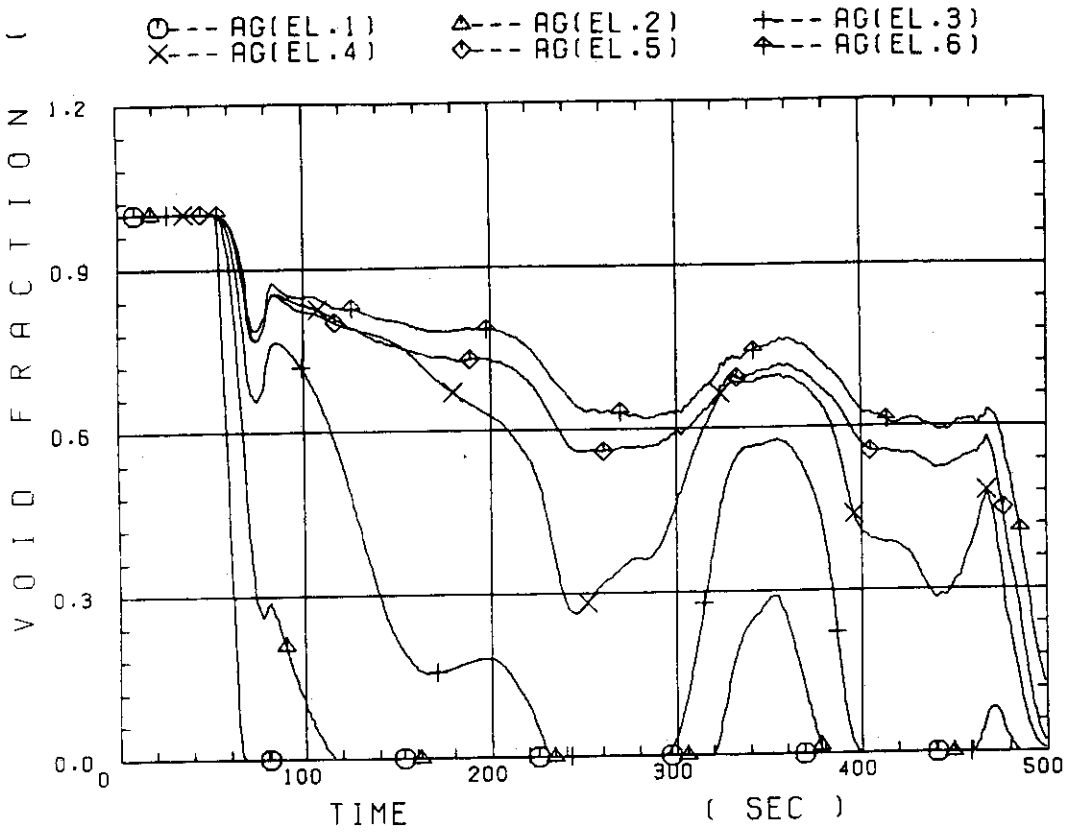

Fig. B-21 Void fraction in core

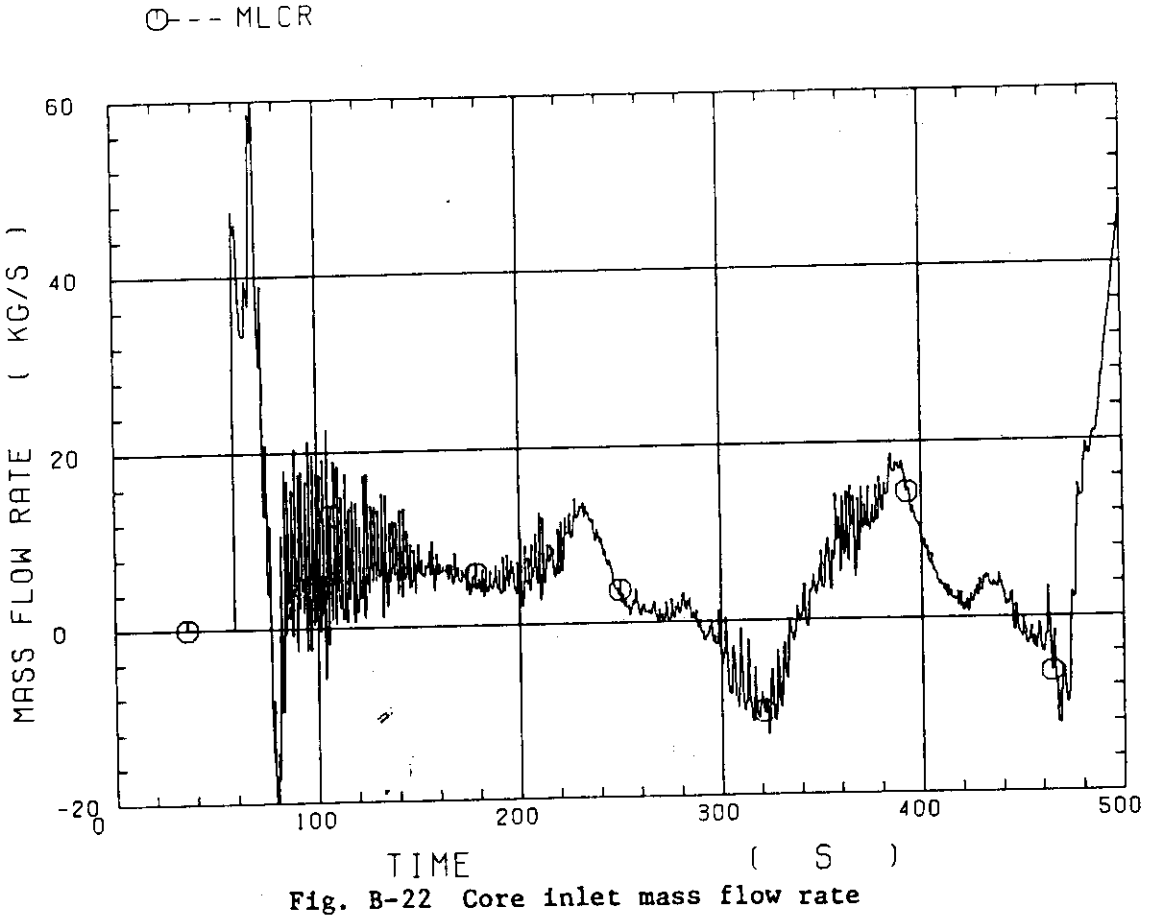

Fig. B-22 Core inlet mass flow rate

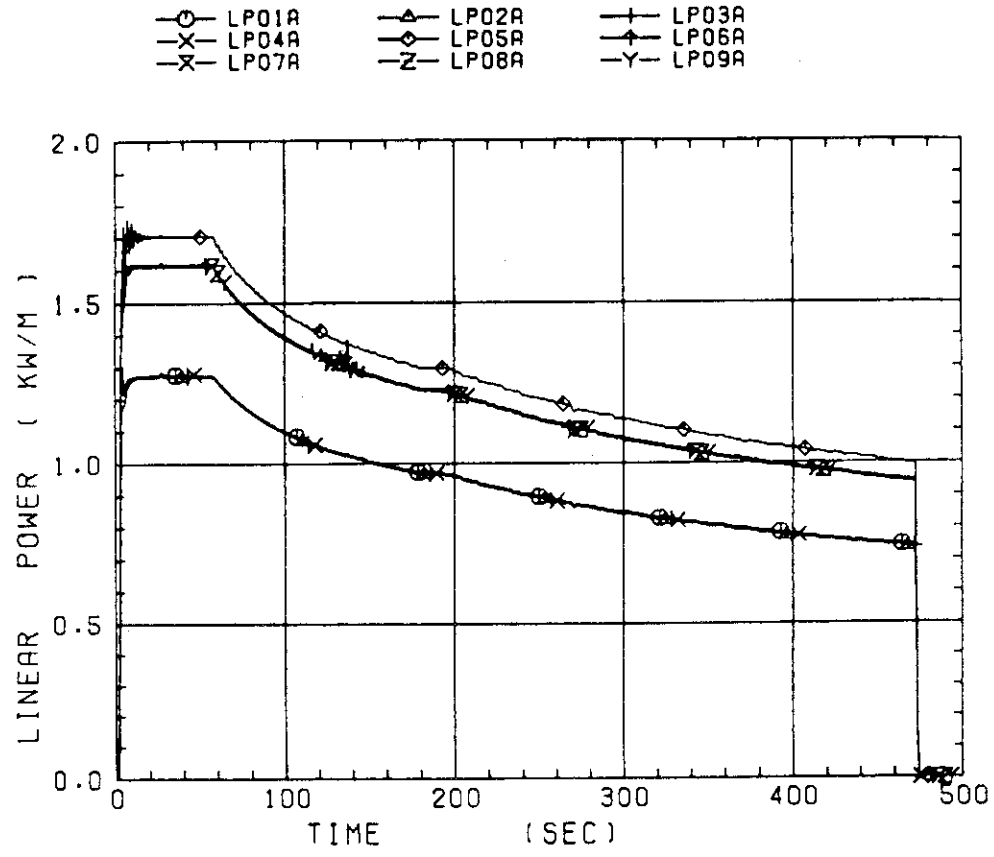

Fig. B-23 Average linear power of heater rod in each power unit zone

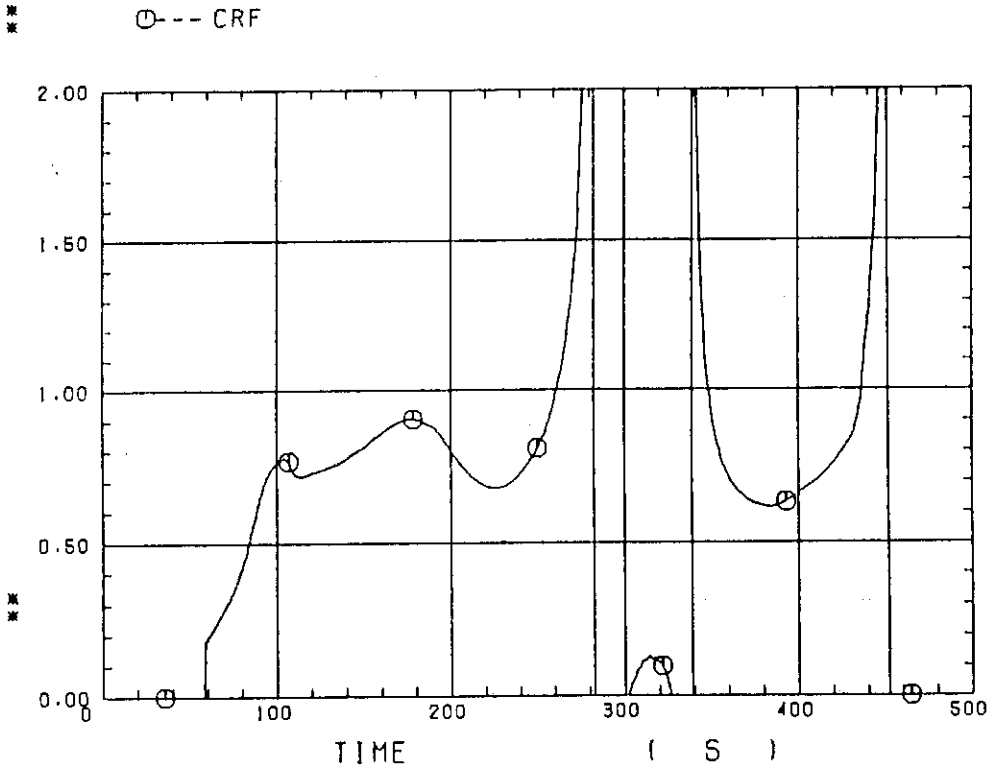

Fig. B-24 Carry-over rate fraction

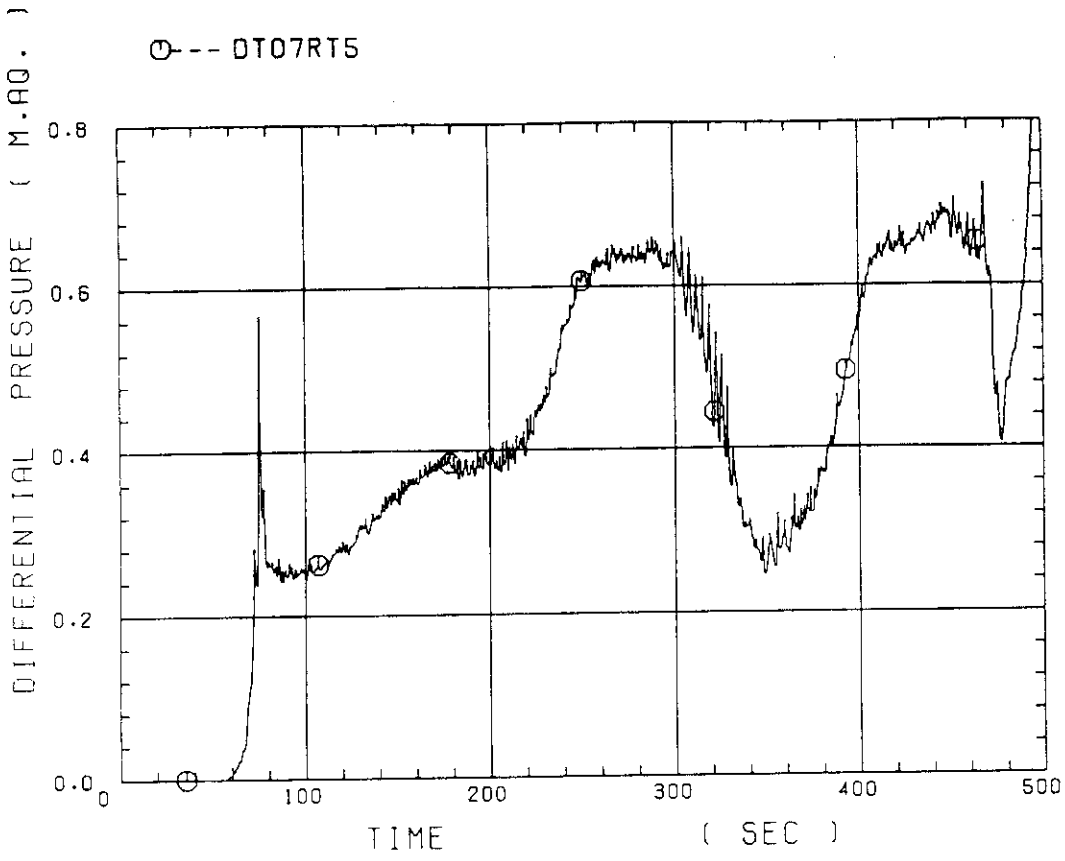

Fig. B-25 Differential pressure through upper plenum

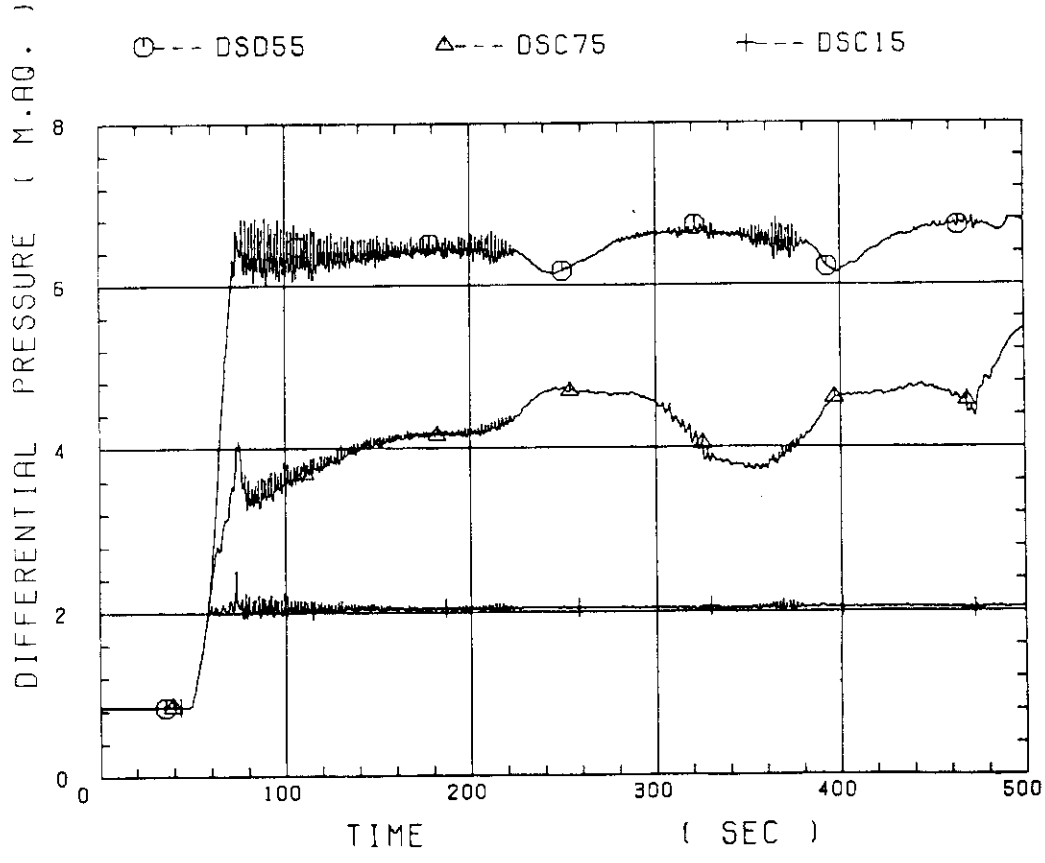

Fig. B-26 Differential pressure through downcomer, core, and lower plenum

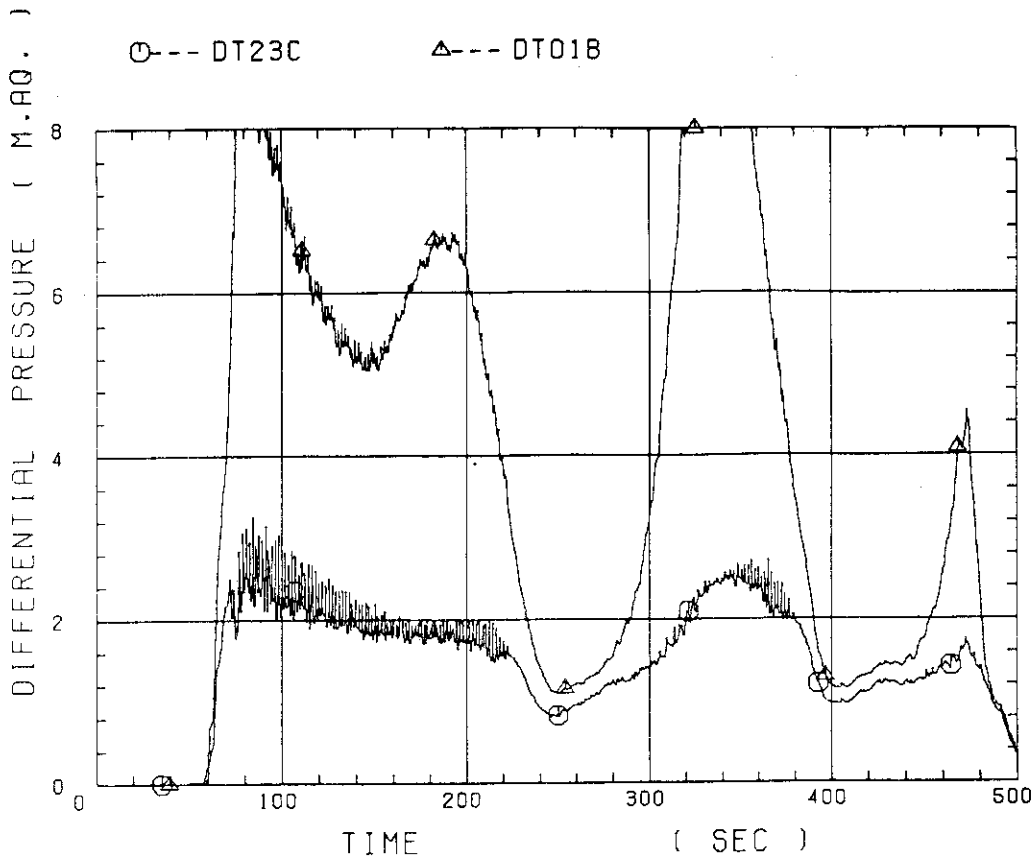

Fig. B-27 Differential pressure through intact and broken loops

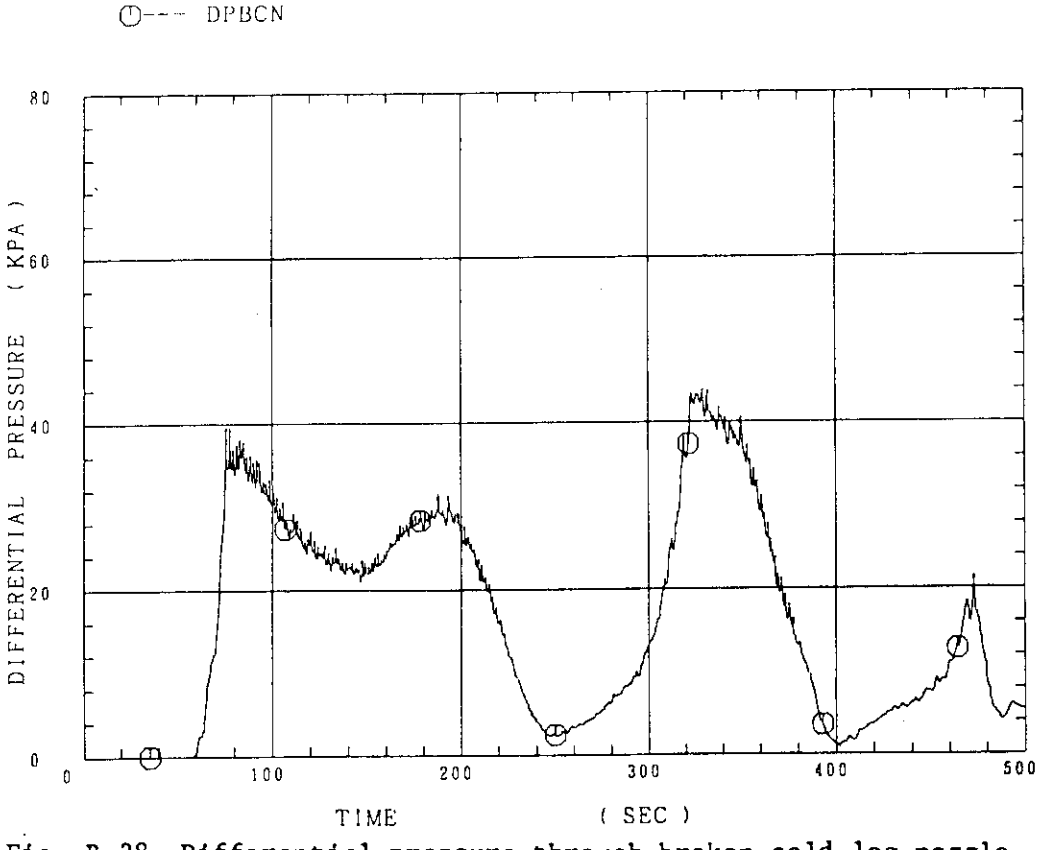

Fig. B-28 Differential pressure through broken cold leg nozzle

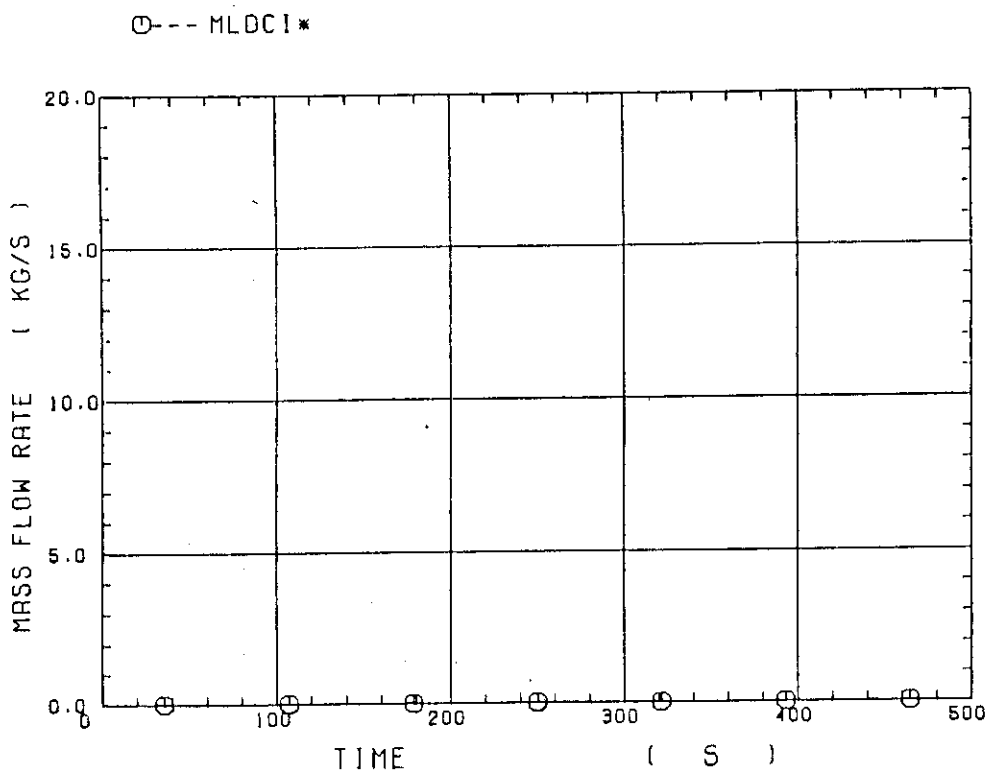

Fig. B-29 Total water mass flow rate from intact loops to downcomer

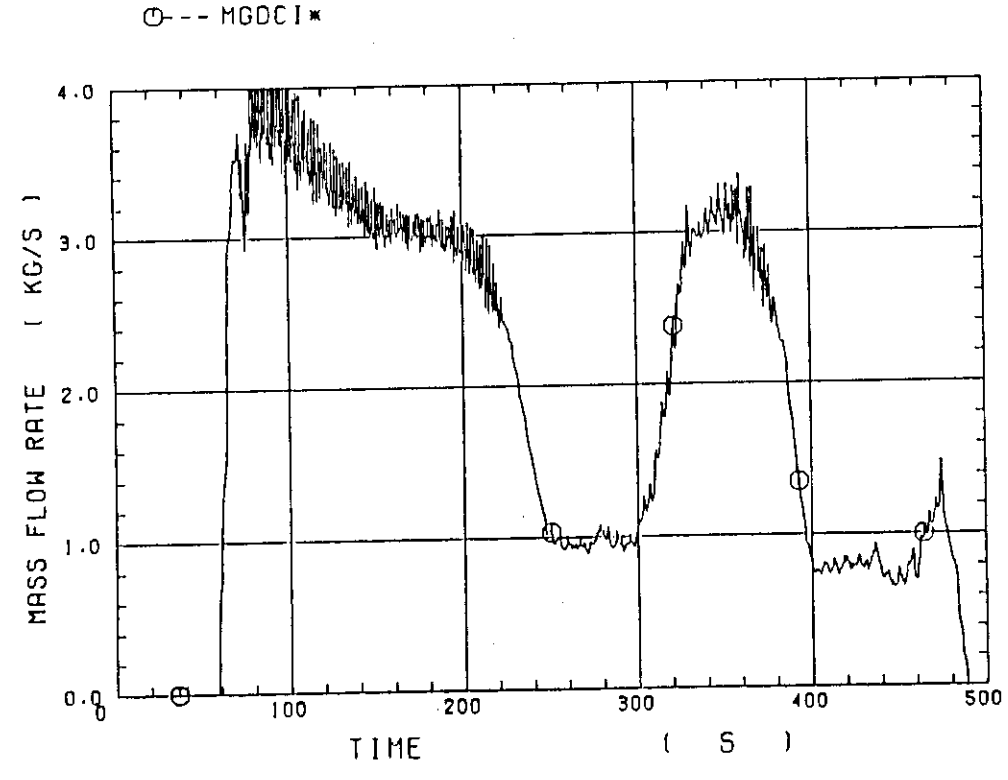

Fig. B-30 Total steam mass flow rate from intact loops to downcomer

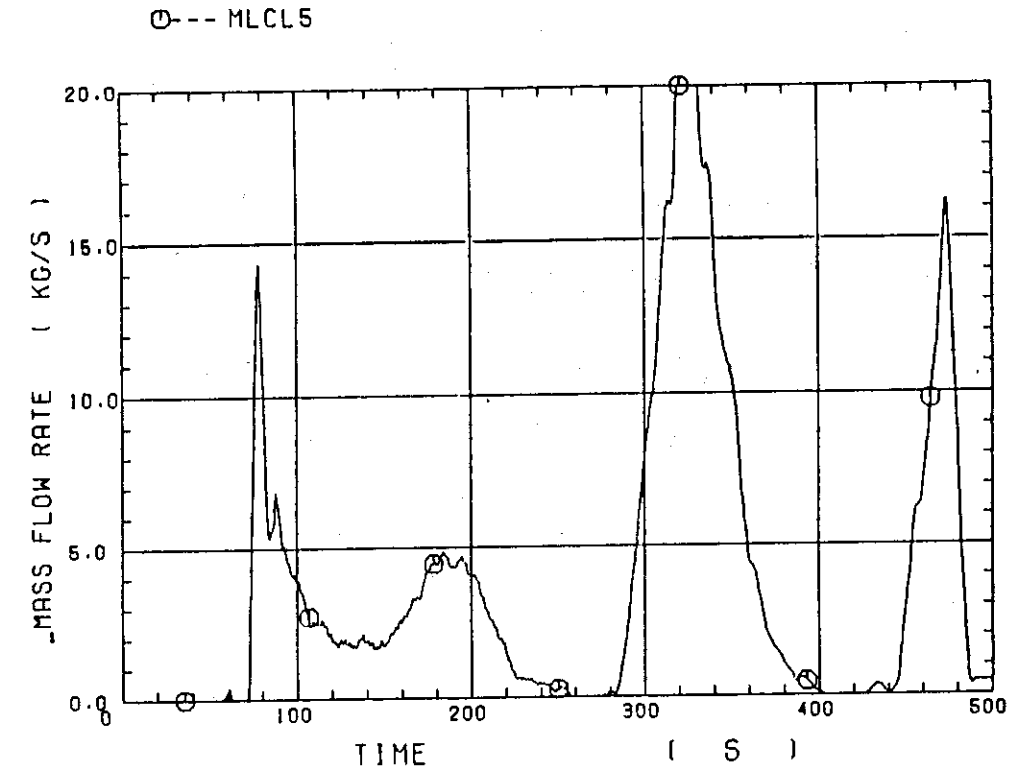

Fig. B-31 Water mass flow rate through broken cold leg nozzle

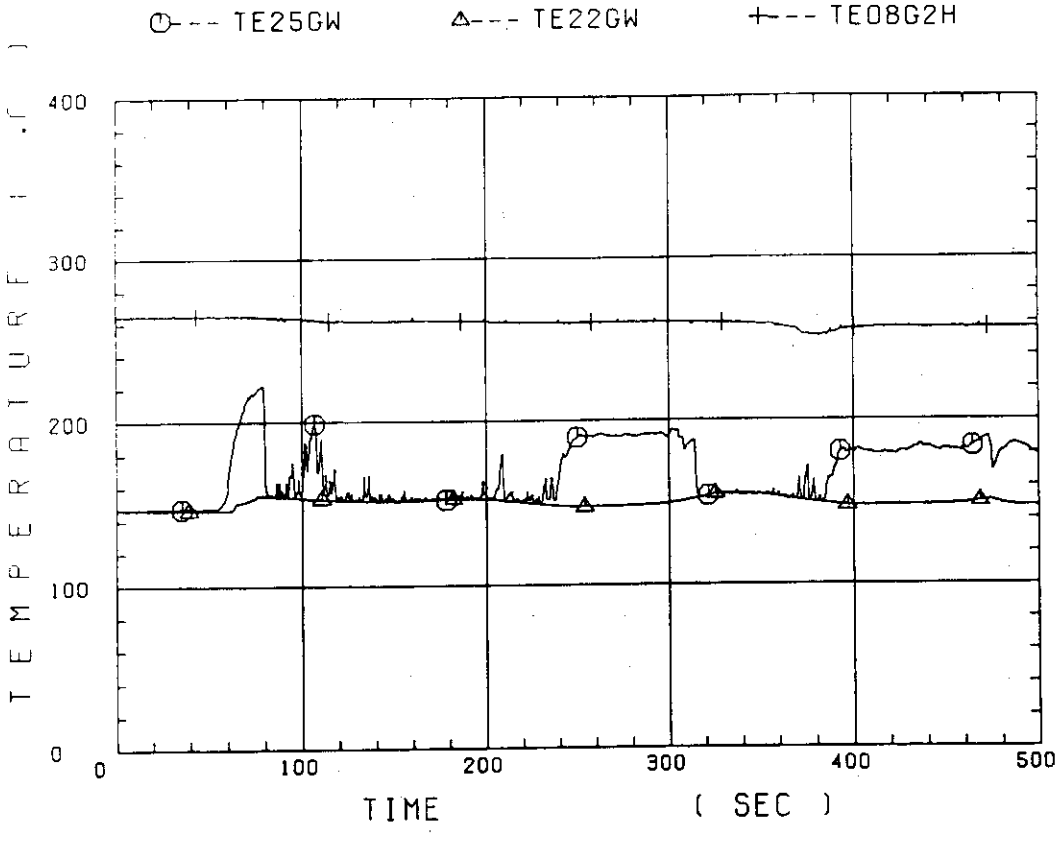

Fig. B-32 Fluid temperature in inlet plenum, outlet plenum, and secondary of steam generator 1

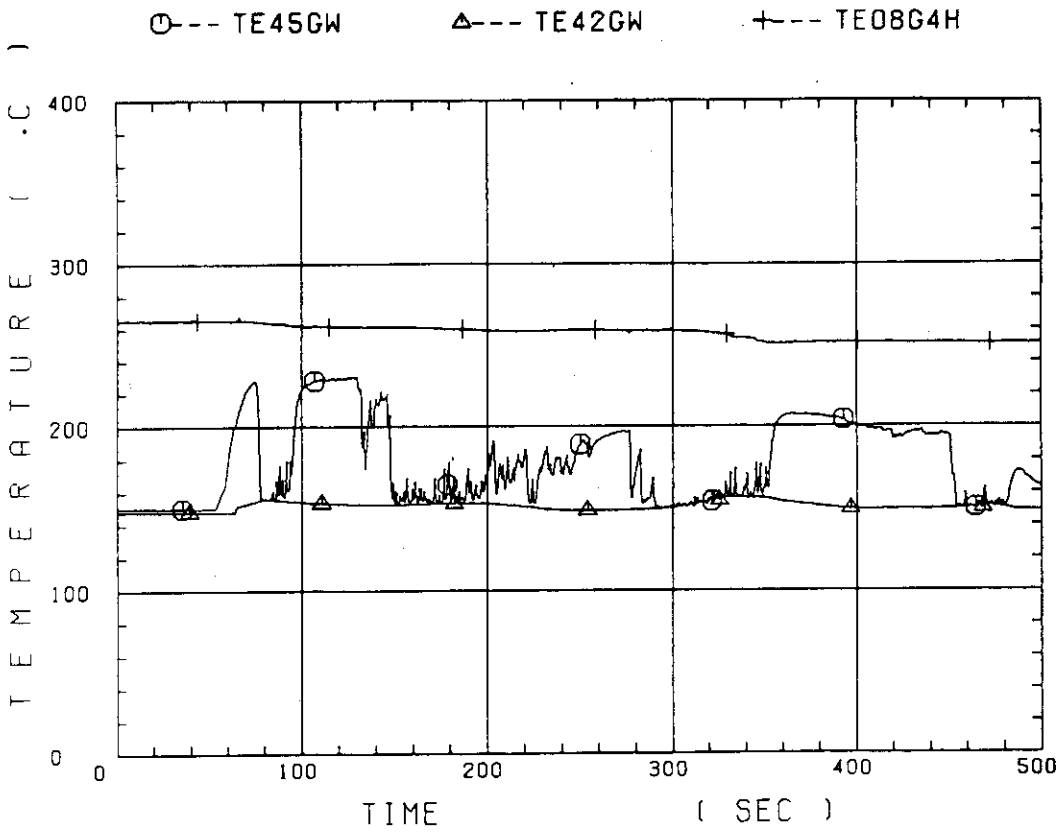

Fig. B-33 Fluid temperature in inlet plenum, outlet plenum, and secondary of steam generator 2

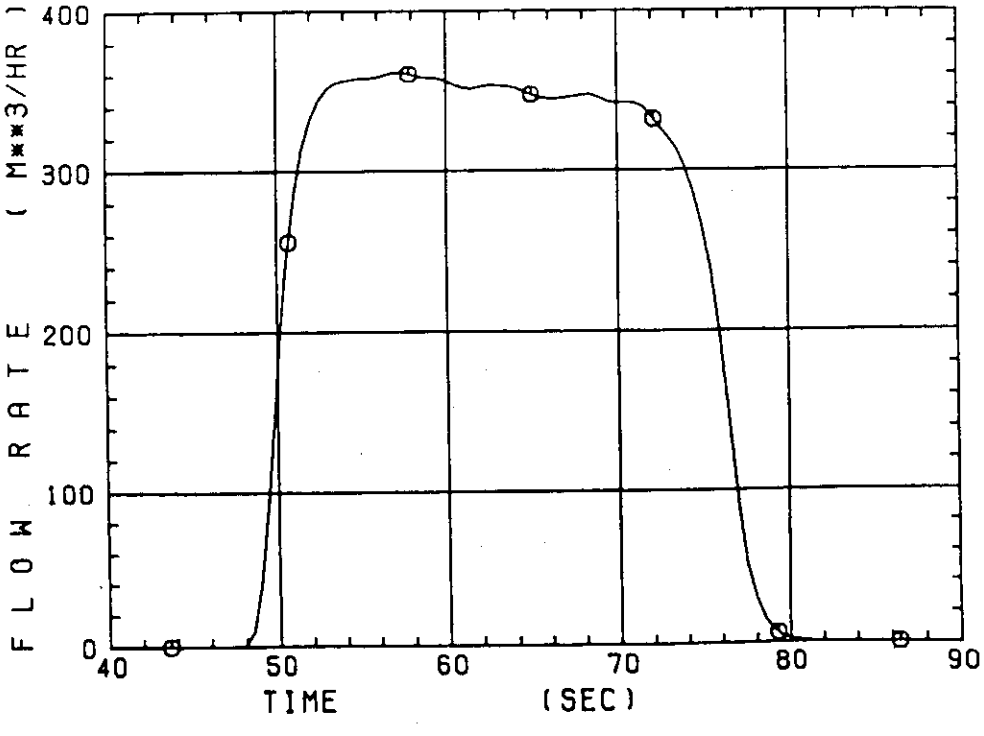

Fig. B-34 Total accumulator injection rate

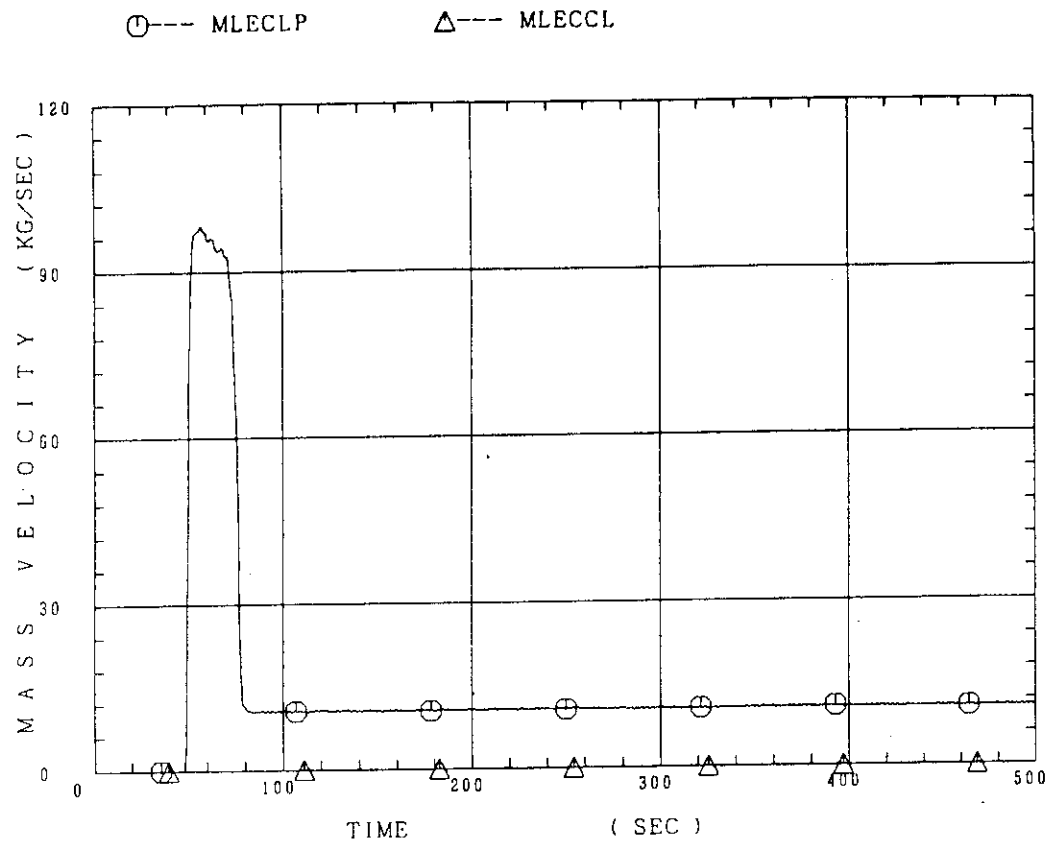

Fig. B-35 ECC water injection rates to lower plenum and to cold legs

Appendix C

Main results of test C1-21 (Run 40)

Table and Figure List

Table C-1 Summary of test conditions

Table C-2 Chronology of events

Fig. C-1 Surface temperature on low power rod (Z-rod) in medium power region (B region) (average power rod)

Fig. C-2 Surface temperature on high power rod (X-rod) in high power region (A region) (peak power rod)

Fig. C-3 Surface temperature on low power rod (Z-rod) in low power region (C region) (lowest power rod)

Fig. C-4 Heat transfer coefficient at midplane of low power rod (Z-rod) in medium power region (B region) (average power rod)

Fig. C-5 Heat transfer coefficient at midplane of high power rod (X-rod) in high power region (A region) (peak power rod)

Fig. C-6 Initial rod surface temperature in high power region (A region)

Fig. C-7 Initial rod surface temperature in medium power region (B region)

Fig. C-8 Initial rod surface temperature in low power region (C region)

Fig. C-9 Turnaround temperature in high power region (A region)

Fig. C-10 Turnaround temperature in medium power region (B region)

Fig. C-11 Turnaround temperature in low power region (C region)

Fig. C-12 Turnaround time in high power region (A region)

Fig. C-13 Turnaround time in medium power region (B region)

Fig. C-14 Turnaround time in low power region (C region)

Fig. C-15 Quench temperature in high power region (A region)

Fig. C-16 Quench temperature in medium power region (B region)

Fig. C-17 Quench temperature in low power region (C region)

Fig. C-18 Quench time in high power region (A region)

Fig. C-19 Quench time in medium power region (B region)

Fig. C-20 Quench time in low power region (C region)

Fig. C-21 Void fraction in core

Fig. C-22 Core inlet mass flow rate

Fig. C-23 Average linear power of heater rod in each power unit zone

Fig. C-24 Carry-over rate fraction

Fig. C-25 Differential pressure through upper plenum
Fig. C-26 Differential pressure through downcomer, core, and lower plenum
Fig. C-27 Differential pressure through intact and broken loops
Fig. C-28 Differential pressure through broken cold leg nozzle
Fig. C-29 Total water mass flow rate from intact loops to downcomer
Fig. C-30 Total steam mass flow rate from intact loops to downcomer
Fig. C-31 Water mass flow rate through broken cold leg nozzle
Fig. C-32 Fluid temperature in inlet plenum, outlet plenum, and secondary of steam generator 1
Fig. C-33 Fluid temperature in inlet plenum, outlet plenum, and secondary of steam generator 2
Fig. C-34 Total accumulator injection rate
Fig. C-35 ECC water injection rates to lower plenum and to cold legs

Table C-1 Summary of test conditions

1. TEST TYPE : FLECHT-SET 27148 COUPLING TEST

2. TEST NUMBER : RUN 040 , C1-21 3. DATE : April 2, 1981

4. POWER : A: TOTAL: 992 MW; B:LINEAR: 1.5 KW/M

5. RELATIVE RADIAL POWER SHAPE :

   A: ZONE: A B C

   B: RATIO: 1.16 1.0 0.79

6. AXIAL POWER SHAPE : CHOPPED COSINE

7. PRESSURE (KG/CM^2A) :

   A: SYSTEM: 1.52 , B: CONTAINMENT 1.52 ,

   C: STEAM GENERATOR SECONDARY: 53

8. TEMPERATURE (DEG.C) :

   A: DOWNCOMER WALL 102 , B: VESSEL INTERNALS 102 ,

   C: PRIMARY PIPING WALL 110 , D: LOWER PELNUM LIQUID 102 ,

   E: ECC LIQUID 67 , F: STEAM GENERATOR SECONDARY 264 ,

   G: CORE TEMPERATURE AT ECC INITIATION 523

9. ECC INJECTION TYPE: B

   A: COLD LEG, B: LOWER PLENUM, C: LOWER PLENUM + COLD LEG

10. PUMP K-FACTOR : ~15

11. ECC FLOW RATES AND DURATION :

    A: ACCUMULATOR 361 M^3/HR FROM 0 TO 24.5 SECONDS

    B: LPCI 39.9 M^3/HR FROM 245 TO 660.5 SECONDS

    C: ECC INJECTION TO LOWER PLENUM : FROM 0 TO 660.5 SECONDS

    (VALVE OPENING AND CLOSING TIMES ARE INCLUDED IN THE INJECTION DURATION)

12. INITIAL WATER LEVEL IN LOWER PLENUM : 0.89 M.

13. POWER CONTROL : ANS x 1.2 + ACTINIDE (30 SEC AFTER SCRAM)

14. EXPECTED BOCREC TIME FROM ECC INITIATION 9 SEC

15. EXPECTED PEAK TEMPERATURE AT BOCREC 600 C

TABLE C-2 CHRONOLOGY OF EVENTS FOR TEST C1-21 (RUN 040)

EVENT	TIME (sec)
Test Initiated (Heater Rods Power on) (Data Recording Initiated)	0
Accumulator Injection Initiated	50.5
Power Decay Initiated (Bottom of Core Recovery)	59.5
Accumulator Injection Switched from Lower Plenum to Cold Leg	———
Accumulator Injection Ended and LPCI Injection Initiated	75
All Heater Rods Quenched	540
Power Off	620
LPCI Injection Ended	711
Test Ended (Data Recording Ended)	930

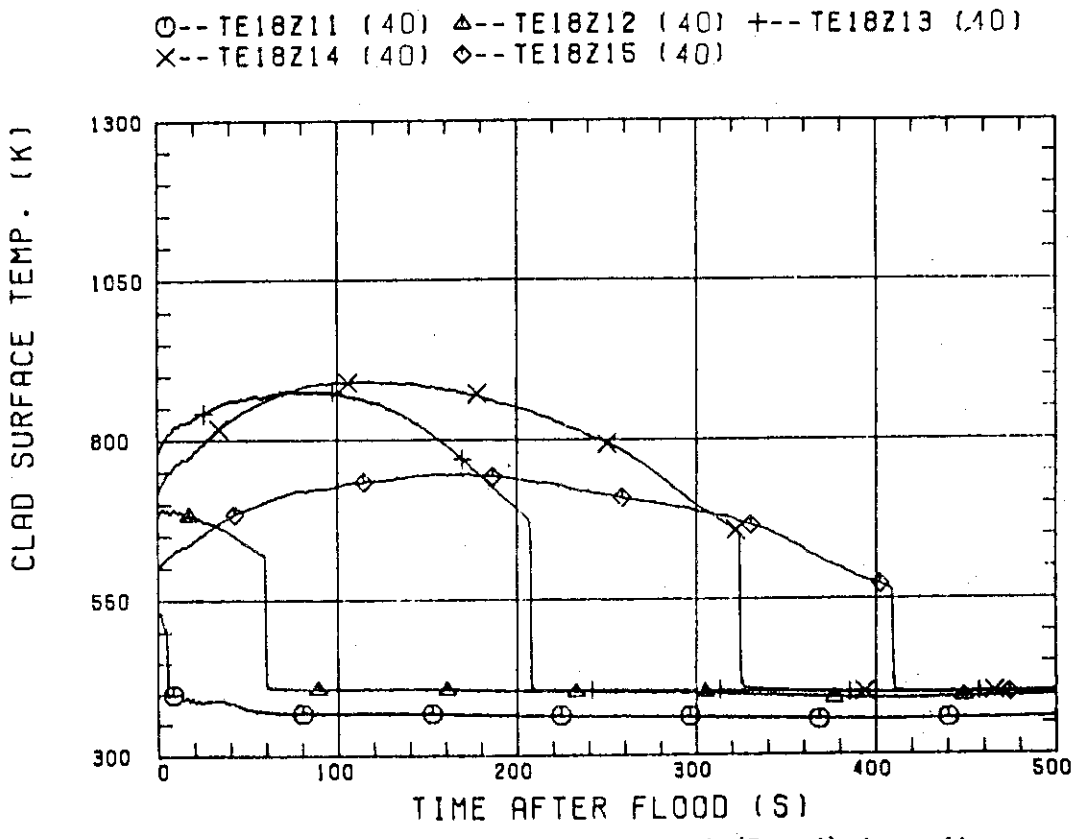

Fig. C-1 Surface temperature on low power rod (Z-rod) in medium power region (B region) (average power rod)

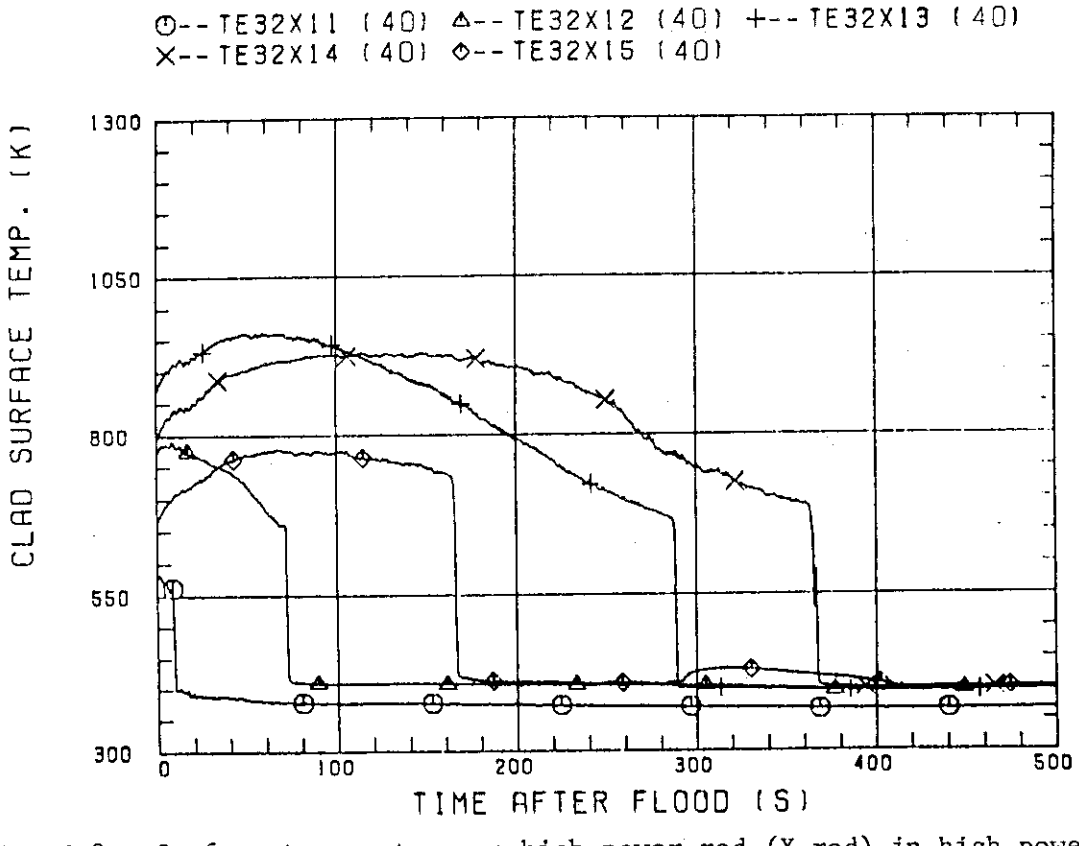

Fig. C-2 Surface temperature on high power rod (X-rod) in high power region (A region) (peak power rod)

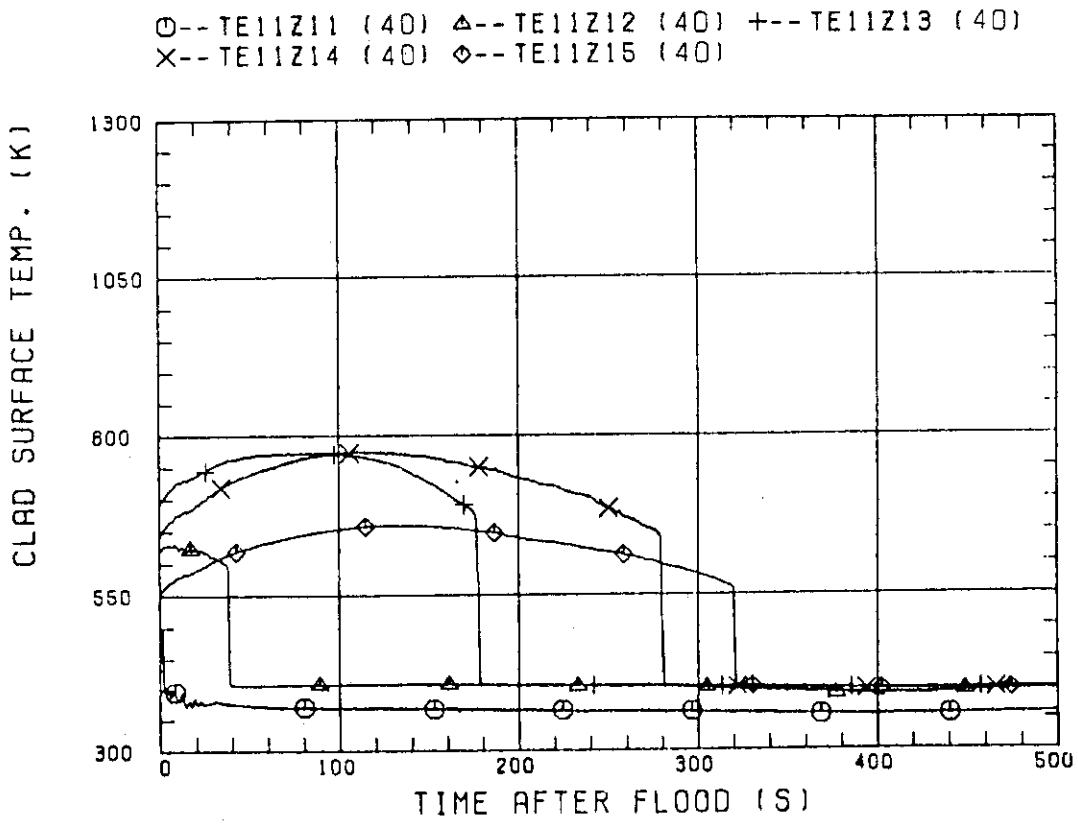

Fig. C-3 Surface temperature on low power rod (Z-rod) in low power region (C region) (lowest power rod)

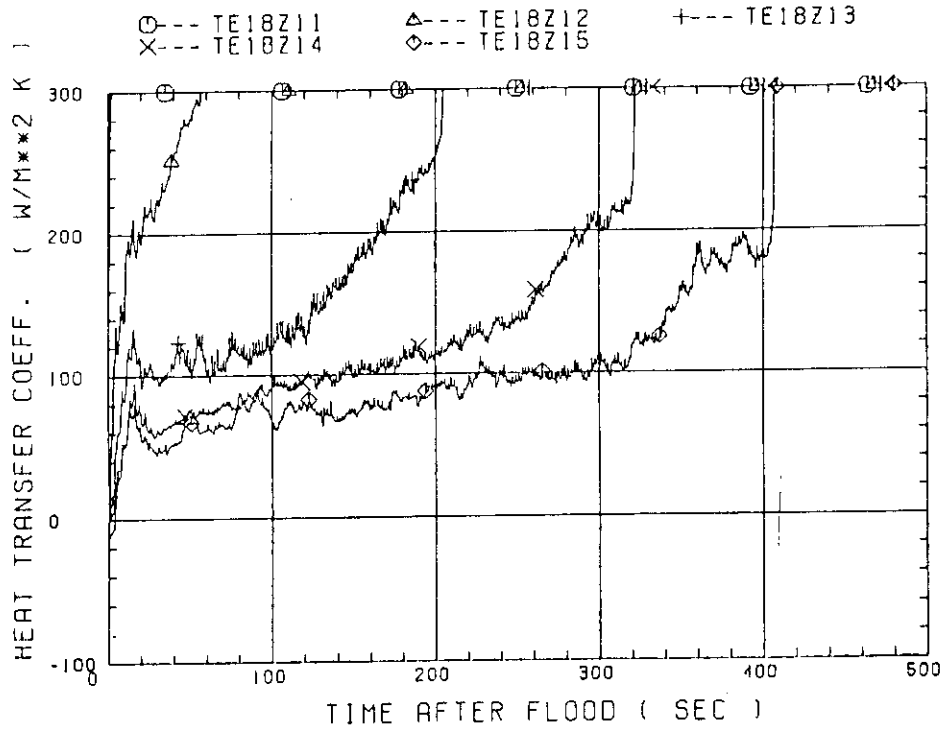

Fig. C-4 Heat transfer coefficient at midplane of low power rod (Z-rod) in medium power region (B region) (average power rod)

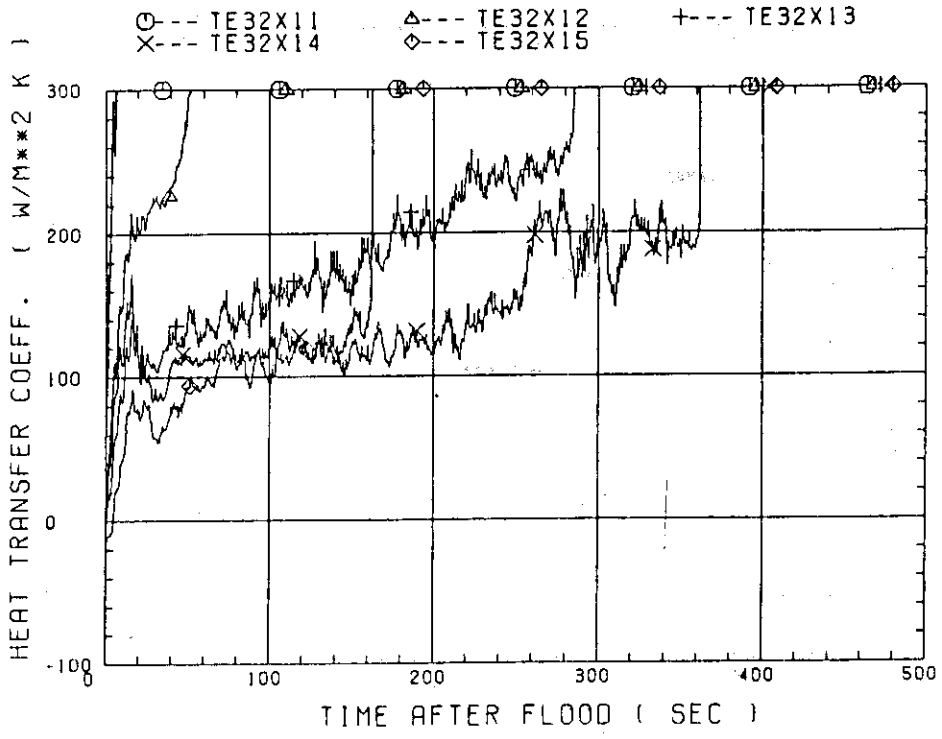

Fig. C-5 Heat transfer coefficient at midplane of high power rod (X-rod) in high power region (A region) (peak power rod)

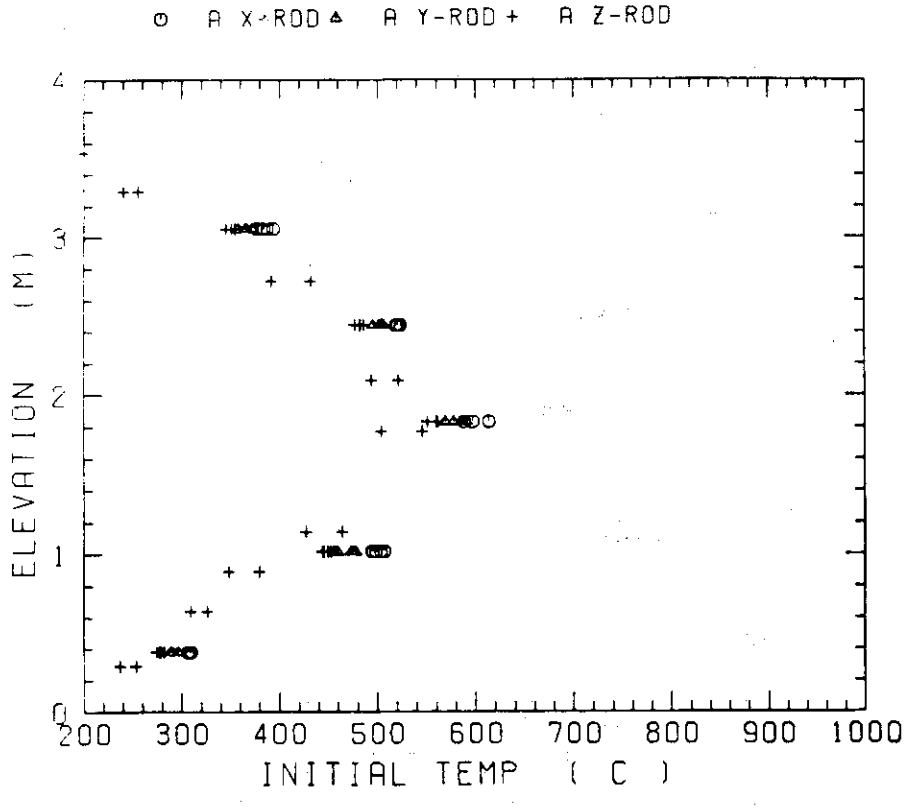

Fig. C-6 Initial rod surface temperature in high power region (A region)

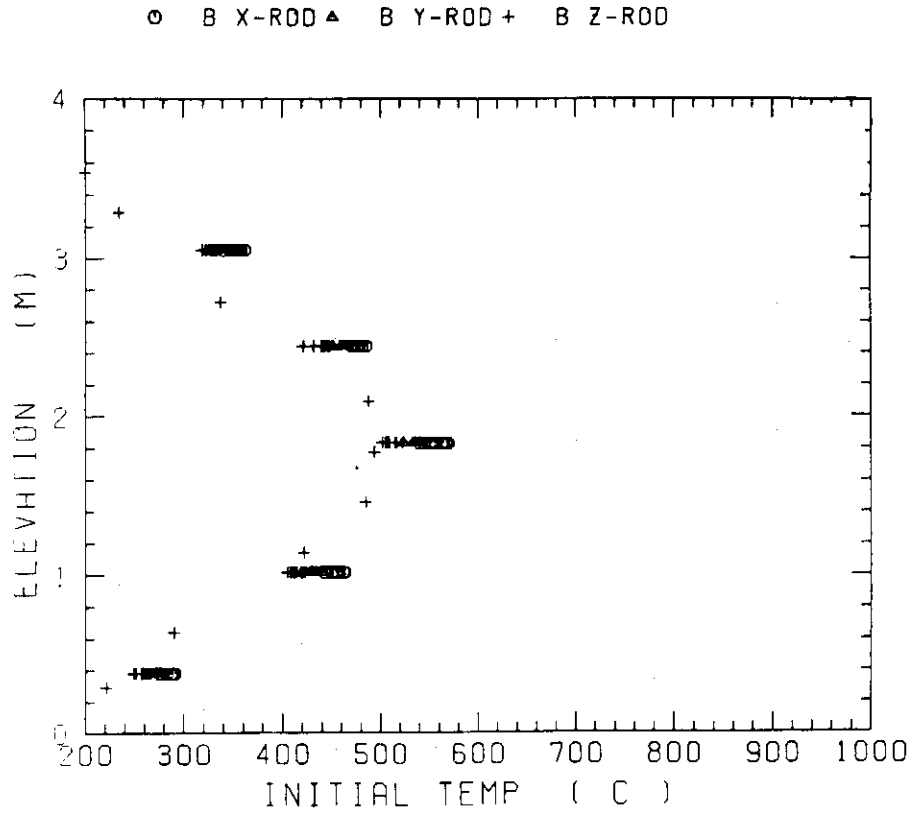

Fig. C-7 Initial rod surface temperature in medium power region (B region)

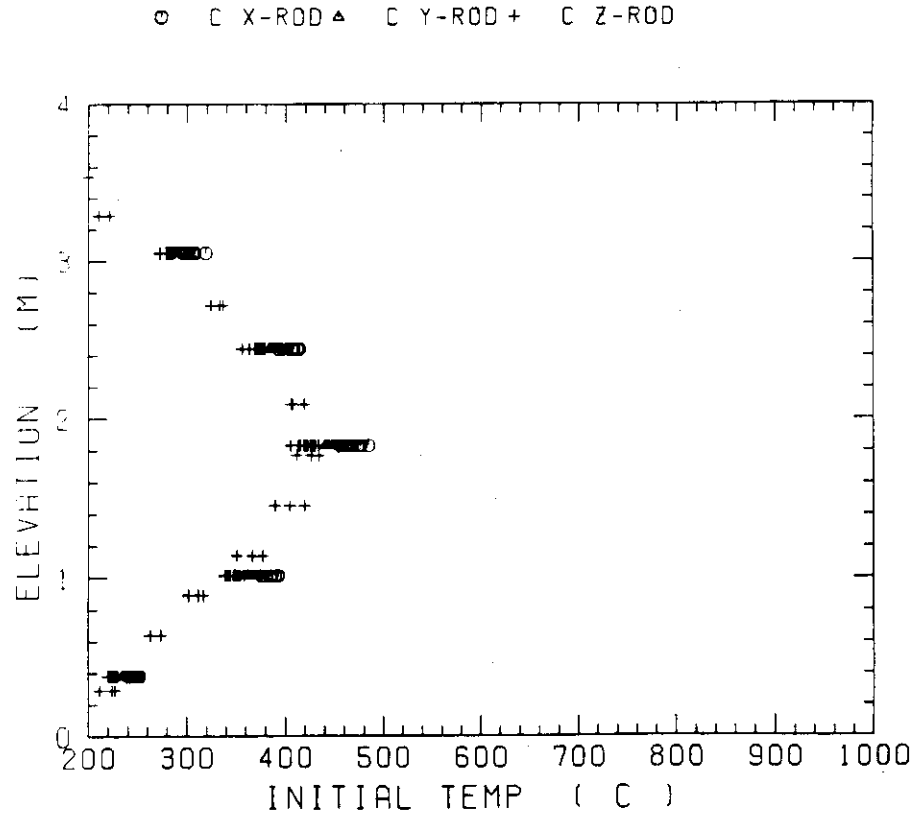

Fig. C-8 Initial rod surface temperature in low power region (C region)

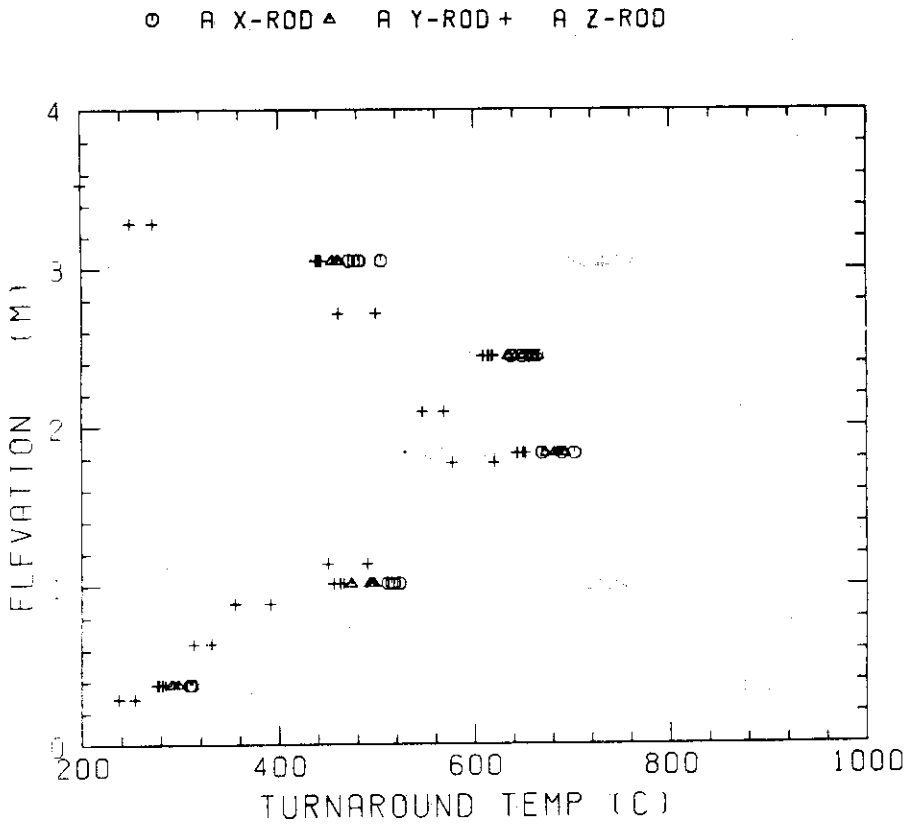

Fig. C-9 Turnaround temperature in high power region (A region)

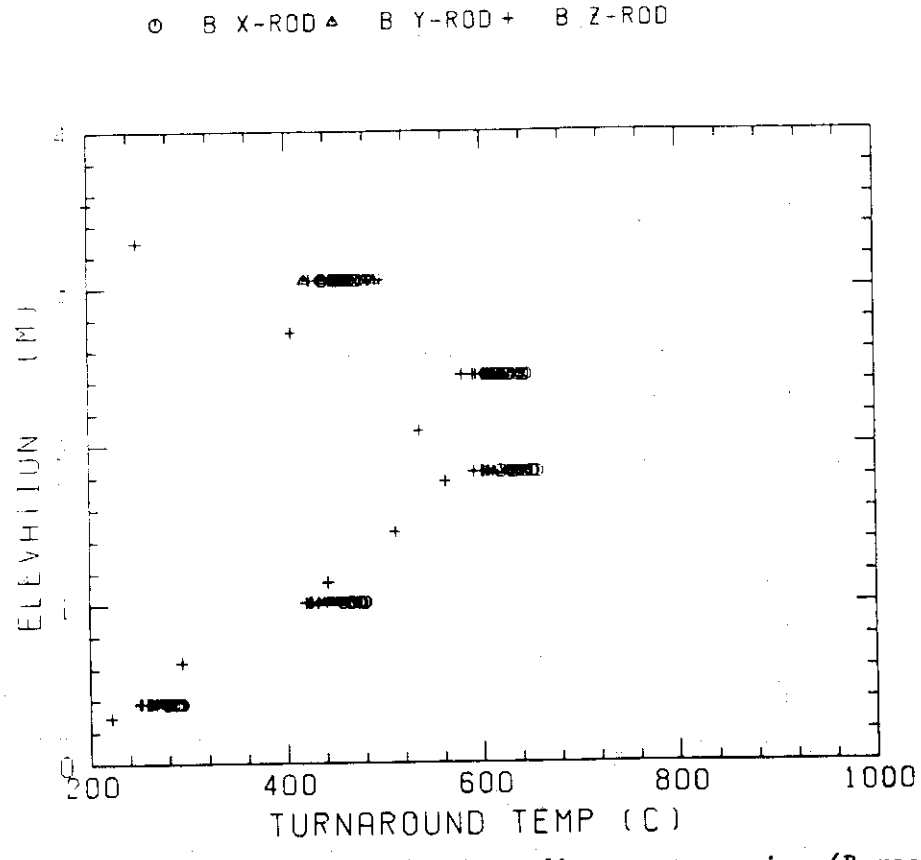

Fig. C-10 Turnaround temperature in medium power region (B region)

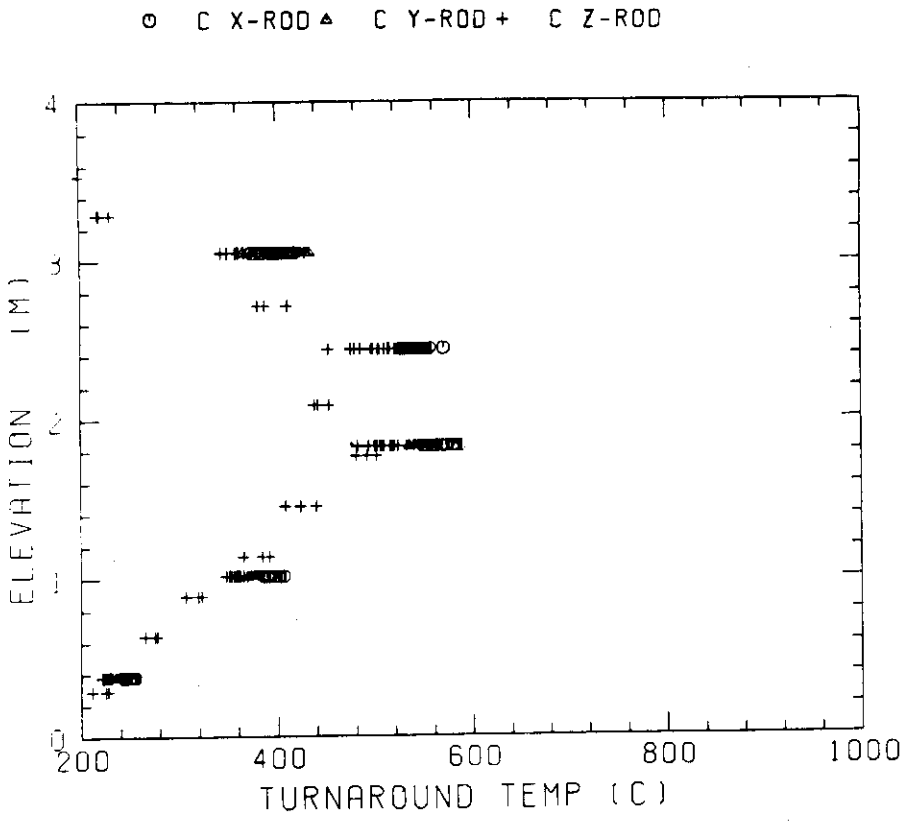

Fig. C-11 Turnaround temperature in low power region (C region)

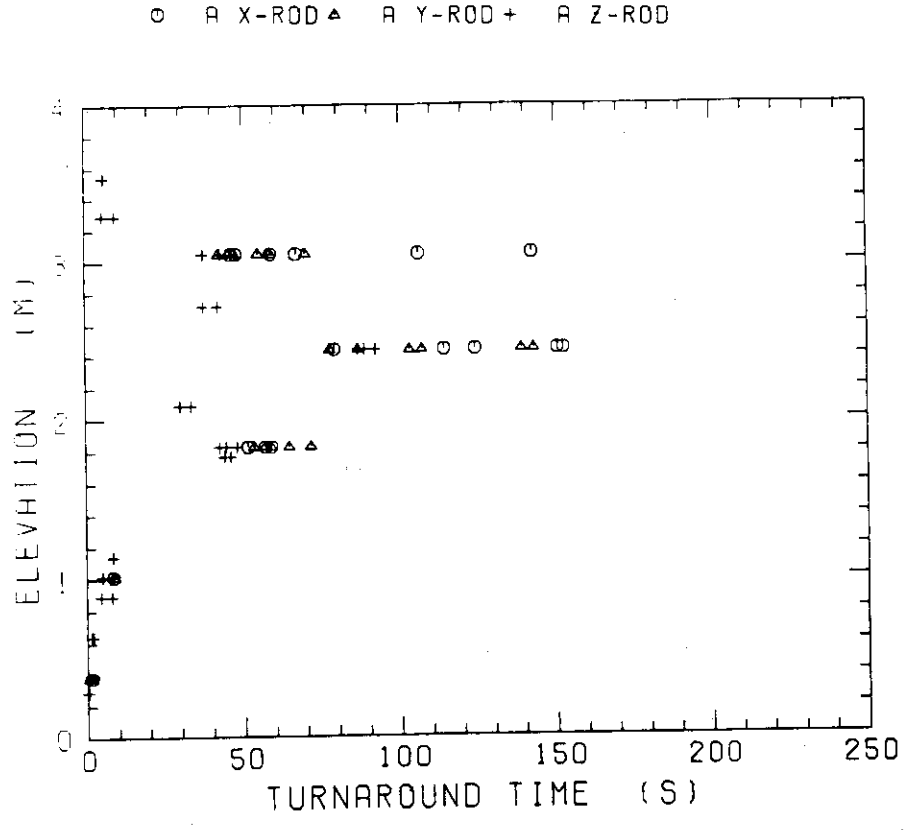

Fig. C-12 Turnaround time in high power region (A region)

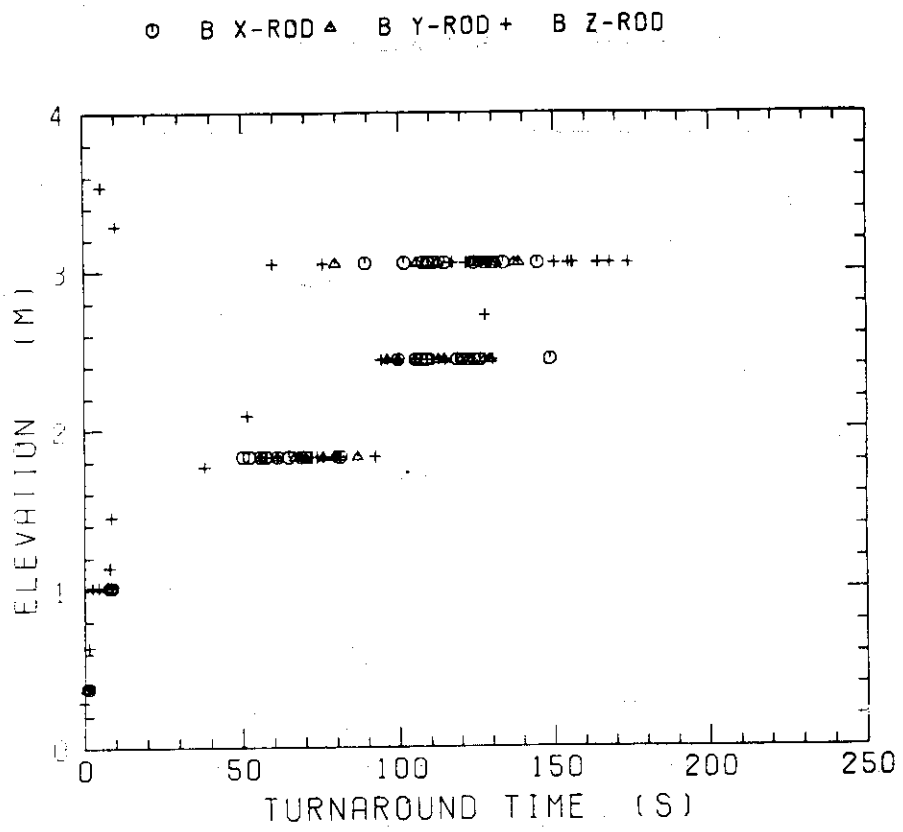

Fig. C-13 Turnaround time in medium power region (B region)

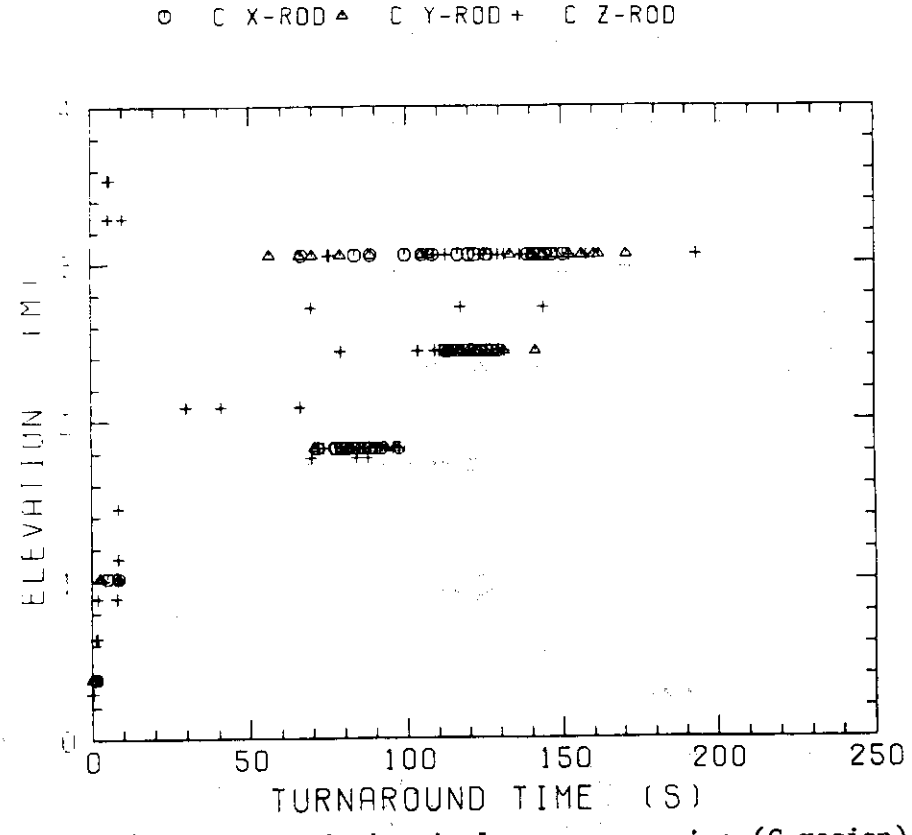

Fig. C-14 Turnaround time in low power region (C region)

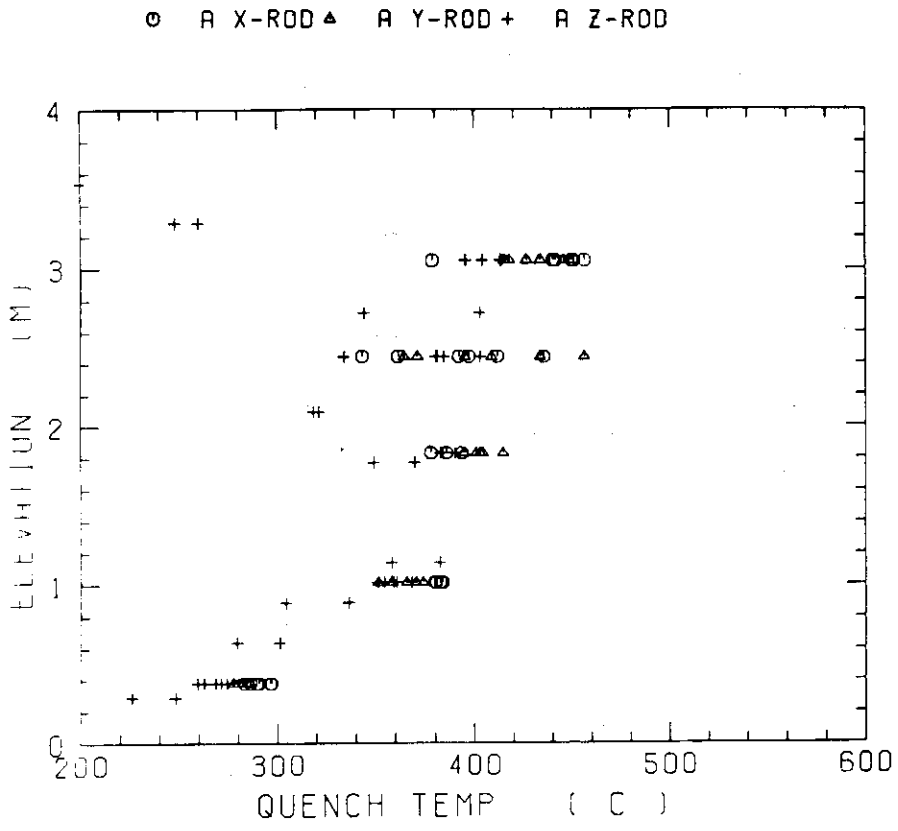

Fig. C-15 Quench temperature in high power region (A region)

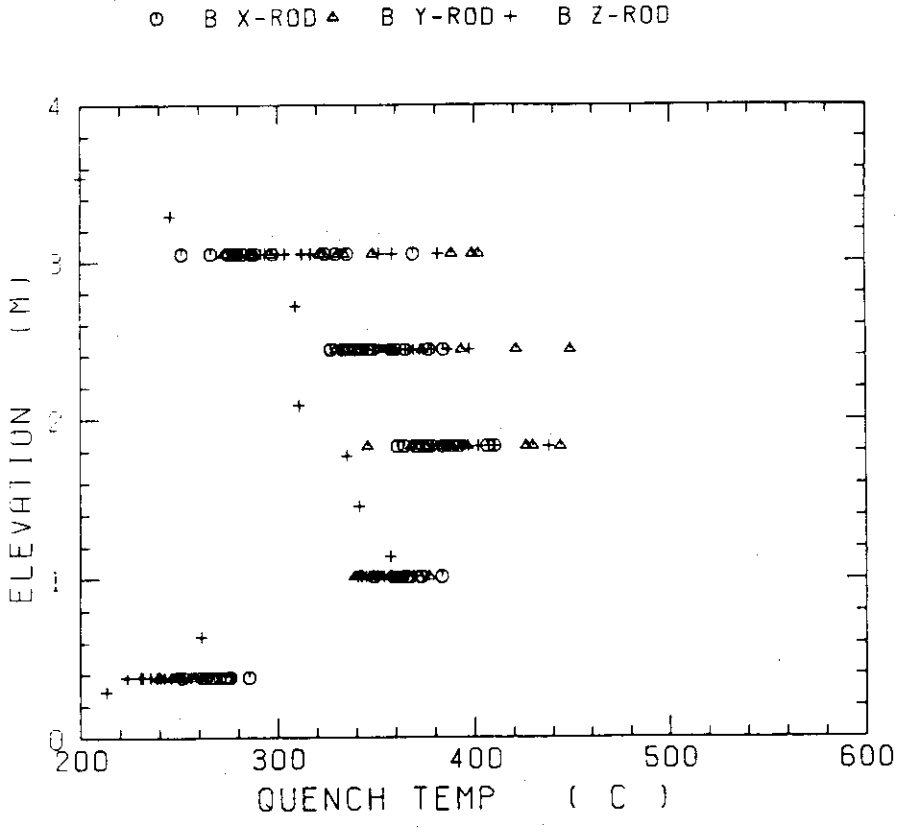

Fig. C-16 Quench temperature in medium power region (B region)

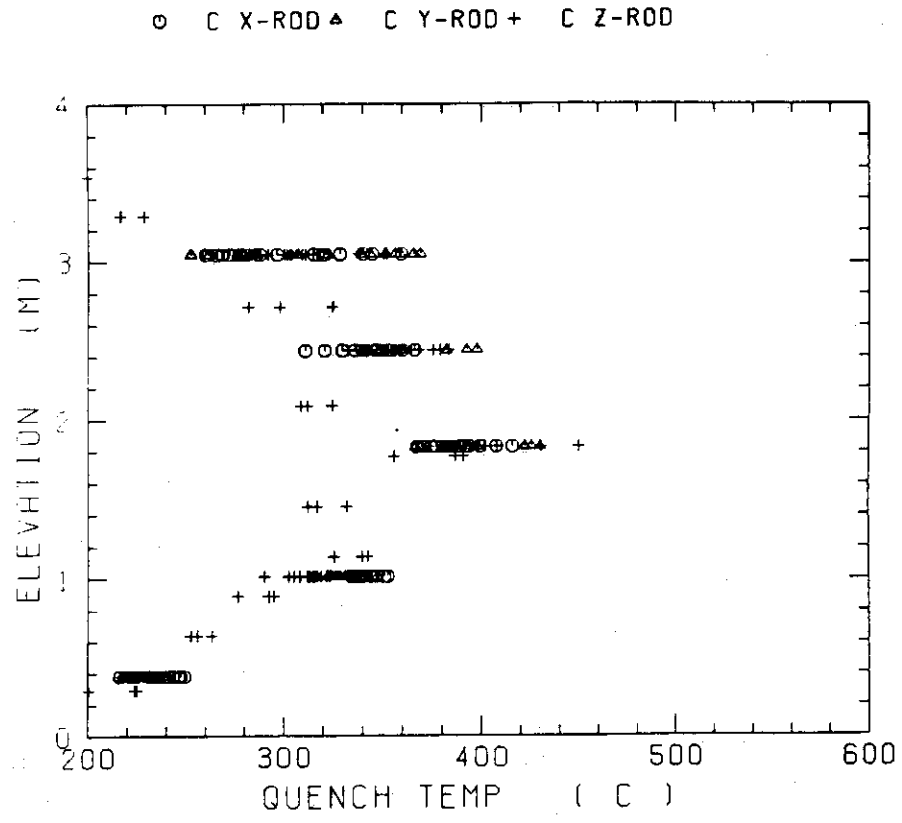

Fig. C-17 Quench temperature in low power region (C region)

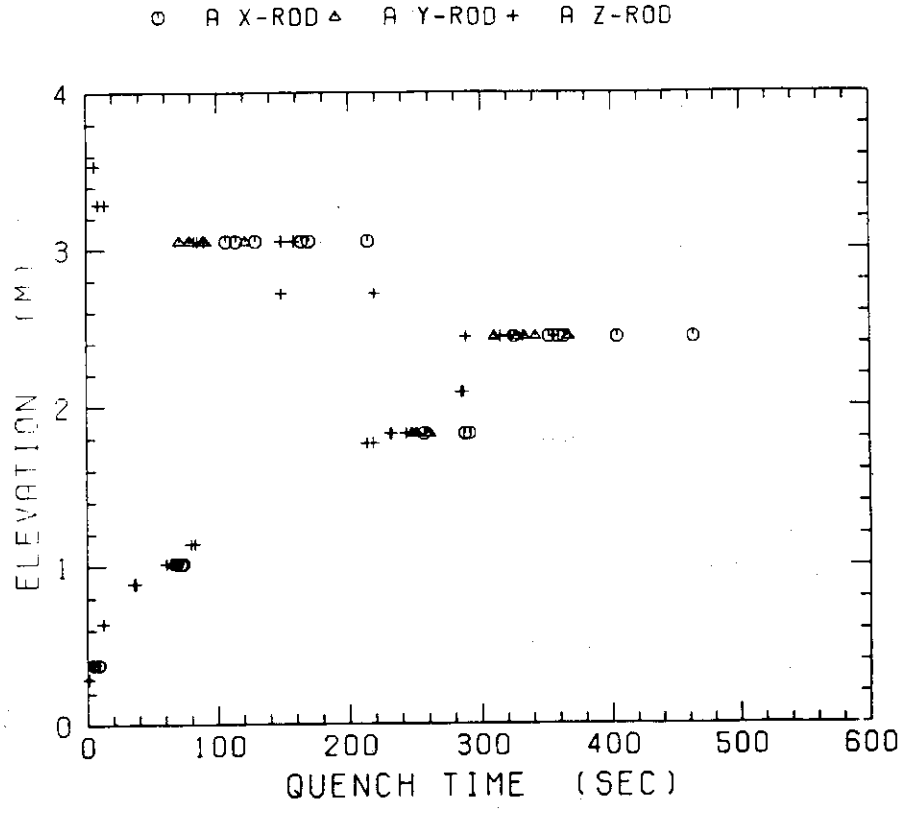

Fig. C-18 Quench time in high power region (A region)

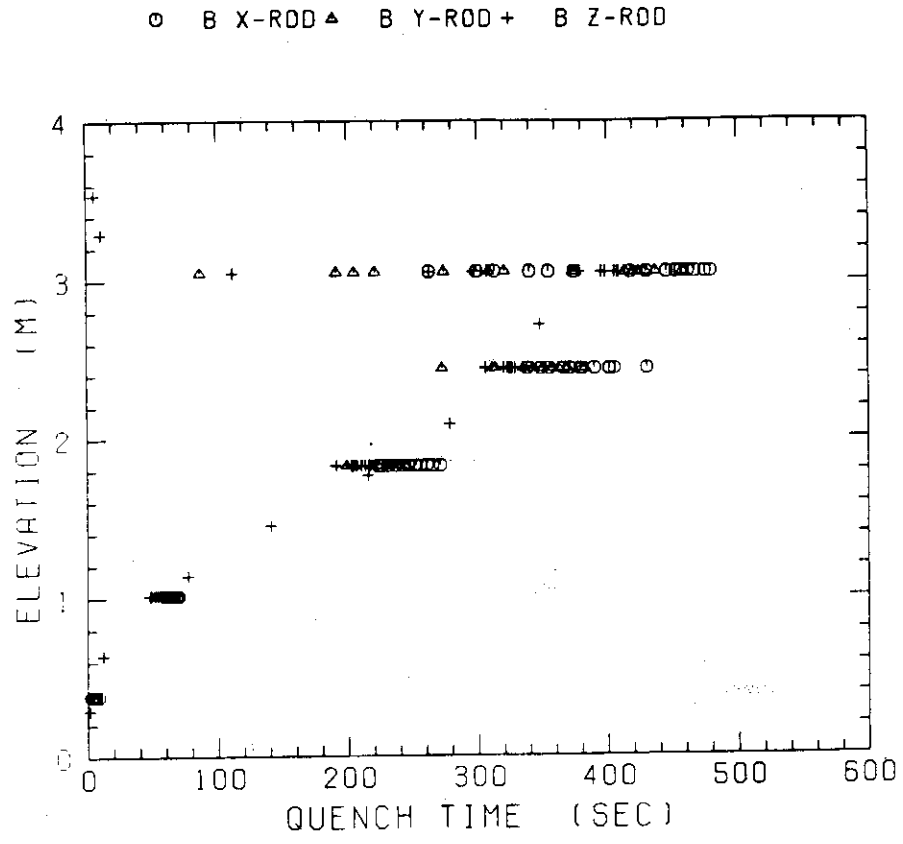

Fig. C-19 Quench time in medium power region (B region)

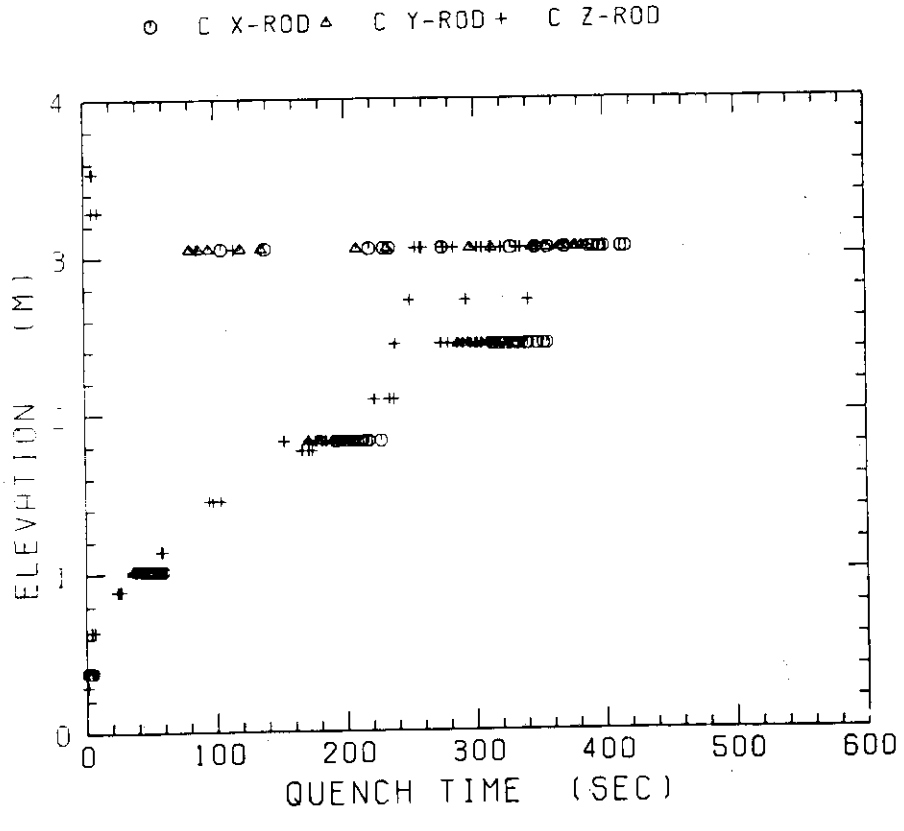

Fig. C-20 Quench time in low power region (C region)

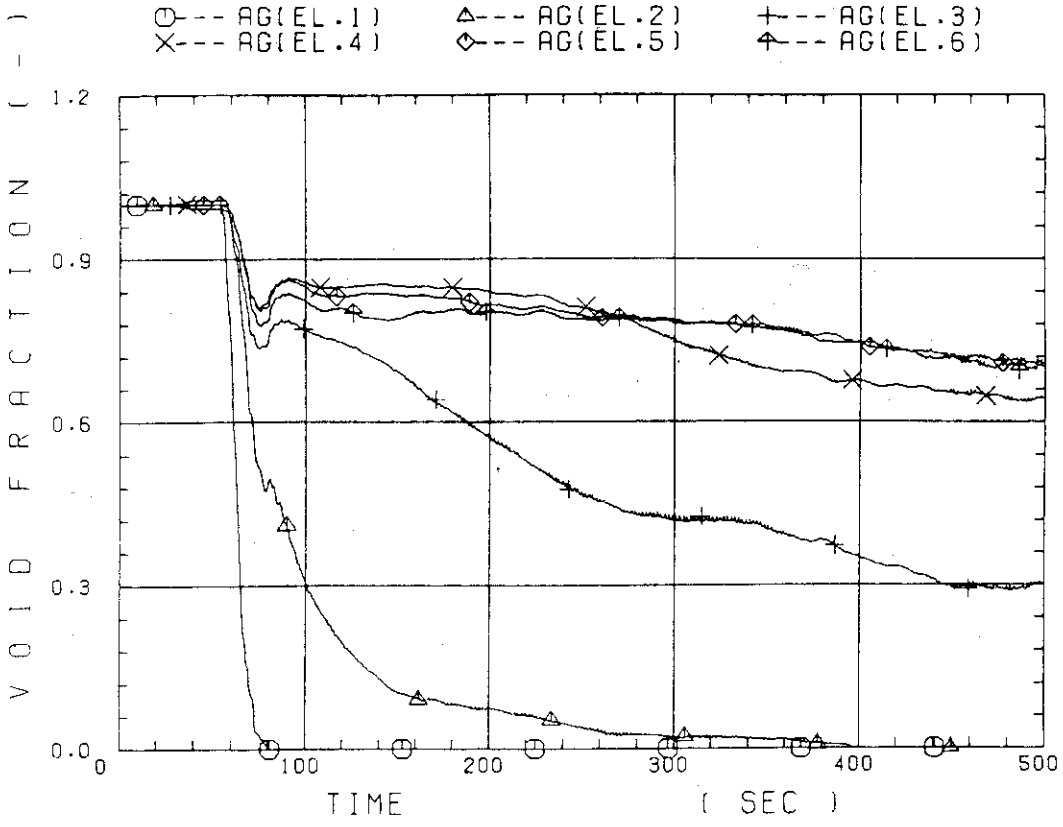

Fig. C-21 Void fraction in core

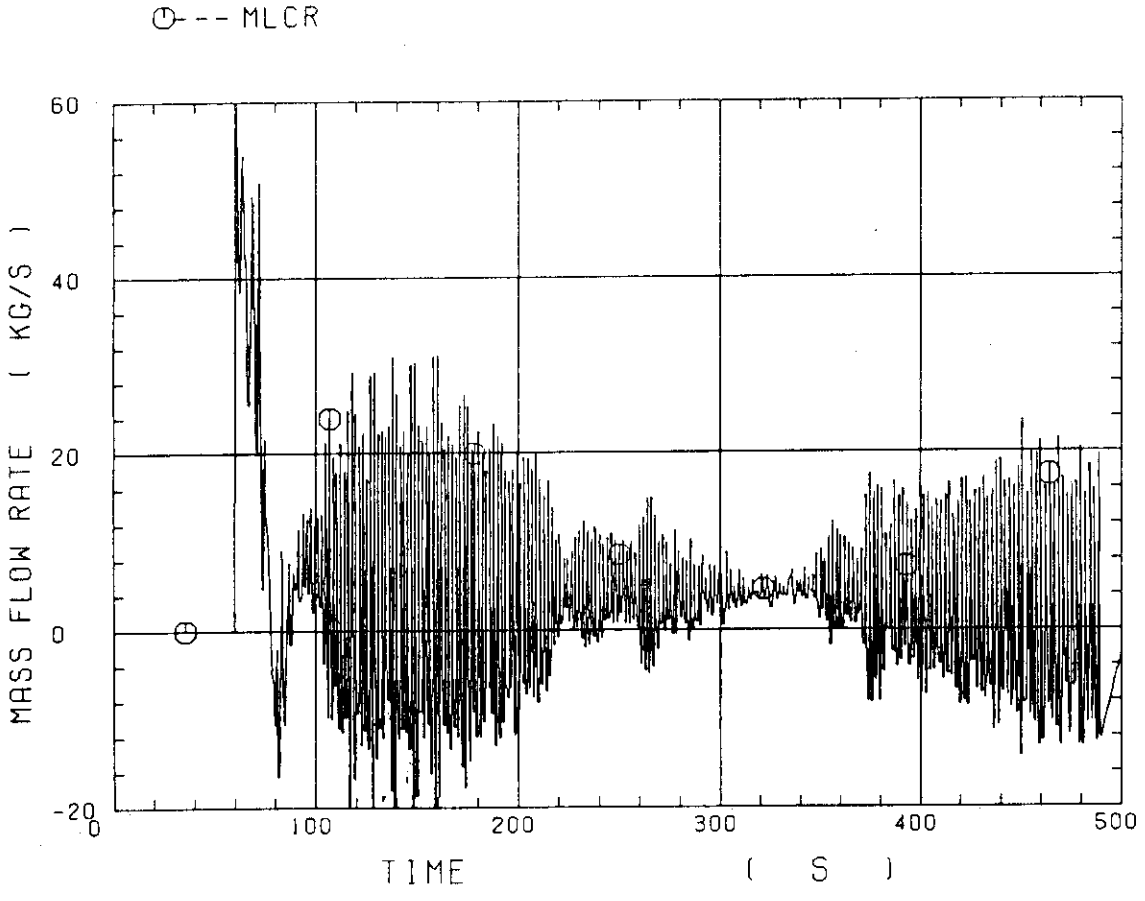

Fig. C-22 Core inlet mass flow rate

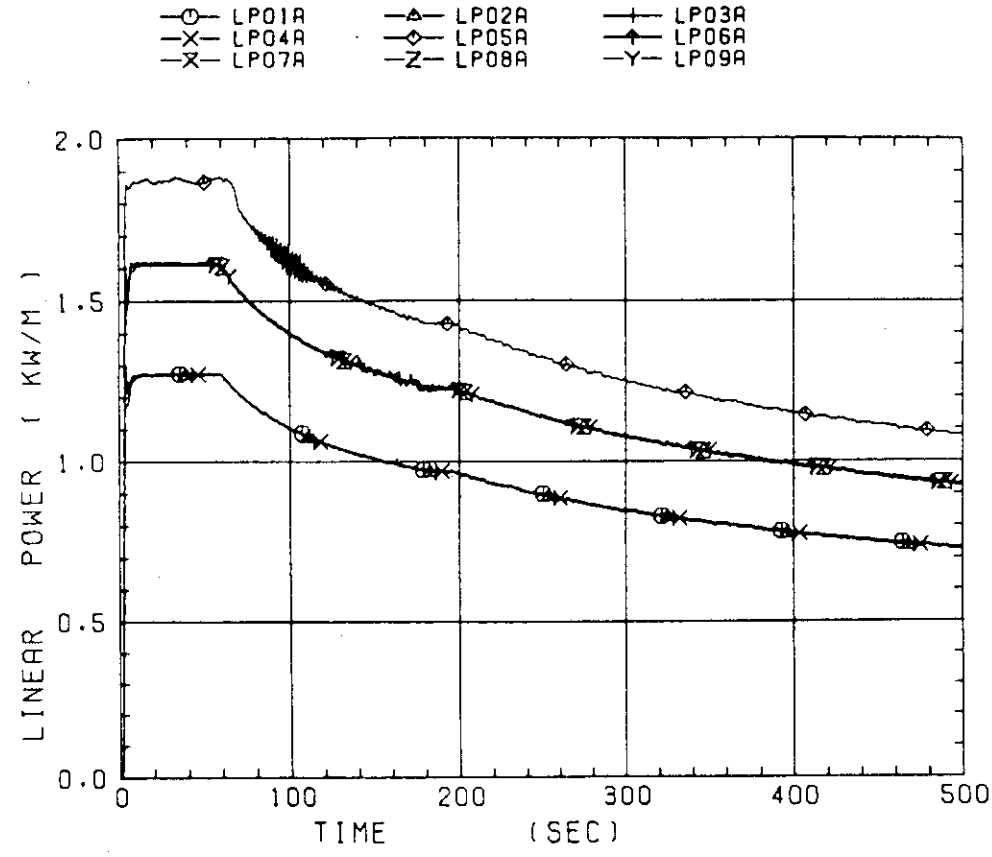

Fig. C-23 Average linear power of heater rod in each power unit zone

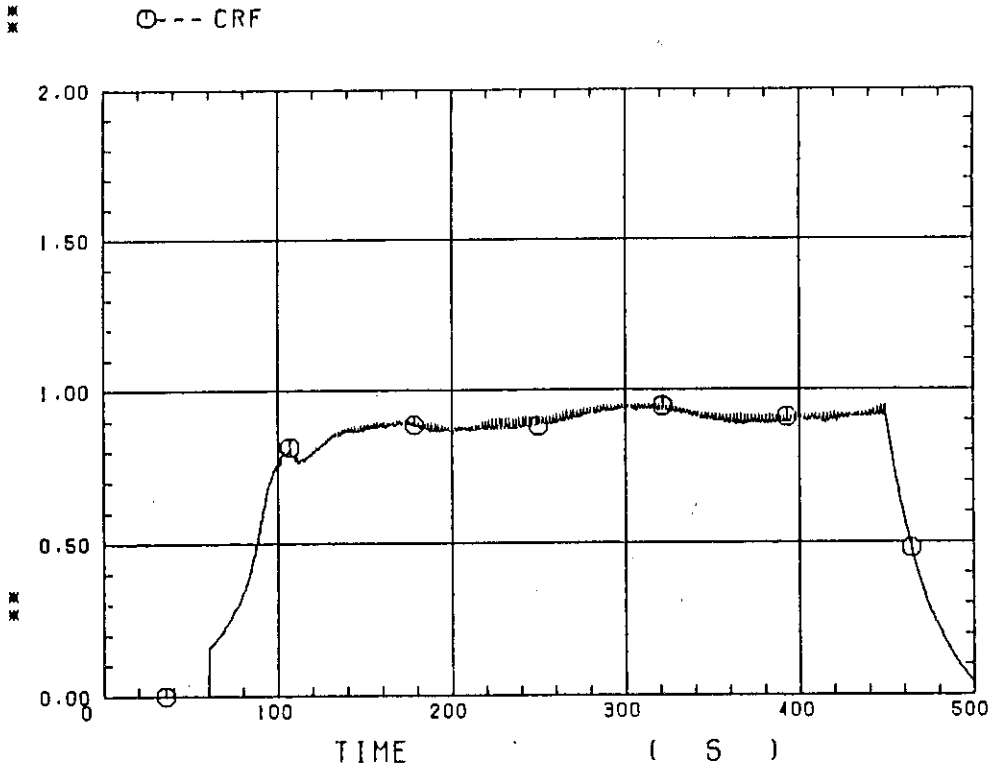

Fig. C-24 Carry-over rate fraction

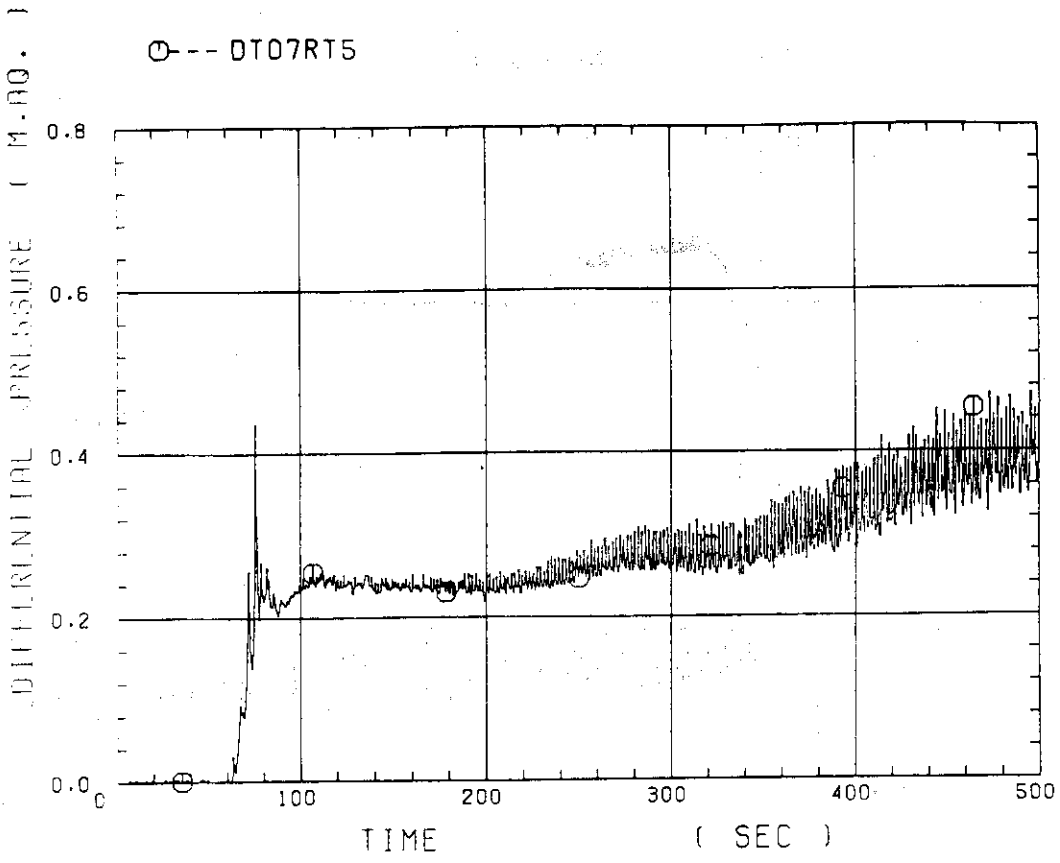

Fig. C-25 Differential pressure through upper plenum

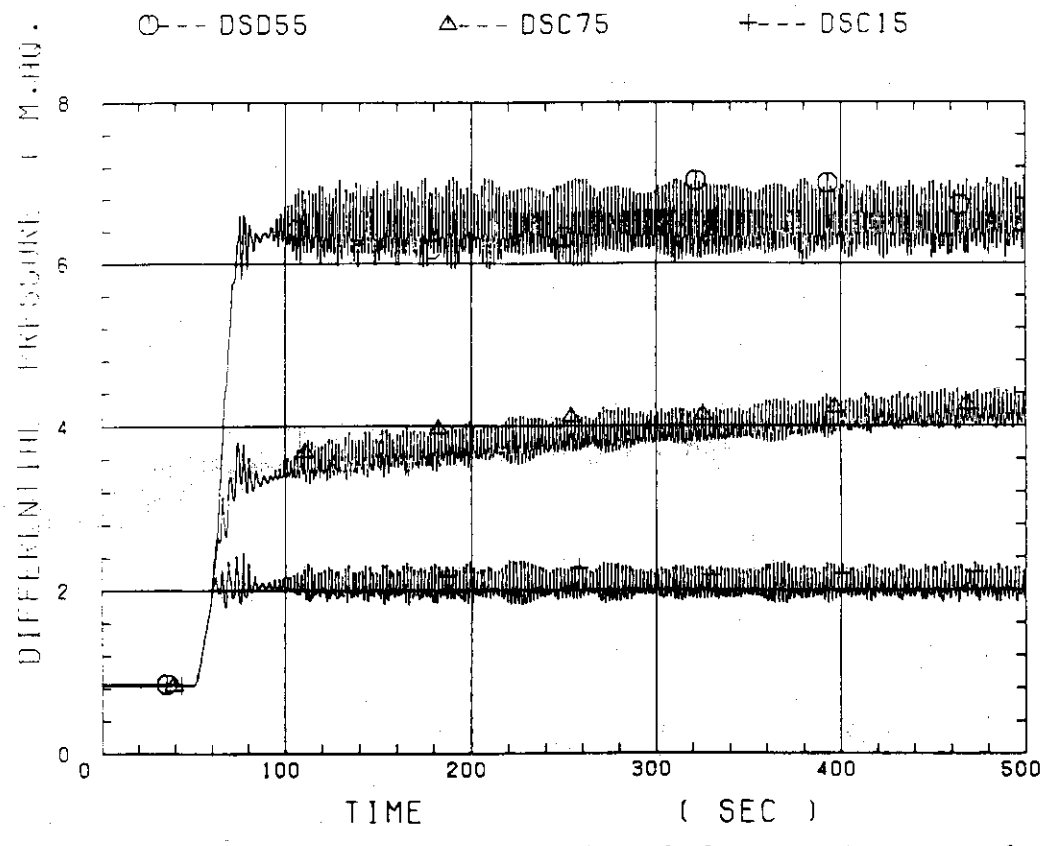

Fig. C-26 Differential pressure through downcomer, core, and lower plenum

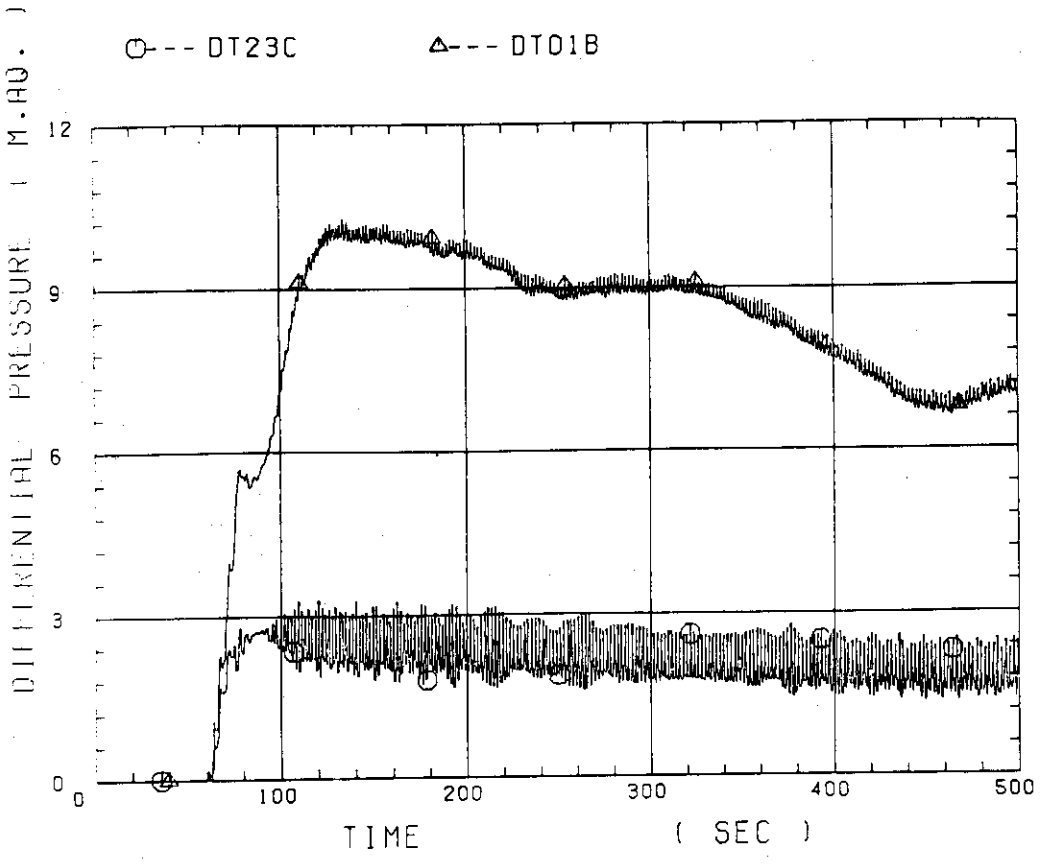

Fig. C-27 Differential pressure through intact and broken loops

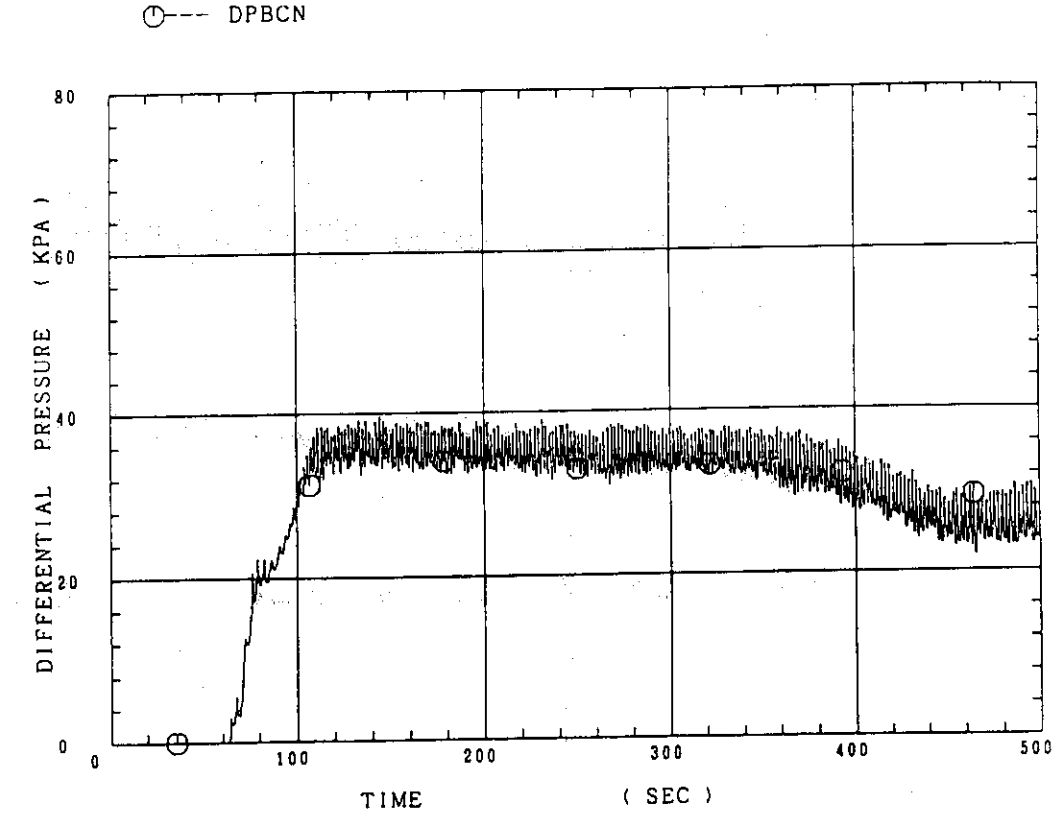

Fig. C-28 Differential pressure through broken cold leg nozzle

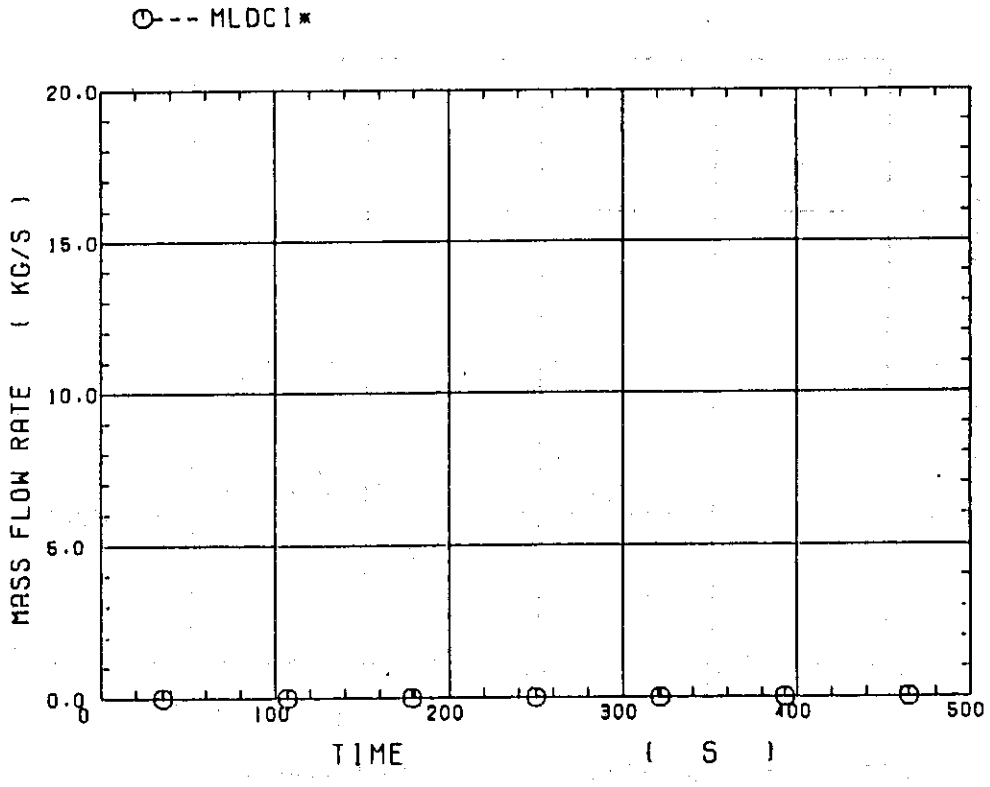

Fig. C-29 Total water mass flow rate from intact loops to downcomer

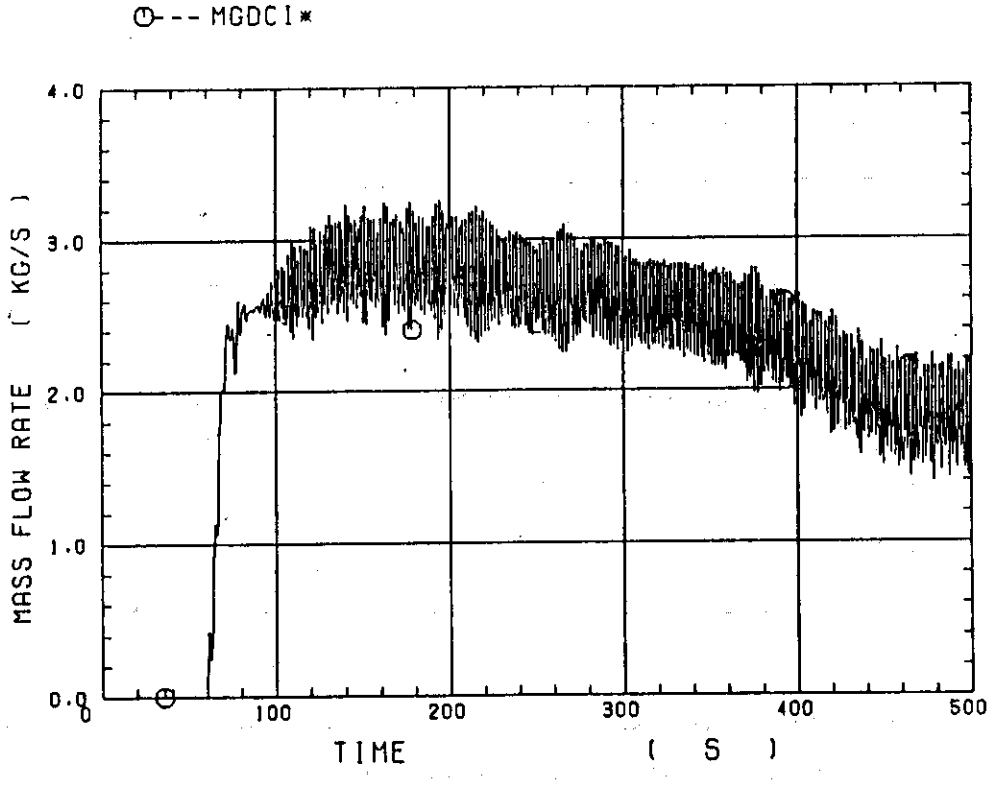

Fig. C-30 Total steam mass flow rate from intact loops to downcomer

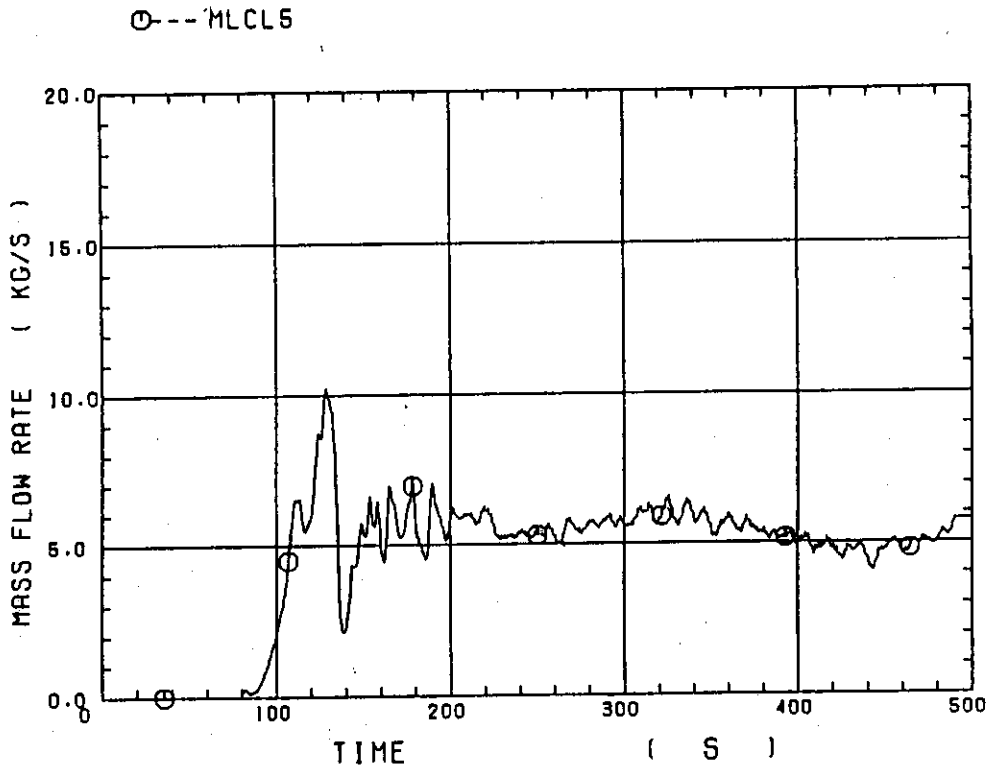

Fig. C-31 Water mass flow rate through broken cold leg nozzle

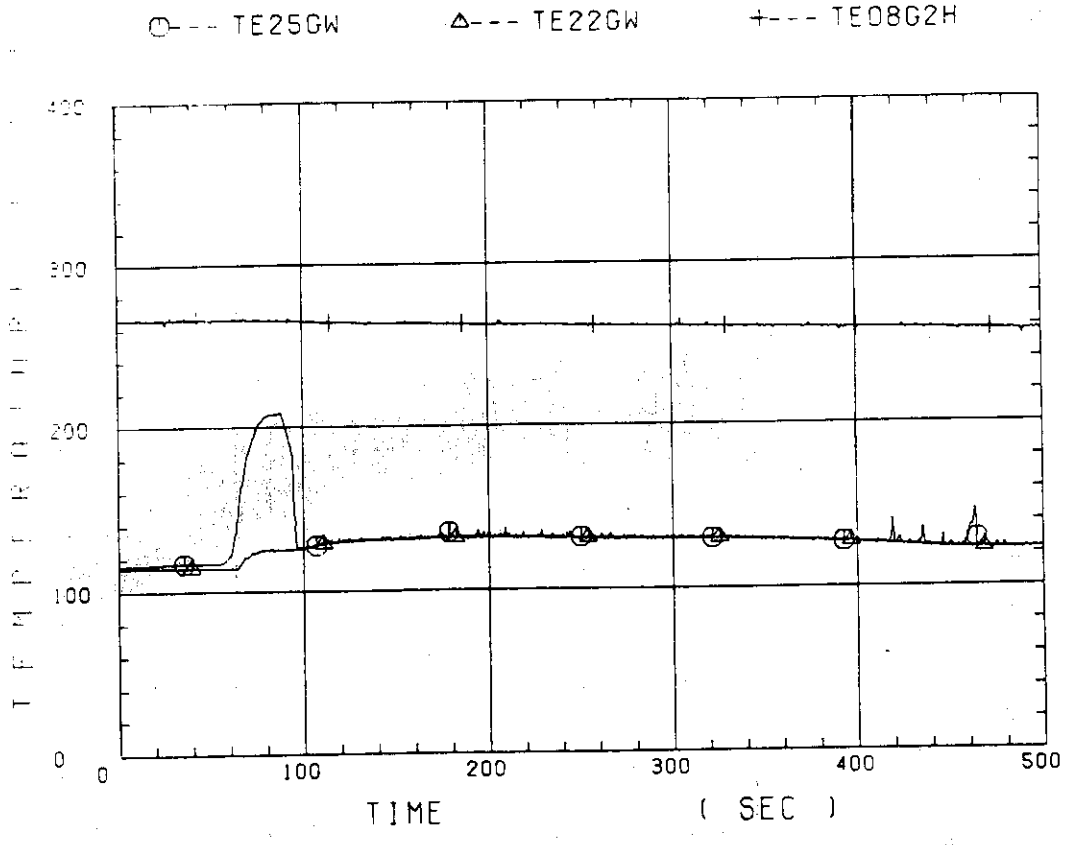

Fig. C-32 Fluid temperature in inlet plenum, outlet plenum, and secondary of steam generator 1

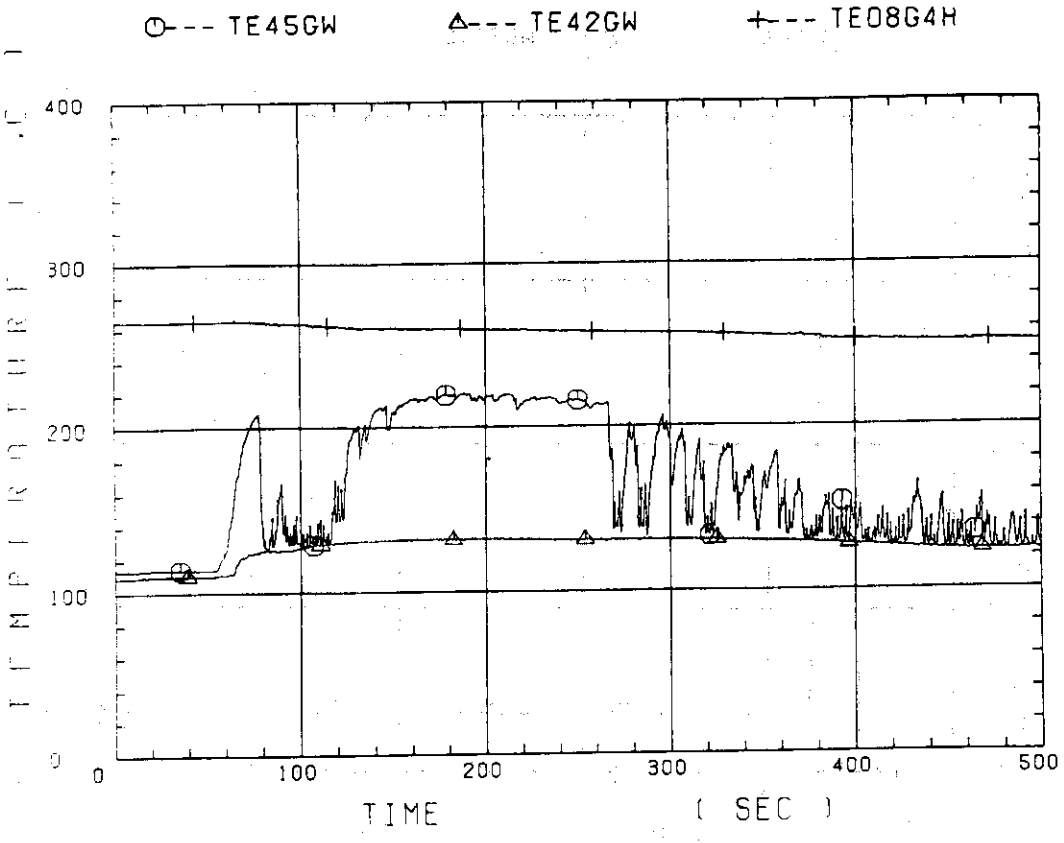

Fig. C-33 Fluid temperature in inlet plenum, outlet plenum, and secondary of steam generator 2

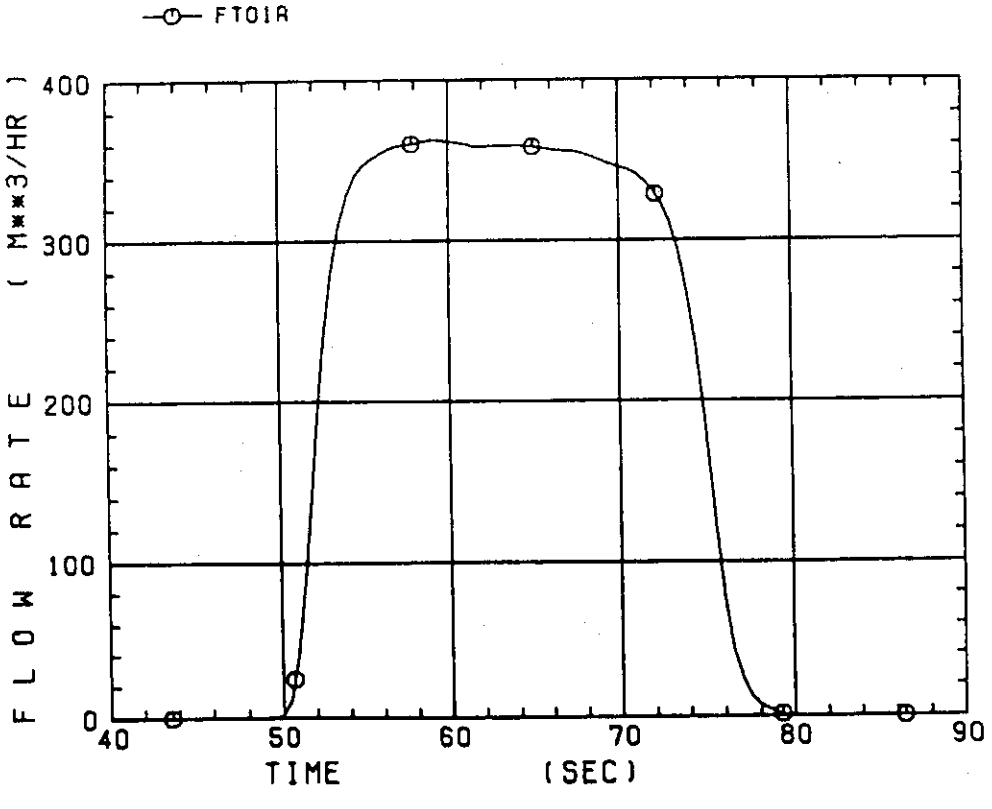

Fig. C-34 Total accumulator injection rate

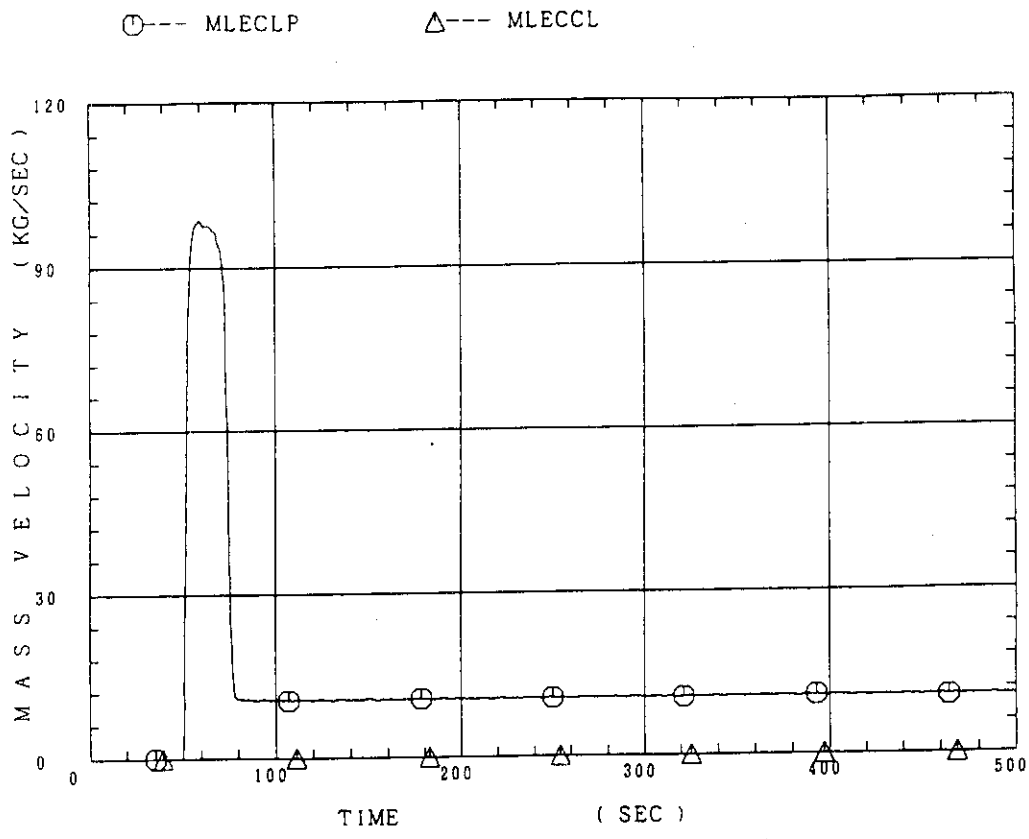

Fig. C-35 ECC water injection rates to lower plenum and to cold legs

Appendix D

Main results of test C1-22 (Run 41)

Table and Figure List

Table D-1 Summary of test conditions
Table D-2 Chronology of events

Fig. D-1 Surface temperature on low power rod (Z-rod) in medium power region (B region) (average power rod)
Fig. D-2 Surface temperature on high power rod (X-rod) in high power region (A region) (peak power rod)
Fig. D-3 Surface temperature on low power rod (Z-rod) in low power region (C region) (lowest power rod)
Fig. D-4 Heat transfer coefficient at midplane of low power rod (Z-rod) in medium power region (B region) (average power rod)
Fig. D-5 Heat transfer coefficient at midplane of high power rod (X-rod) in high power region (A region) (peak power rod)
Fig. D-6 Initial rod surface temperature in high power region (A region)
Fig. D-7 Initial rod surface temperature in medium power region (B region)
Fig. D-8 Initial rod surface temperature in low power region (C region)
Fig. D-9 Turnaround temperature in high power region (A region)
Fig. D-10 Turnaround temperature in medium power region (B region)
Fig. D-11 Turnaround temperature in low power region (C region)
Fig. D-12 Turnaround time in high power region (A region)
Fig. D-13 Turnaround time in medium power region (B region)
Fig. D-14 Turnaround time in low power region (C region)
Fig. D-15 Quench temperature in high power region (A region)
Fig. D-16 Quench temperature in medium power region (B region)
Fig. D-17 Quench temperature in low power region (C region)
Fig. D-18 Quench time in high power region (A region)
Fig. D-19 Quench time in medium power region (B region)
Fig. D-20 Quench time in low power region (C region)
Fig. D-21 Void fraction in core
Fig. D-22 Core inlet mass flow rate
Fig. D-23 Average linear power of heater rod in each power unit zone

Fig. D-24 Carry-over rate fraction
Fig. D-25 Differential pressure through upper plenum
Fig. D-26 Differential pressure through downcomer, core, and lower plenum
Fig. D-27 Differential pressure through intact and broken loops
Fig. D-28 Differential pressure through broken cold leg nozzle
Fig. D-29 Total water mass flow rate from intact loops to downcomer
Fig. D-30 Total steam mass flow rate from intact loops to downcomer
Fig. D-31 Water mass flow rate through broken cold leg nozzle
Fig. D-32 Fluid temperature in inlet plenum, outlet plenum, and secondary of steam generator 1
Fig. D-33 Fluid temperature in inlet plenum, outlet plenum, and secondary of steam generator 2
Fig. D-34 Total accumulator injection rate
Fig. D-35 ECC water injection rates to lower plenum and to cold legs

TABLE D-1 SUMMARY OF TEST CONDITIONS

1. TEST TYPE : FLECHT-SET 3420 B COUPLING TEST
2. TEST NUMBER : RUN 041, C1-22 3. DATA : April 6, 1981
4. POWER : A: TOTAL: 9.92 MW; B: LINEAR: 1.5 KW/M
5. RELATIVE RADIAL POWER SHAPE :

A: ZONE:	A	B	C
B: RATIO:	1.16	1.0	0.79

6. AXIAL POWER SHAPE : CHOPPED COSINE
7. PRESSURE ($KG?CM^2A$):
   A: SYSTEM: 1.6 , B: CONTAINMENT 1.6 ,
   C: STEAM GENERATOR SECONDARY: 52
8. TEMPERATURE (DEG.C) :
   A: DOWNCOMER WALLS 101 , B: VESSEL INTERNALS 98 ,
   C: PRIMARY PIPING WALLS 111 , D: LOWER PEINUM LIQUID 100 ,
   E: ECC LIQUID 112 , F: STEAM GENERATOR SECONDARY 265 ,
   G: CORE TEMPERATURE AT ECC INITIATION 530
9. ECC. INJECTION TYPE: B
   A: COLD LEG, B: LOWER PLENUM, C: LOWER PLENUM + COLD LEG
10. PUMP K-FACTOR : $\sim$ 15
11. ECC FLOW RATES AND DURATION:
    A: ACCUMULATOR 362 M^3/HR FROM 0 TO 24 SECONDS
    B: LPCI 39.9 M^3/HR FROM 24 TO 717 SECONDS
    C: ECC INJECTION TO LOWER PLENUM : FROM 0 TO 717 SECONDS
    (VALVE OPENING AND CLOSING TIMES ARE INCLUDED IN THE INJECTION DURATION)
12. INITIAL WATER LEVEL IN LOWER PLENUM : 0.87 M.
13. POWER CONTROL : ANS $\times$ 1.2 + ACTINIDE (30 SEC AFTER SCRAM)
14. EXPECTED BOCREC TIME FROM ECC INITIATION 9 SEC
15. EXPECTED PEAK TEMPERATURE AT BOCREC 600 C

Table D-2 CHRONOLOGY OF EVENTS FOR TEST C1-22 (RUN 041)

EVENT	TIME (sec)
Test initiated (Heater rods power on) (Data recording initiated)	0
Accumulator injection initiated	51
Power decay initiated (Bottom of core recovery)	60.5
Accumulator injection switched from lower plenum to cold leg	—
Accumulator injection ended and LPCI injection initiated	75
All heater rods quenched	565
Power off	648
LPCI injection ended	768
Test ended (Data recording ended)	990

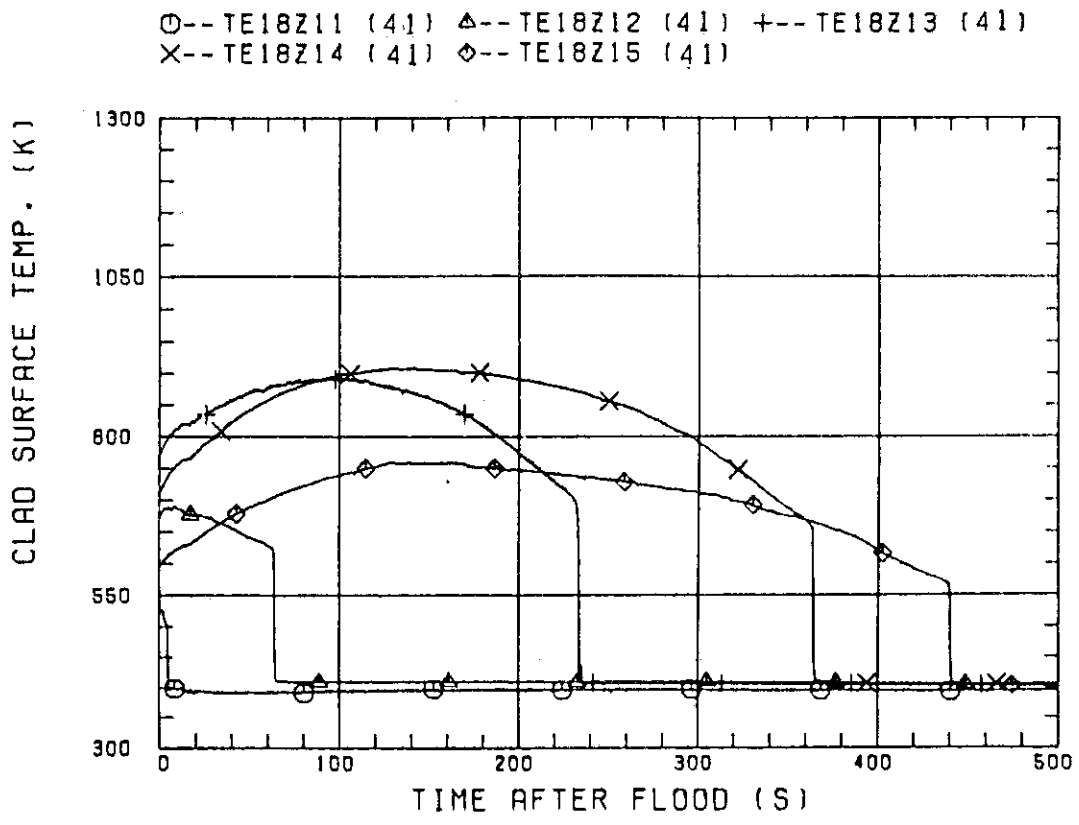

Fig. D-1 Surface temperature on low power rod (Z-rod) in medium power region (B region) (average power rod)

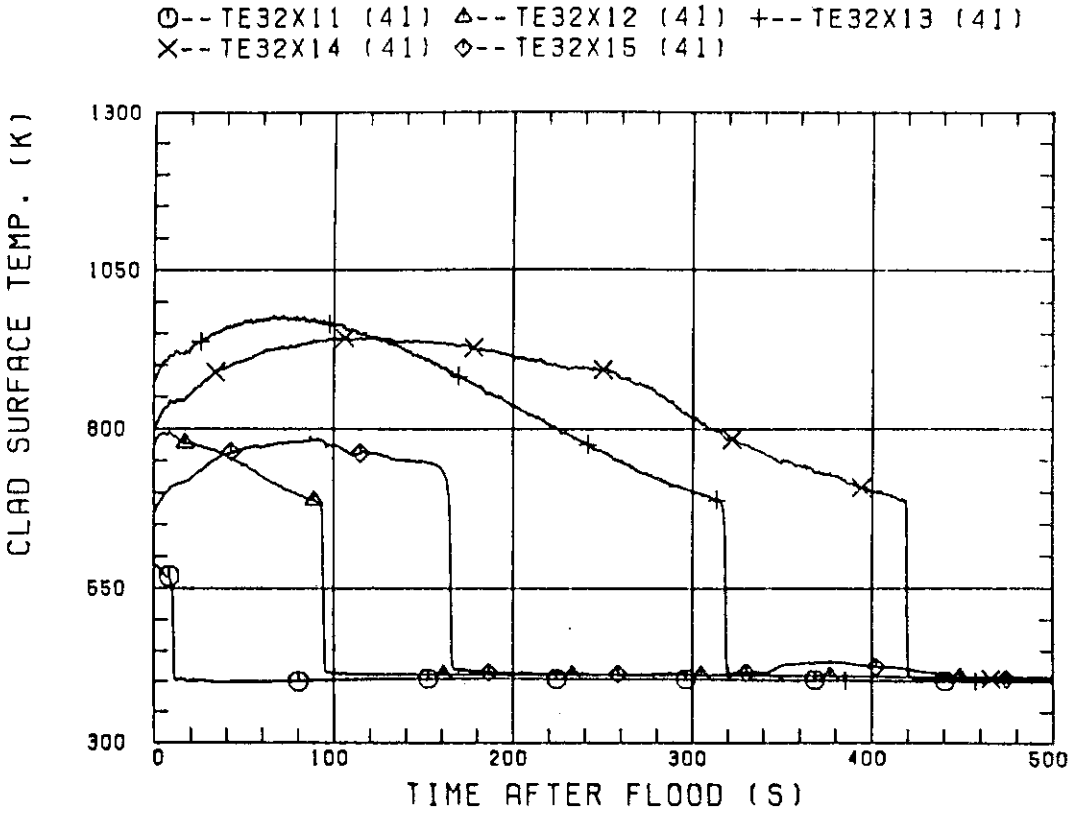

Fig. D-2 Surface temperature on high power rod (X-rod) in high power region (A region) (peak power rod)

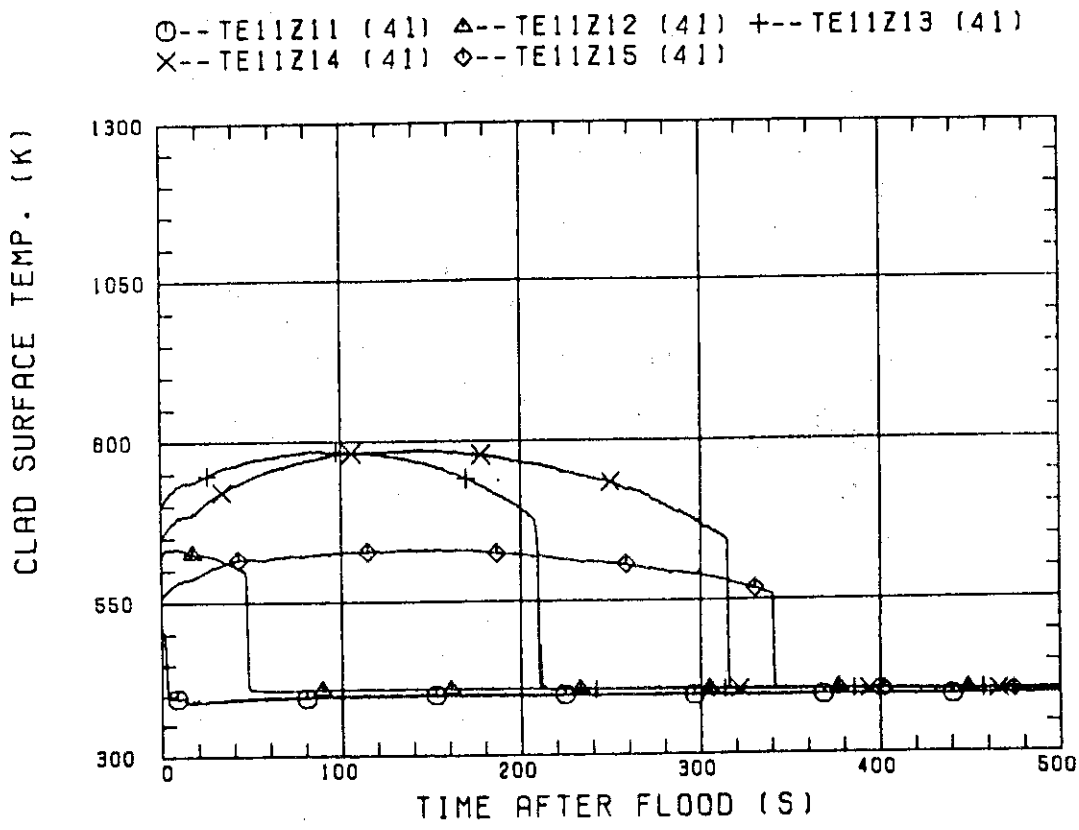

Fig. D-3 Surface temperature on low power rod (Z-rod) in low power region (C region) (lowest power rod)

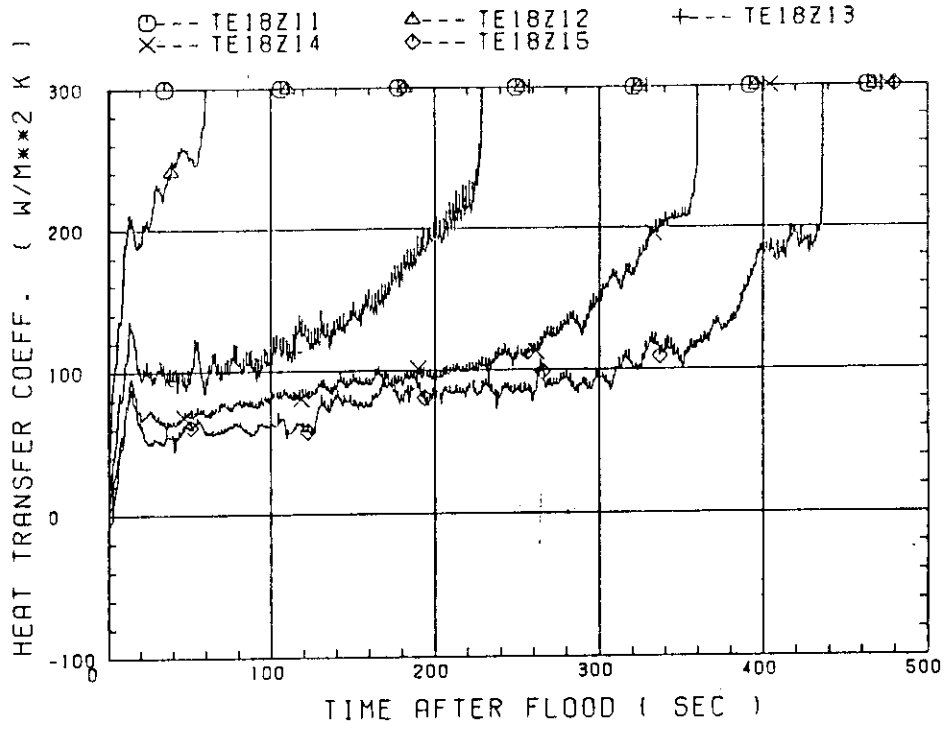

Fig. D-4 Heat transfer coefficient at midplane of low power rod (Z-rod) in medium power region (B region) (average power rod)

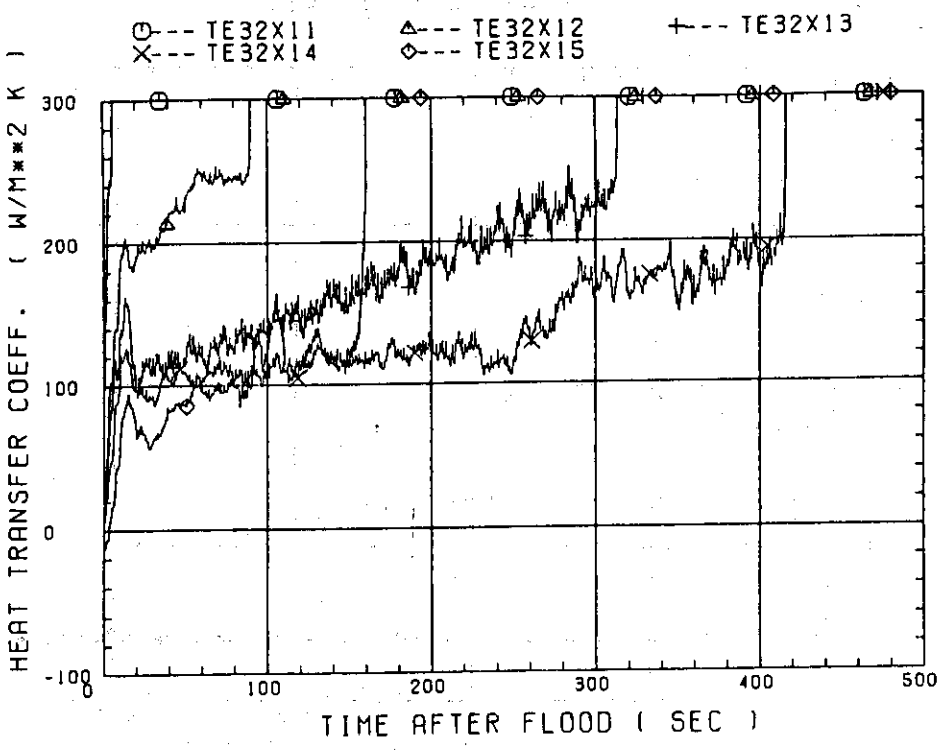

Fig. D-5 Heat transfer coefficient at midplane of high power rod (X-rod) in high power region (A region) (peak power rod)

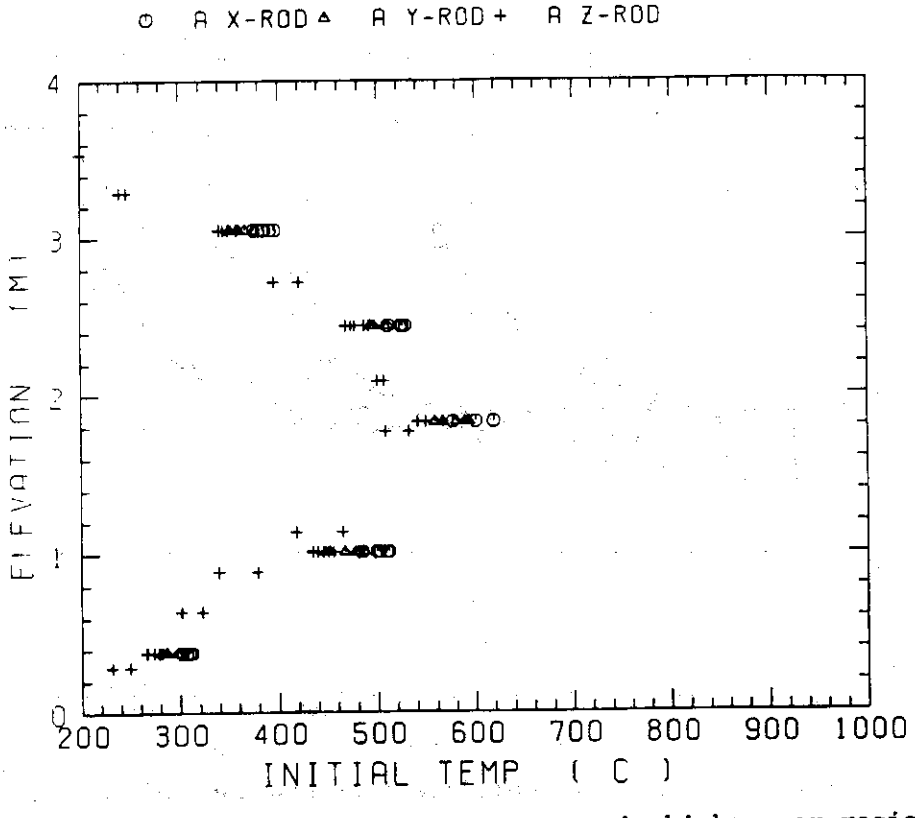

Fig. D-6 Initial rod surface temperature in high power region (A region)

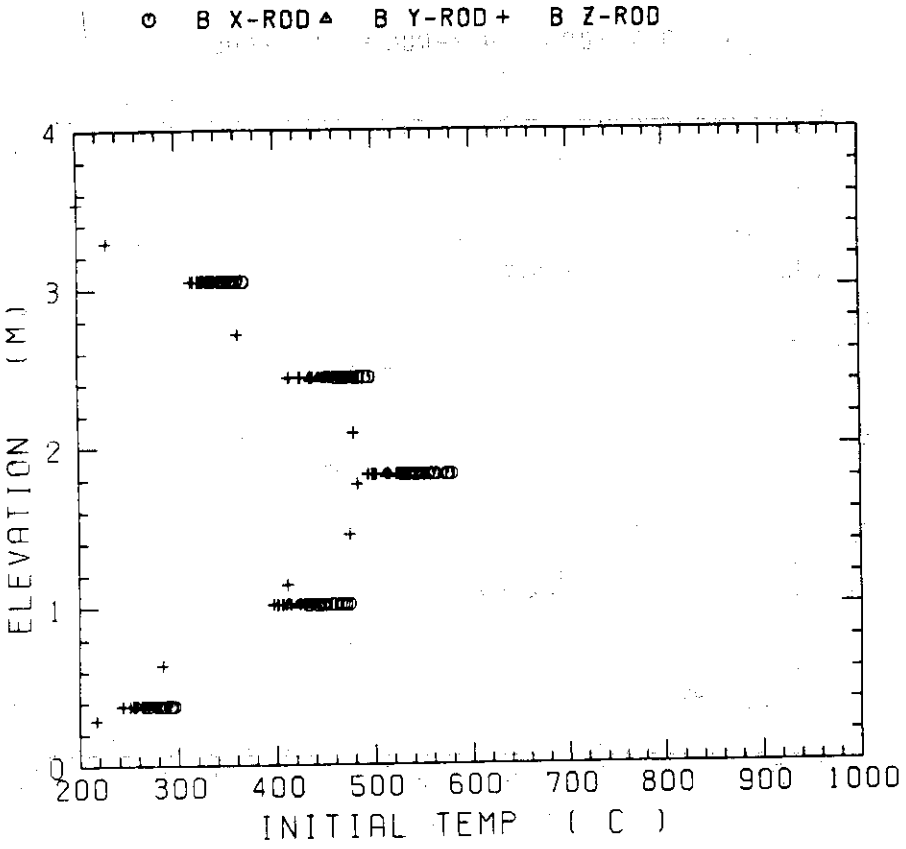

Fig. D-7 Initial rod surface temperature in medium power region (B region)

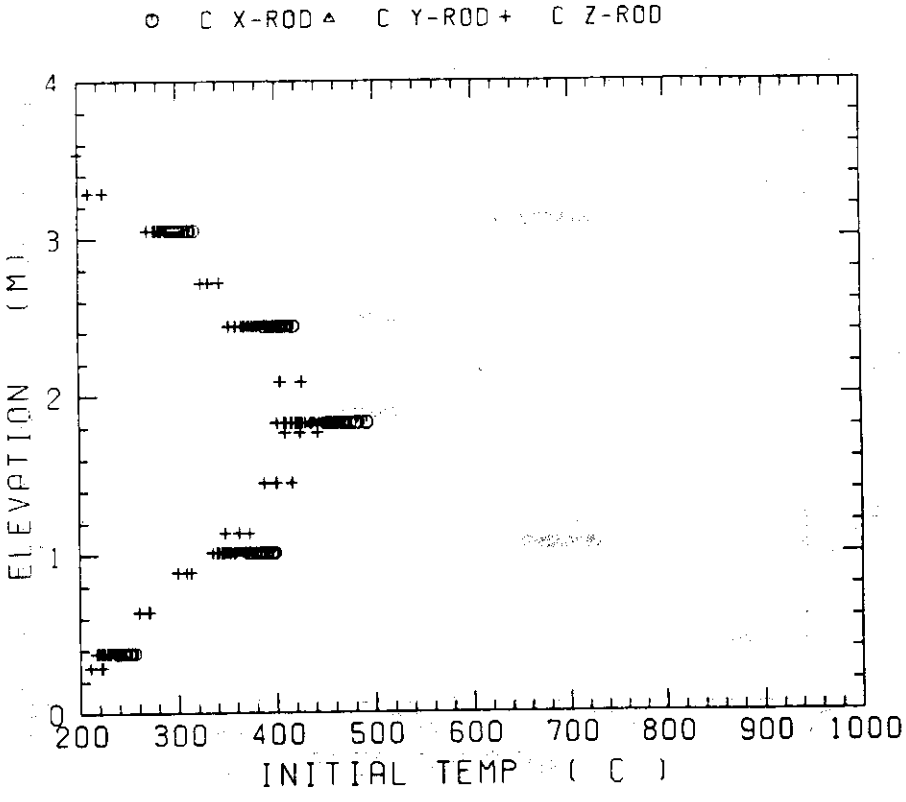

Fig. D-8 Initial rod surface temperature in low power region (C region)

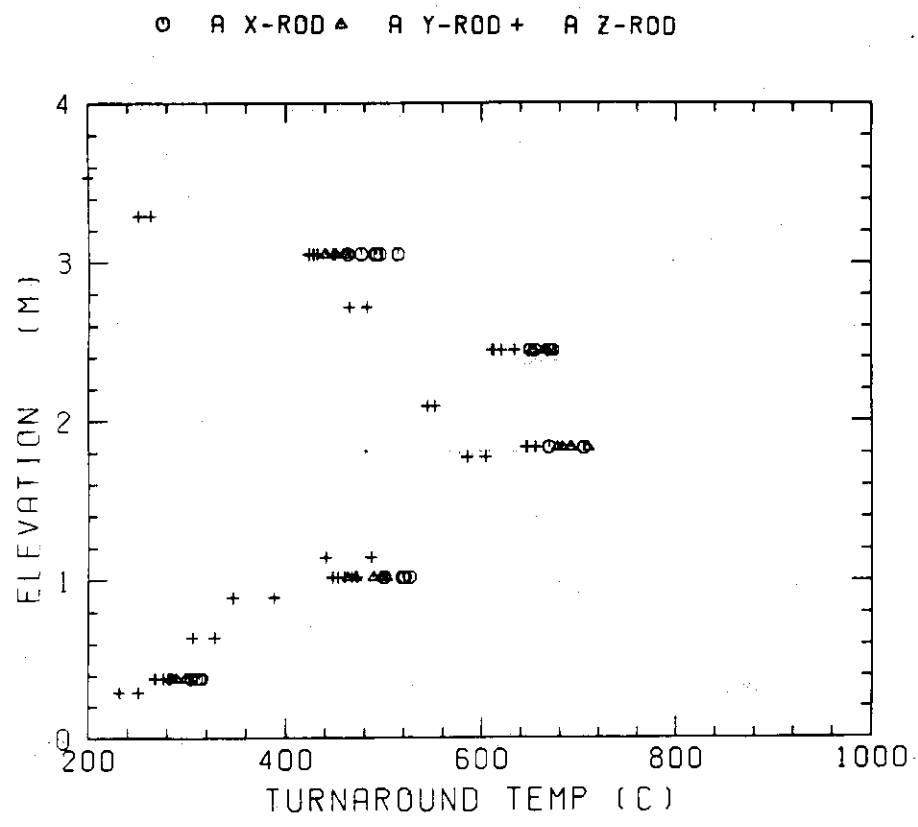

Fig. D-9 Turnaround temperature in high power region (A region)

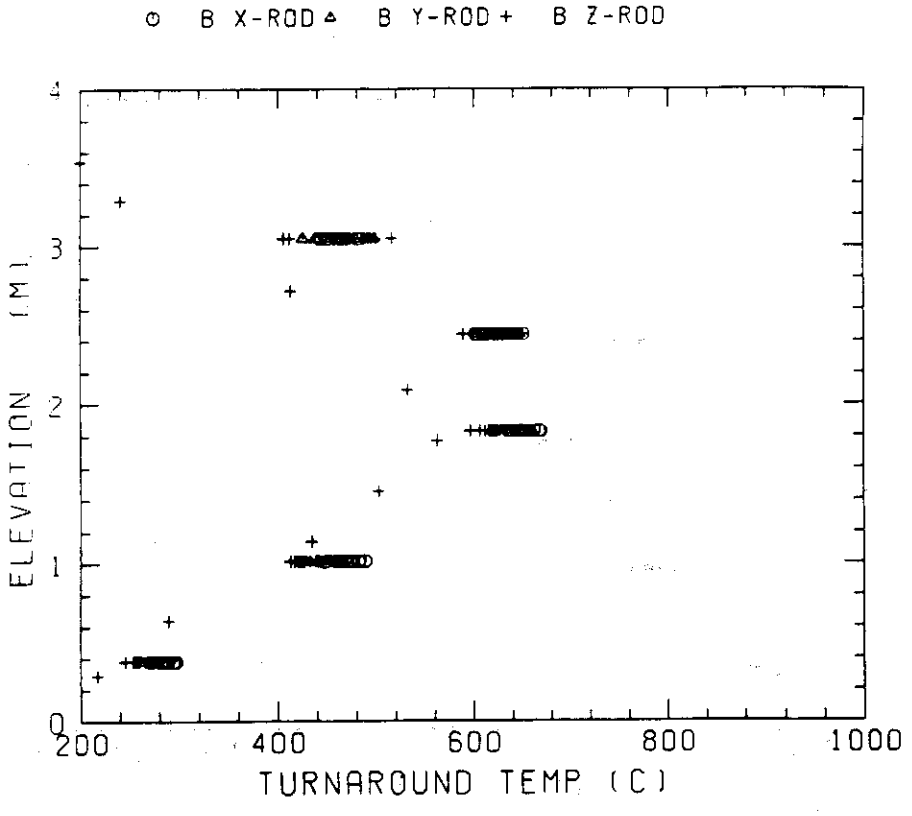

Fig. D-10 Turnaround temperature in medium power region (B region)

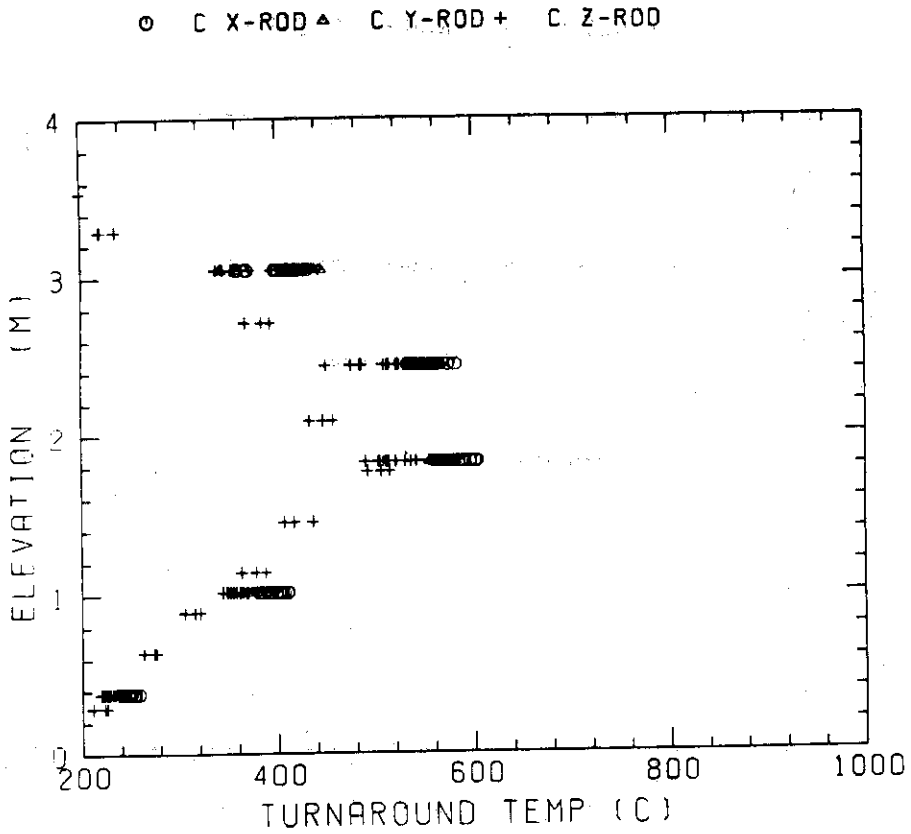

Fig. D-11 Turnaround temperature in low power region (C region)

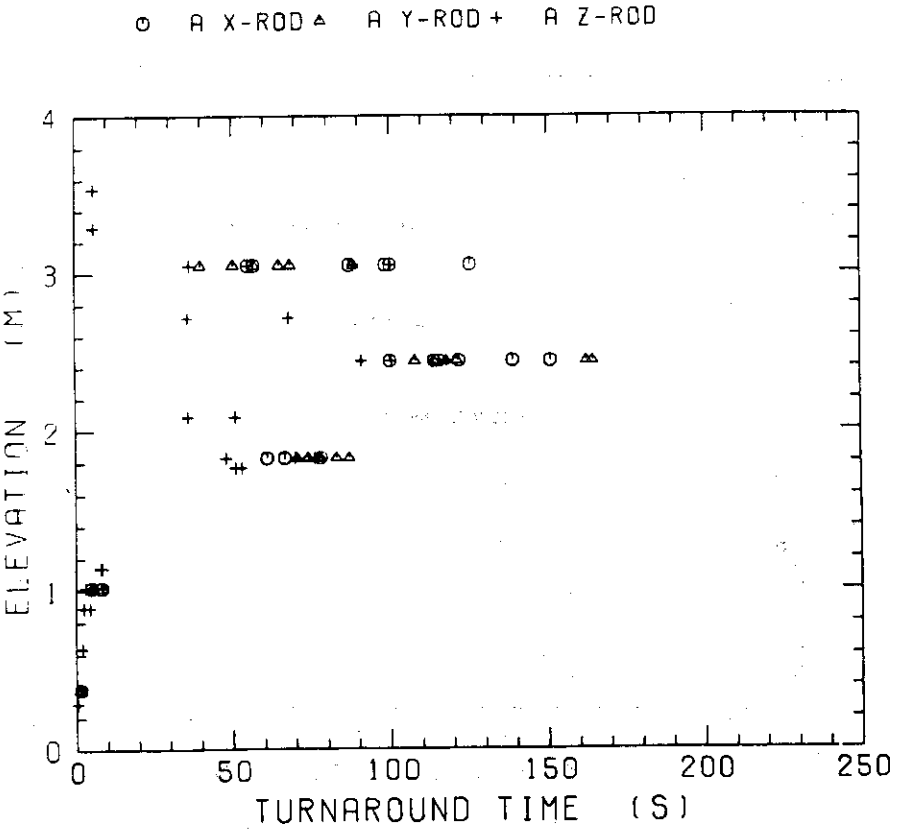

Fig. D-12 Turnaround time in high power region (A region)

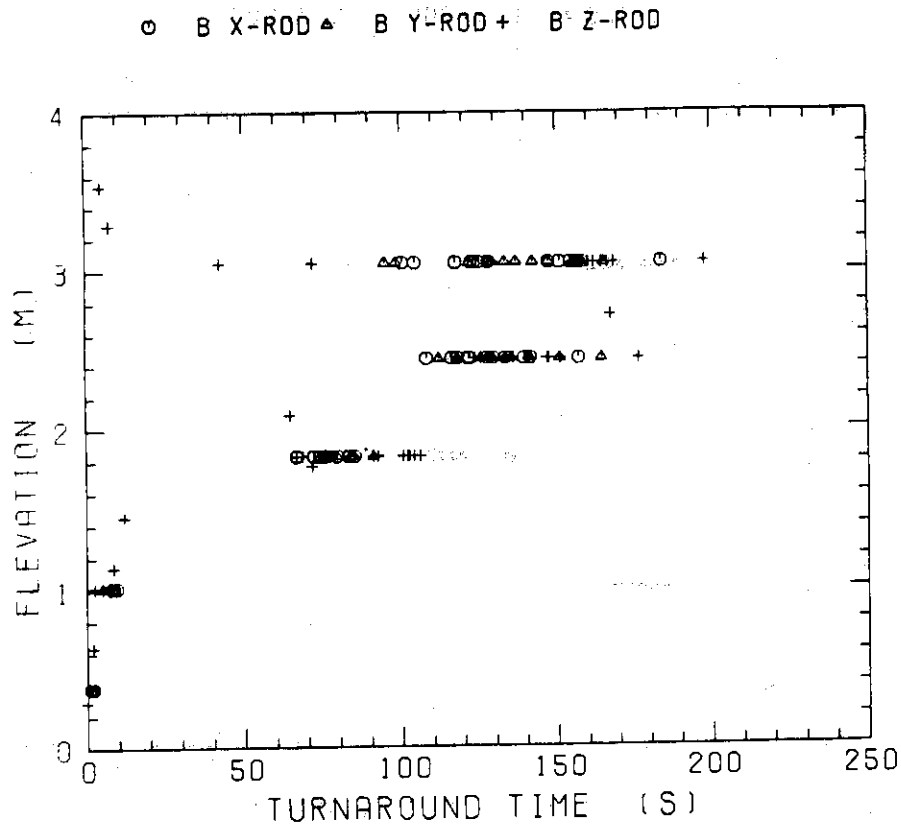

Fig. D-13 Turnaround time in medium power region (B region)

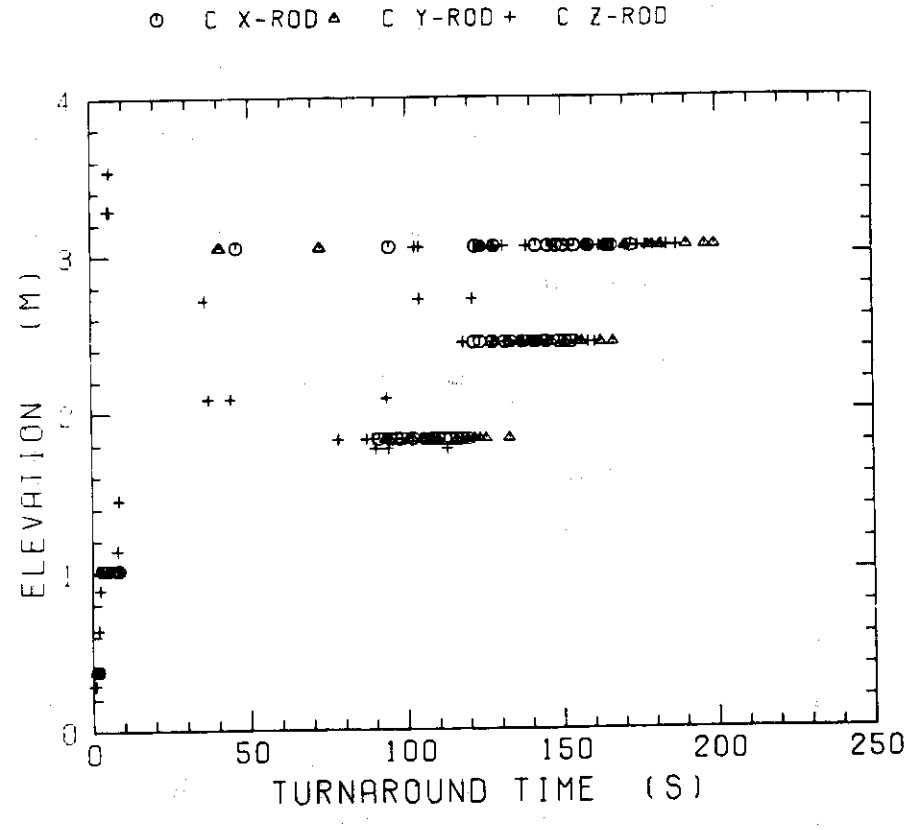

Fig. D-14 Turnaround time in low power region (C region)

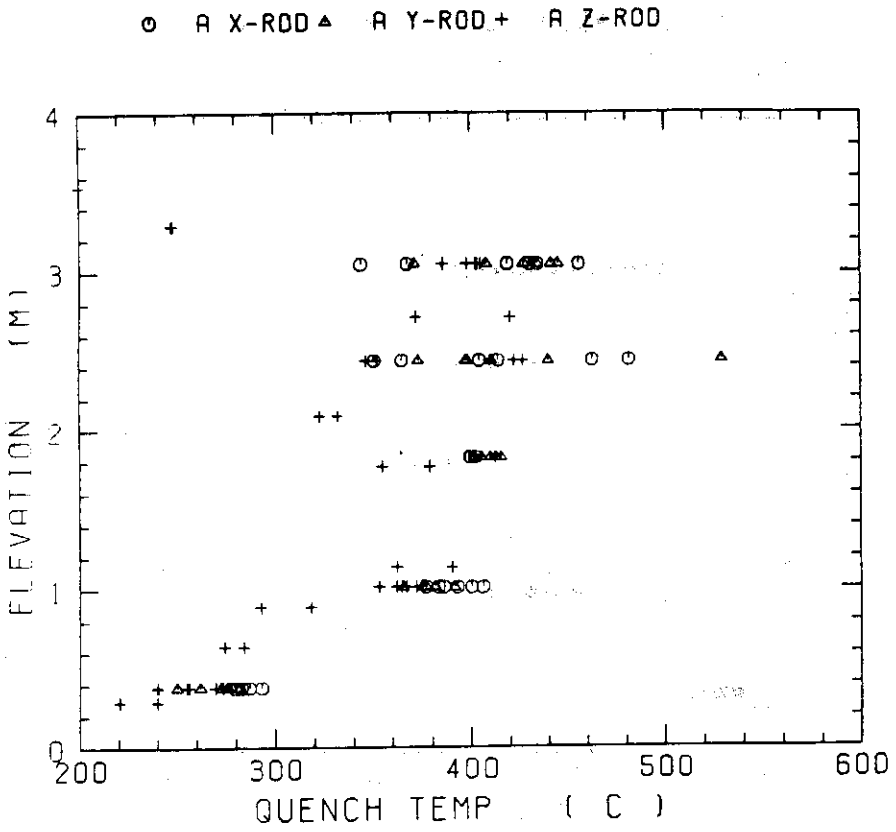

Fig. D-15 Quench temperature in high power region (A region)

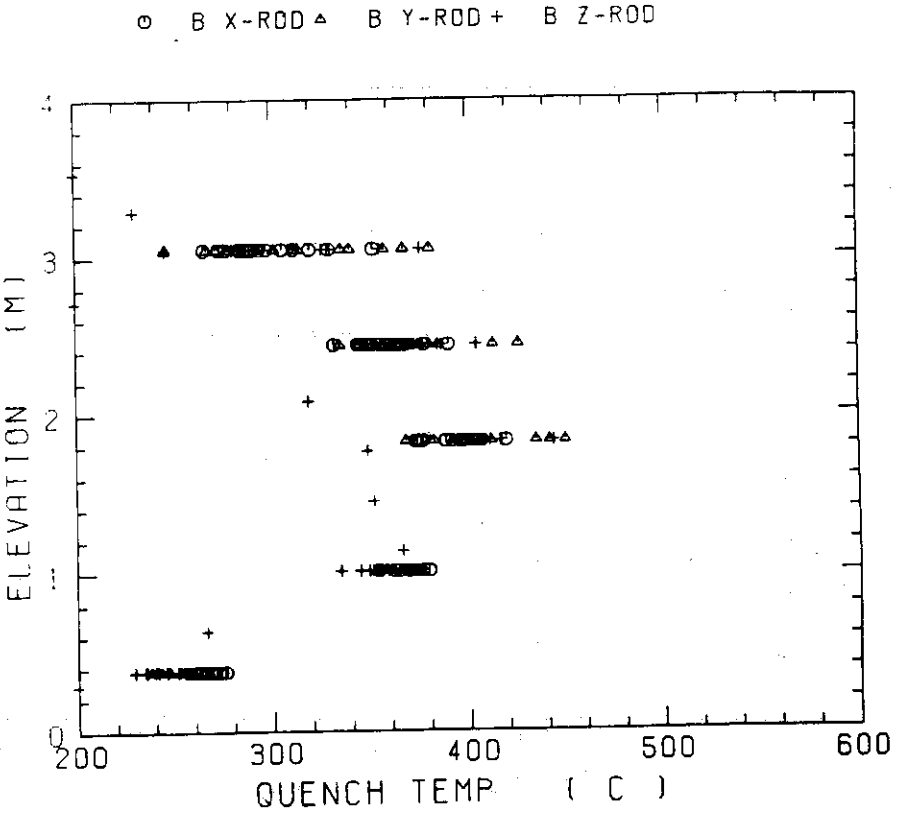

Fig. D-16 Quench temperature in medium power region (B region)

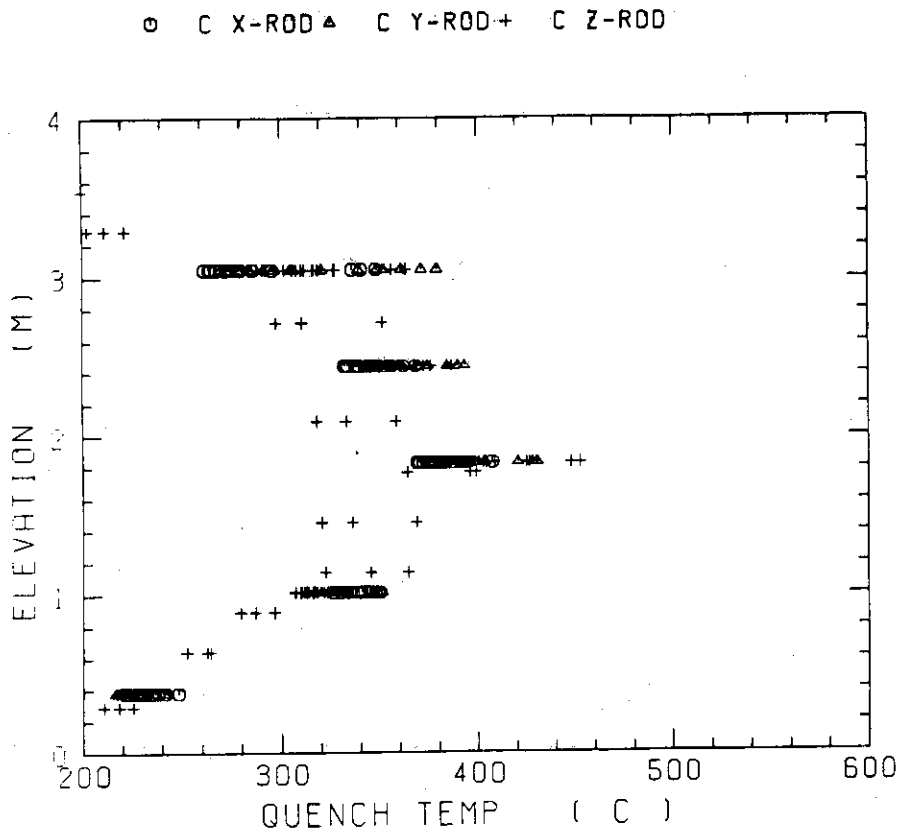

Fig. D-17 Quench temperature in low power region (C region)

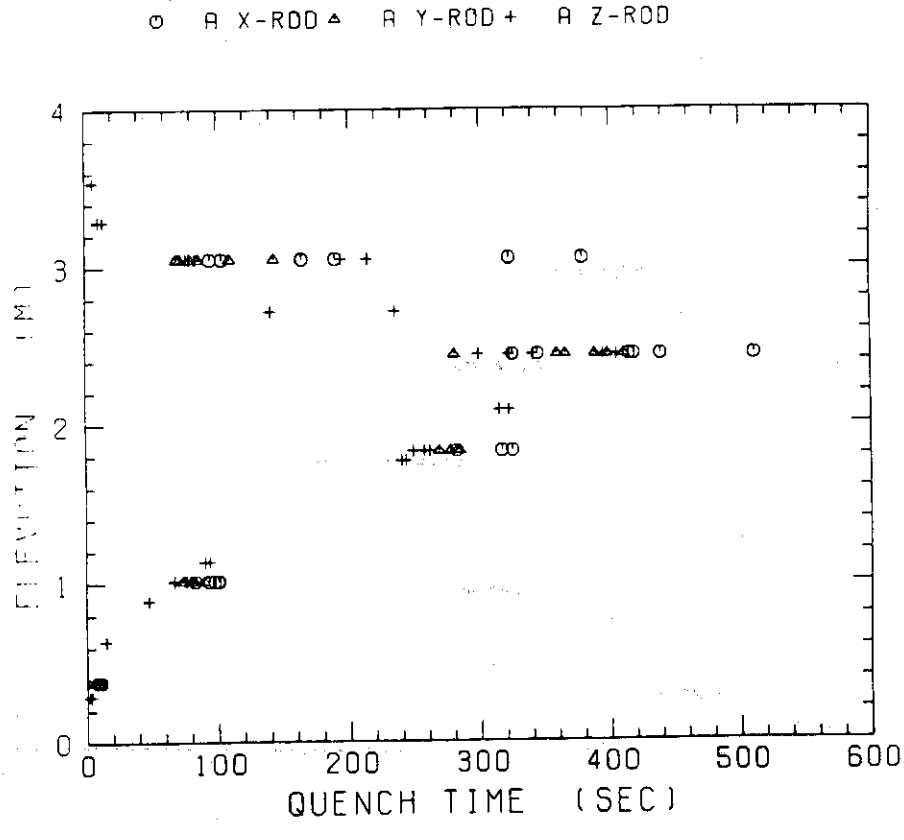

Fig. D-18 Quench time in high power region (A region)

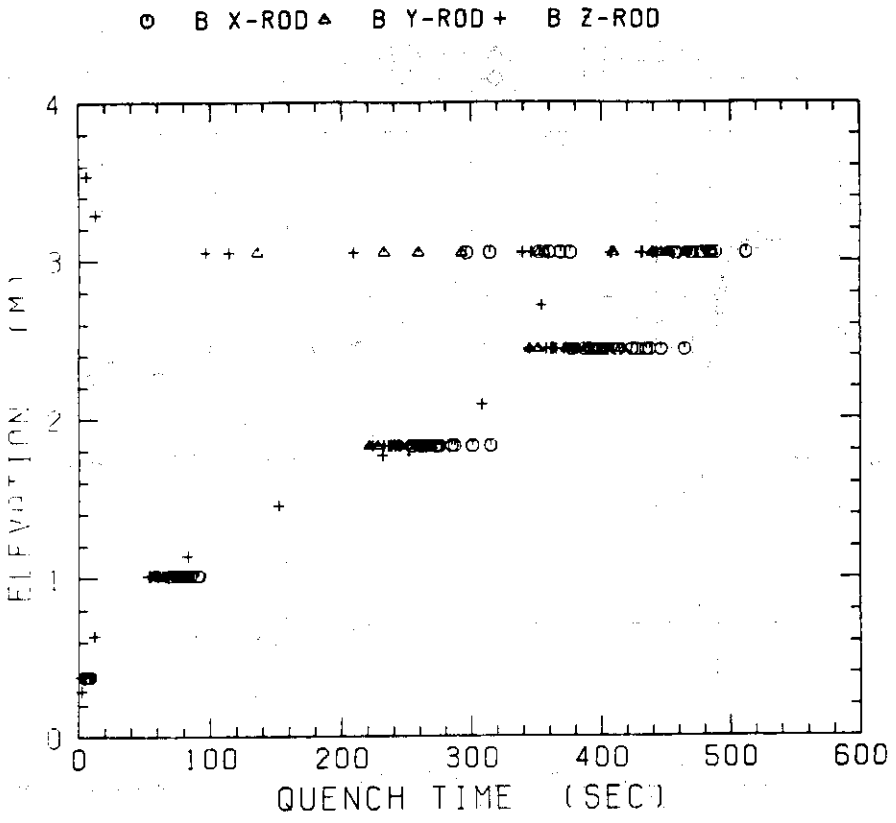

Fig. D-19 Quench time in medium power region (B region)

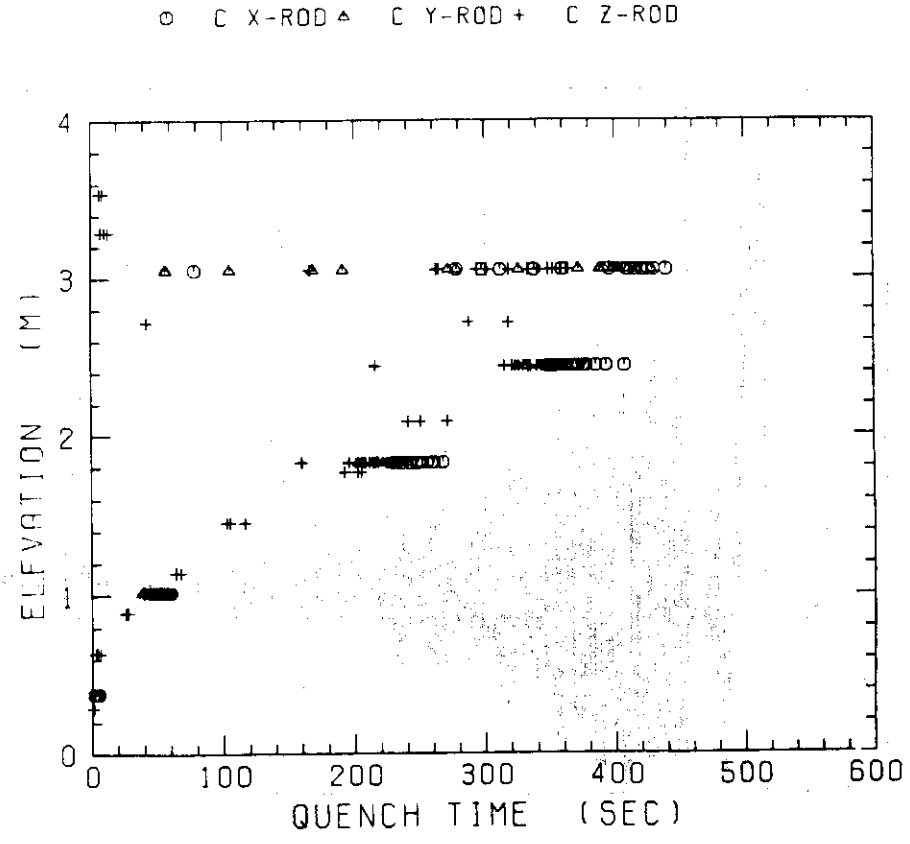

Fig. D-20 Quench time in low power region (C region)

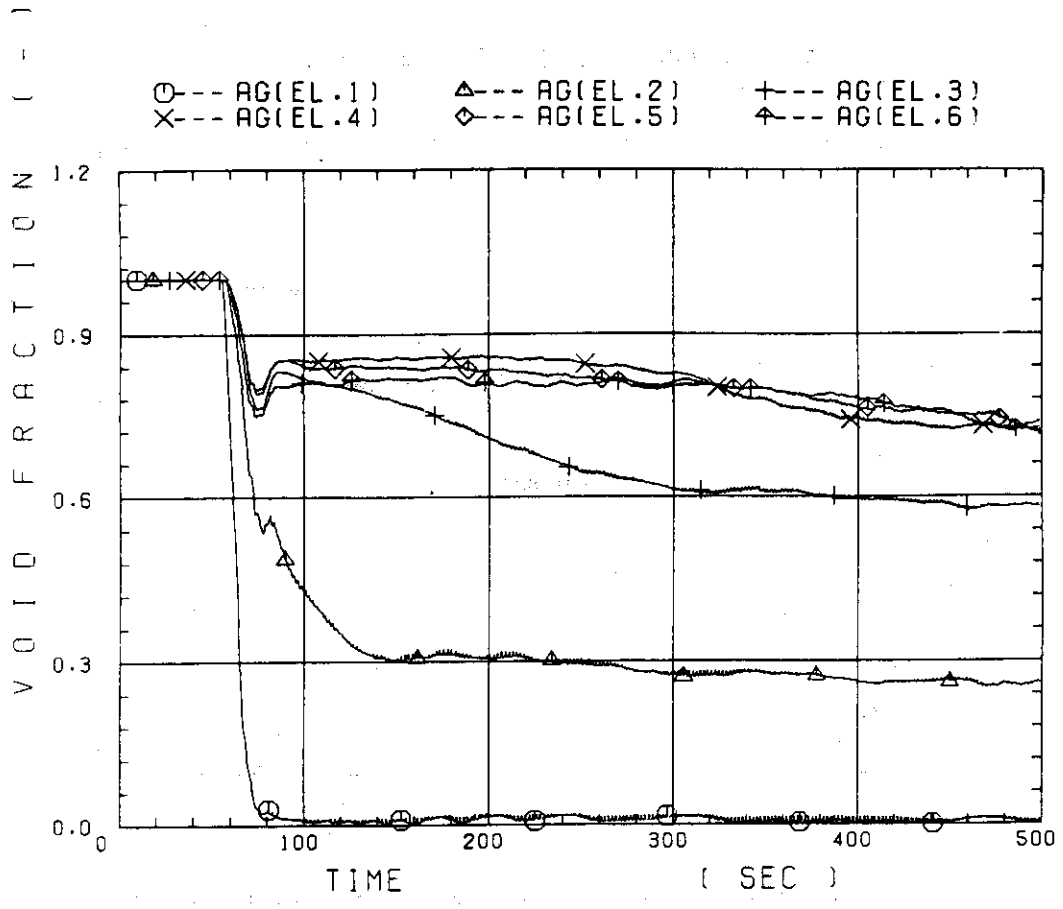

Fig. D-21 Void fraction in core

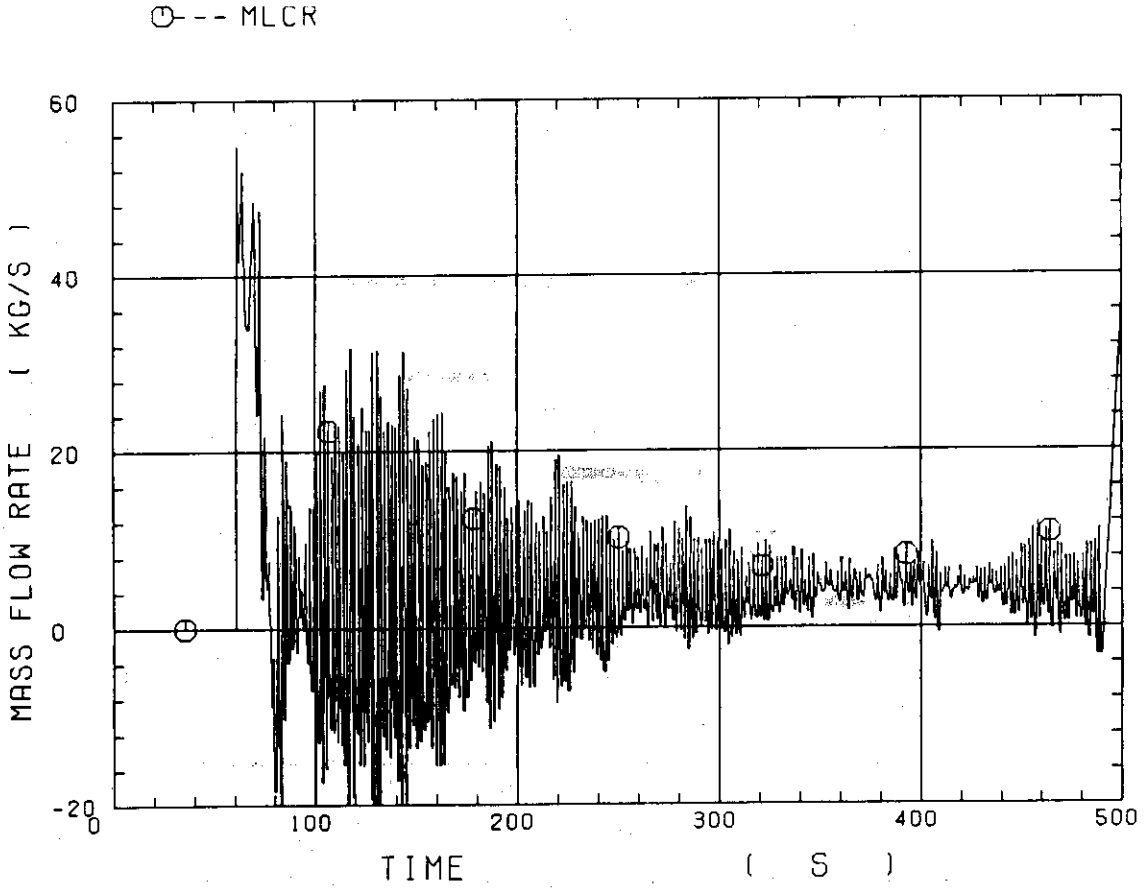

Fig. D-22 Core inlet mass flow rate

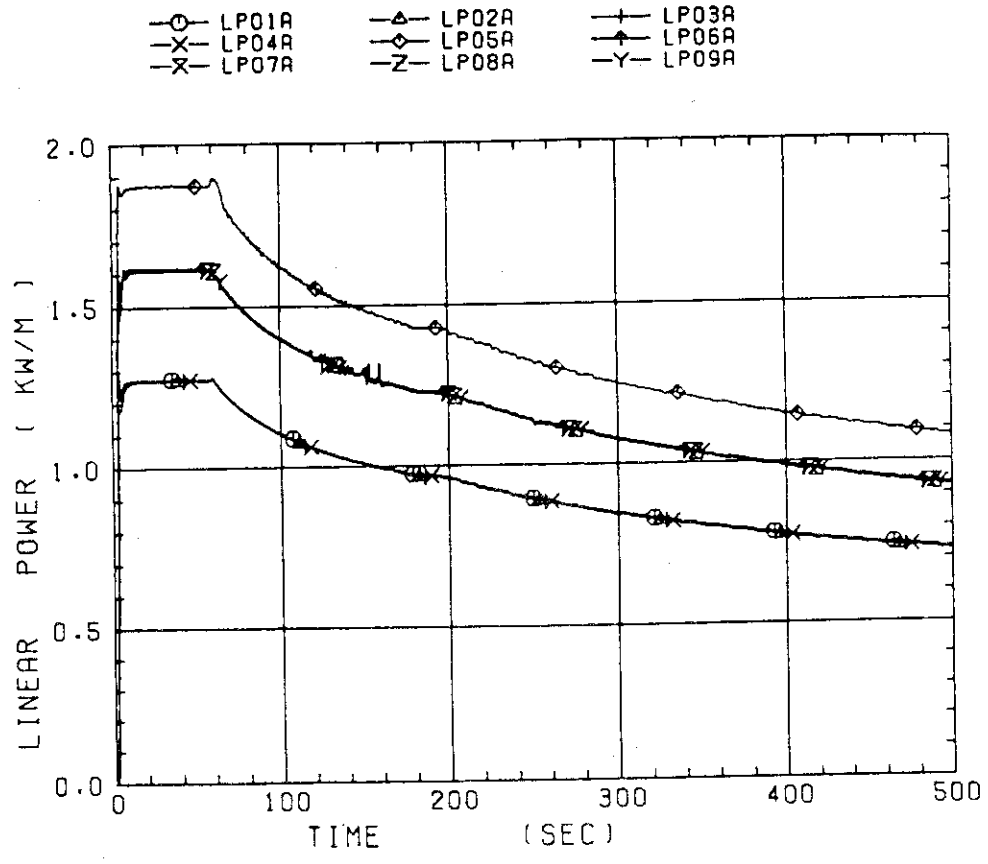

Fig. D-23 Average linear power of heater rod in each power unit zone

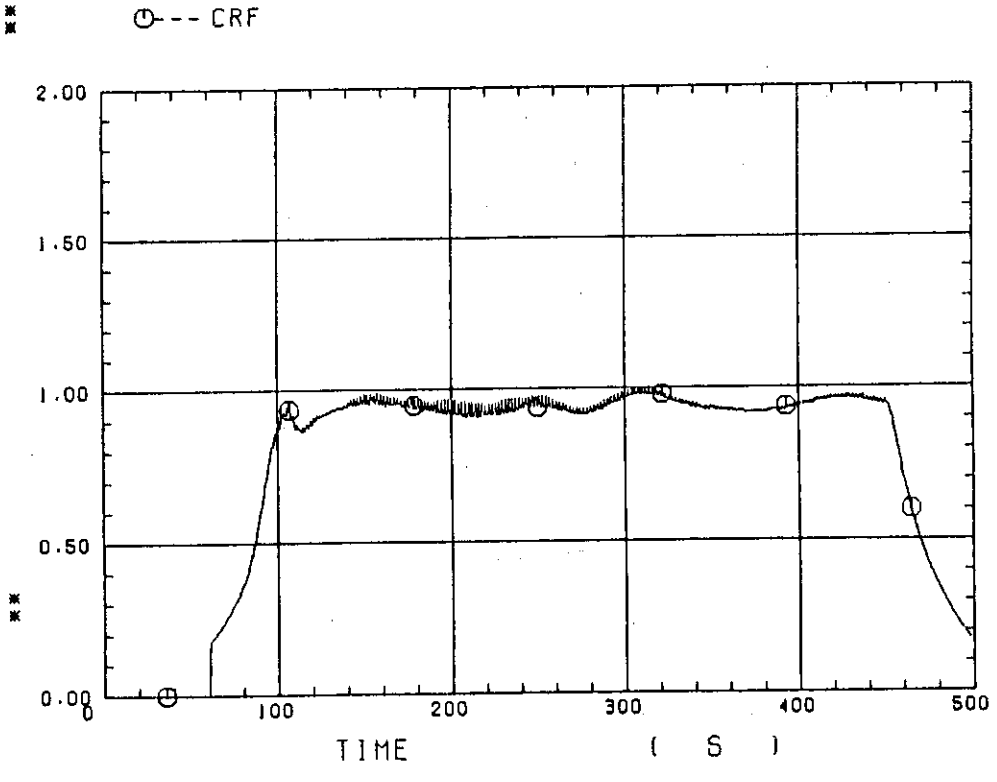

Fig. D-24 Carry-over rate fraction

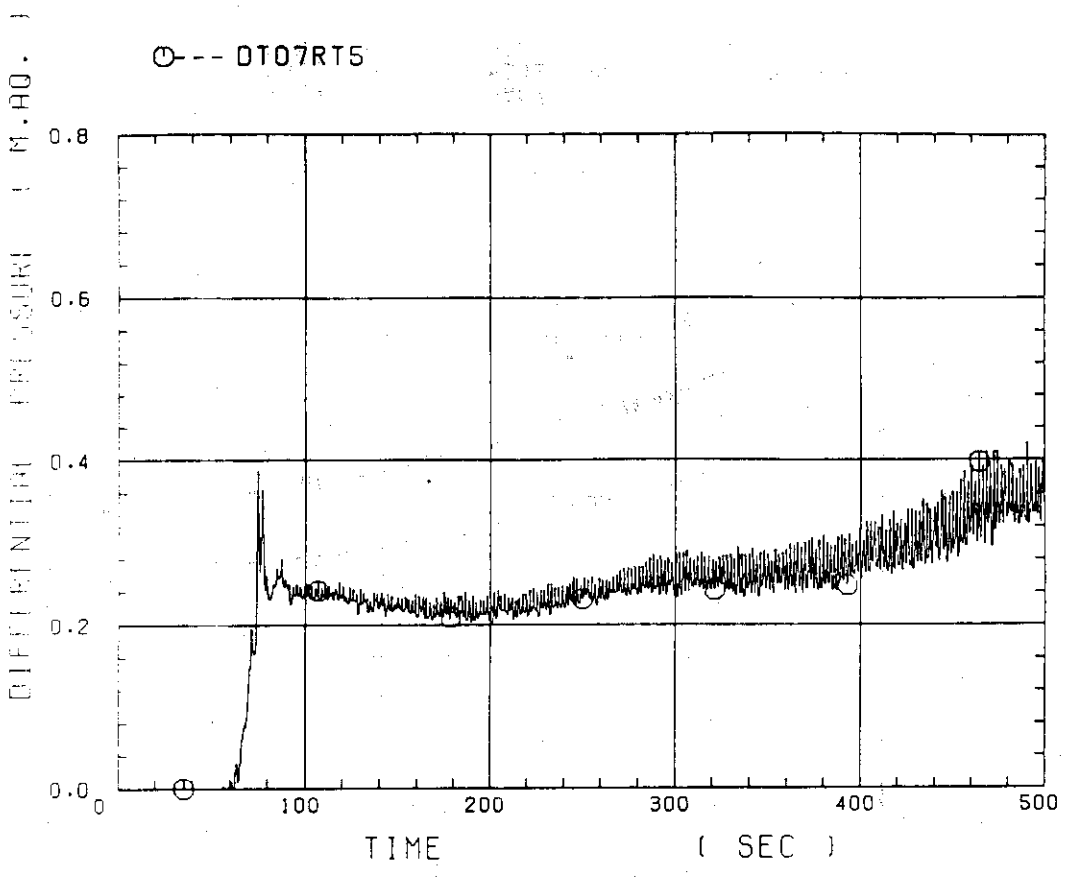

Fig. D-25 Differential pressure through upper plenum

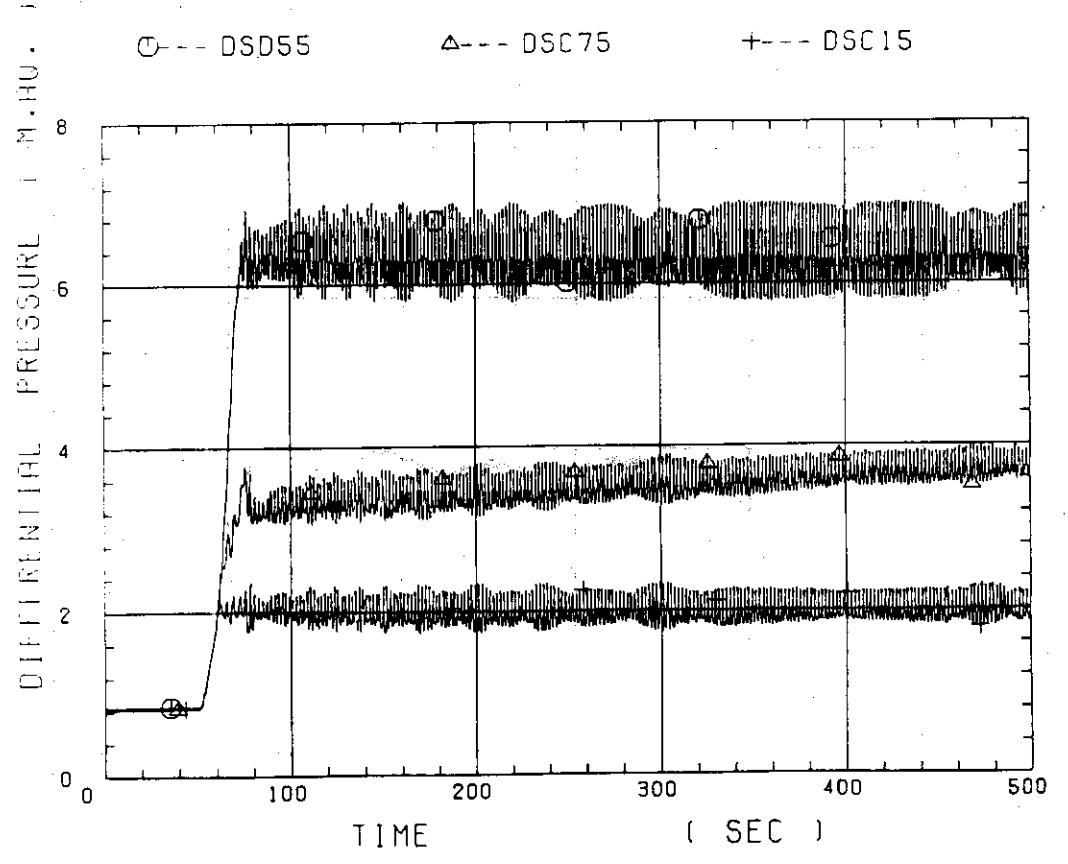

Fig. D-26 Differential pressure through downcomer, core, and lower plenum

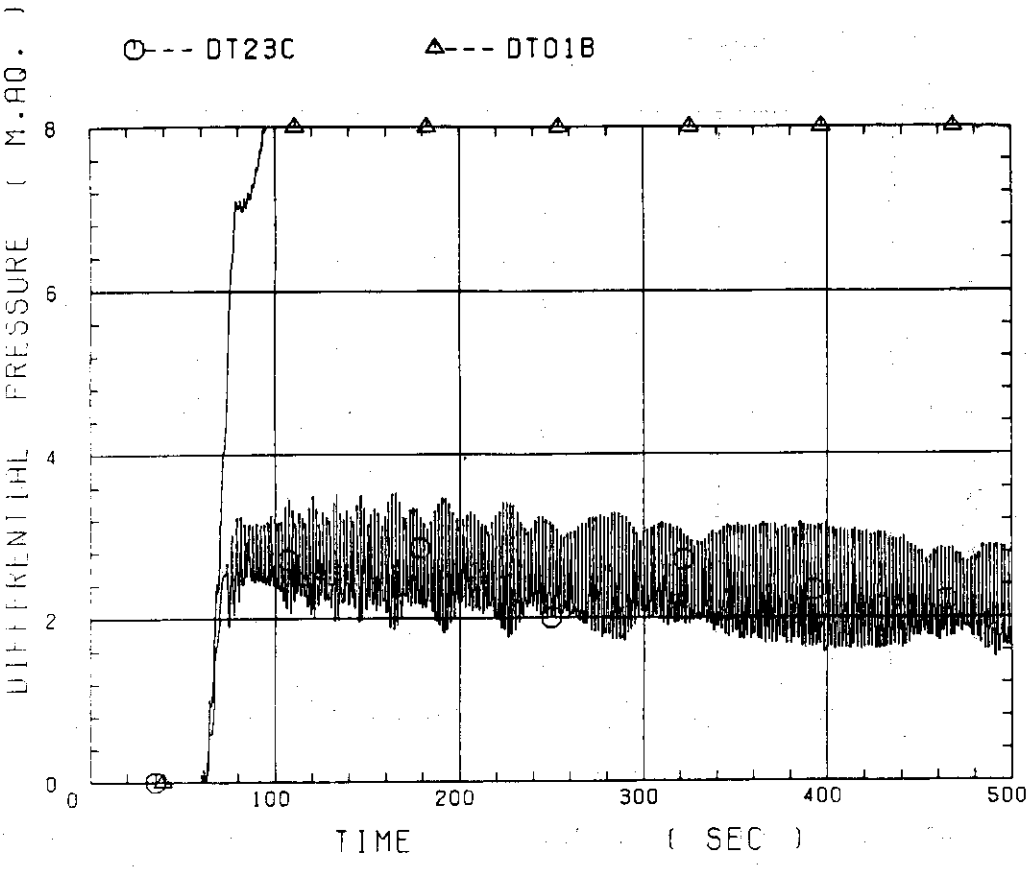

Fig. D-27 Differential pressure through intact and broken loops

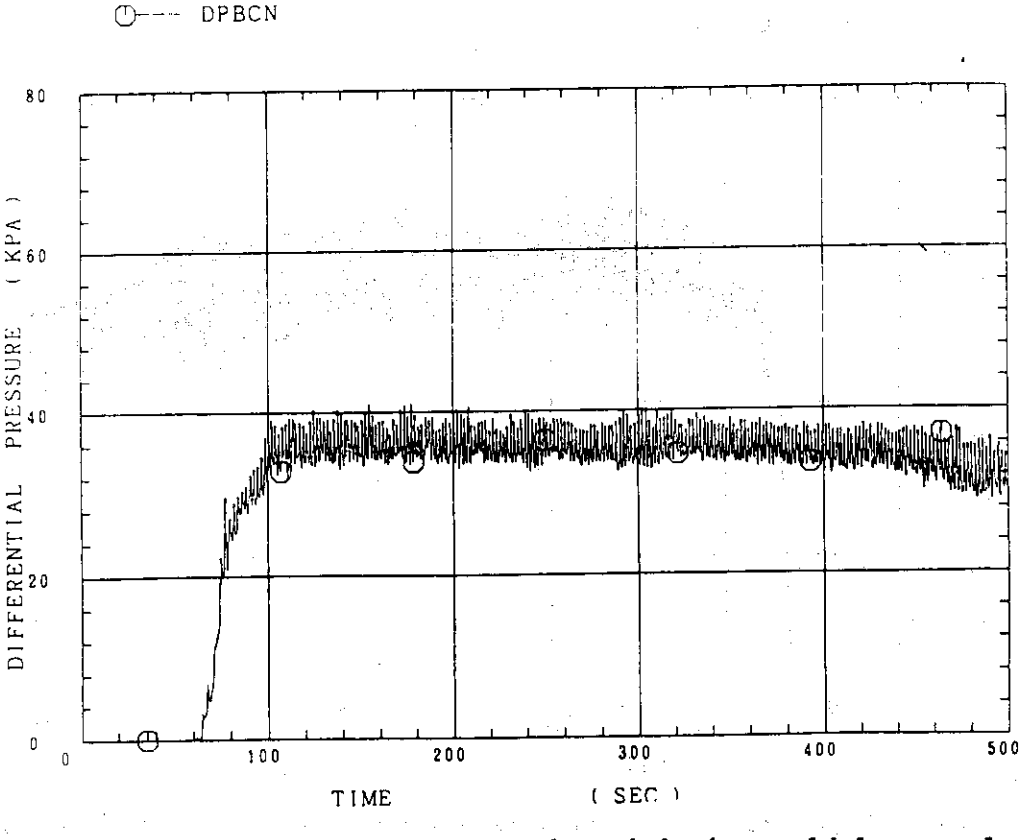

Fig. D-28 Differential pressure through broken cold leg nozzle

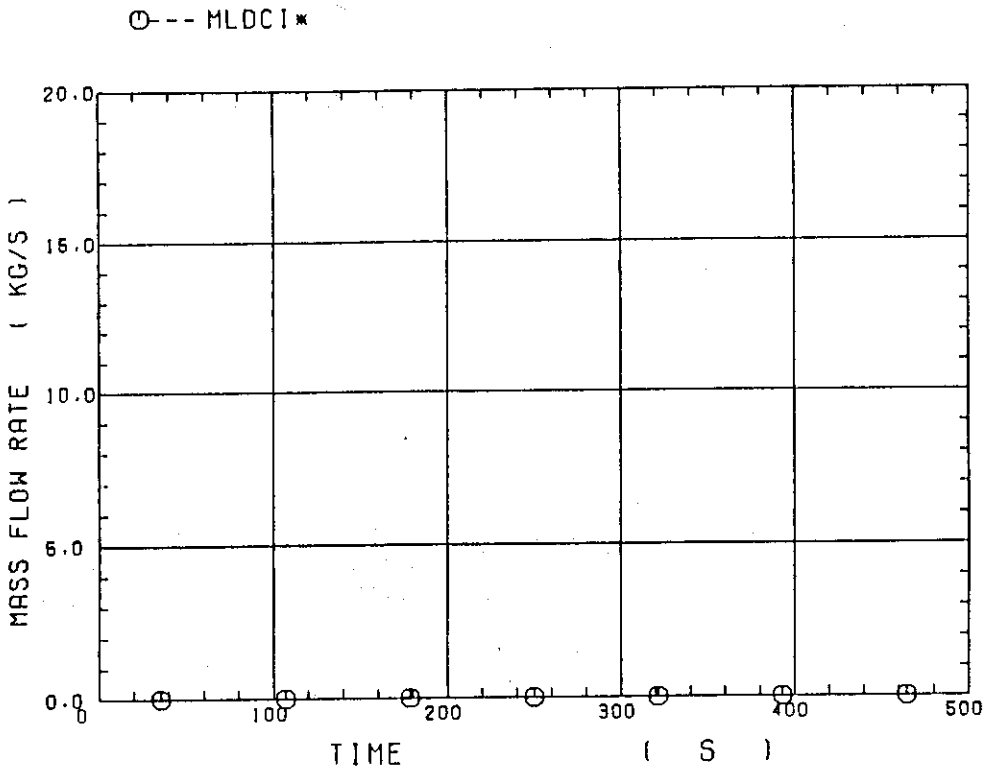

Fig. D-29 Total water mass flow rate from intact loops to downcomer

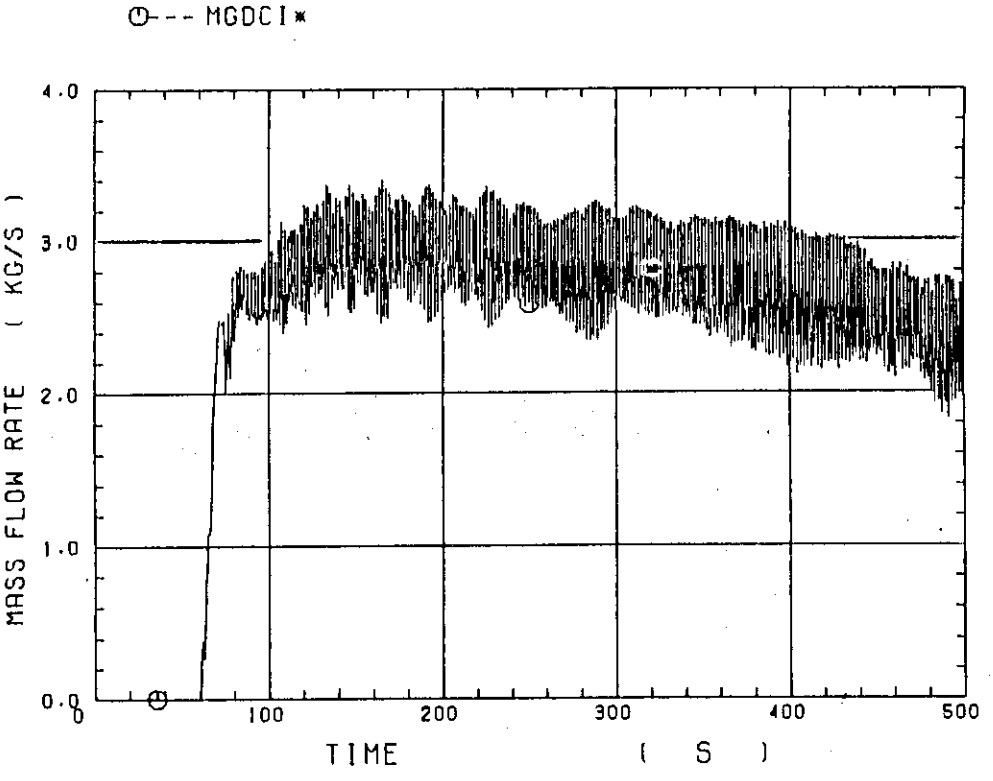

Fig. D-30 Total steam mass flow rate from intact loops to downcomer

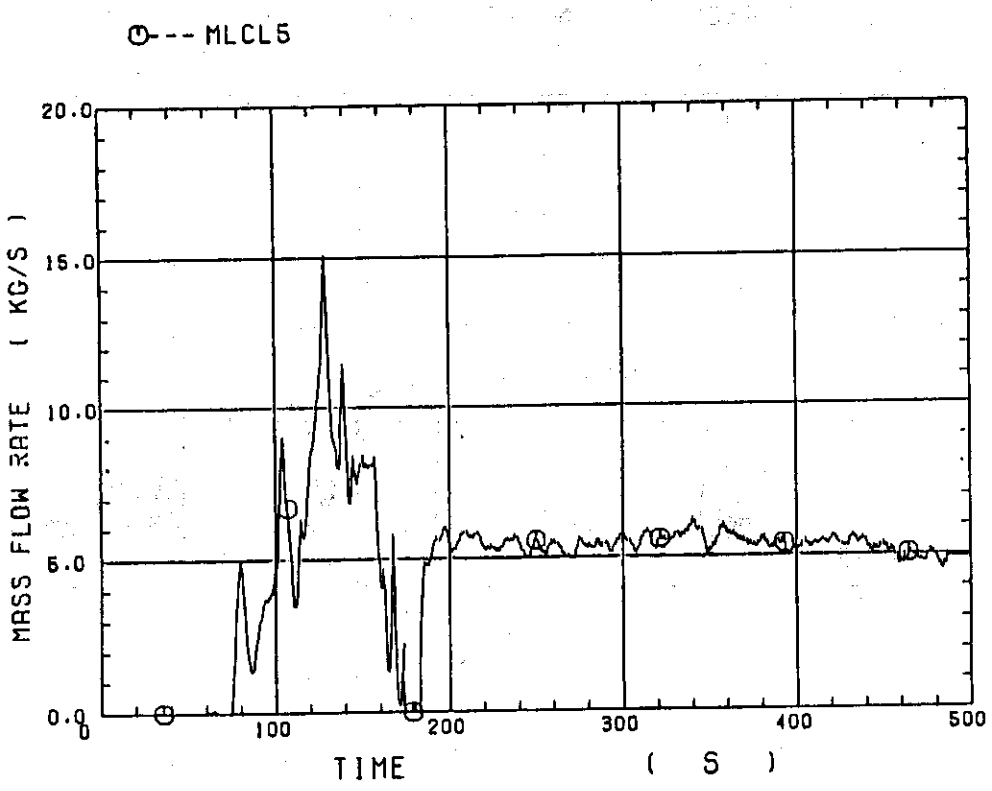

Fig. D-31 Water mass flow rate through broken cold leg nozzle

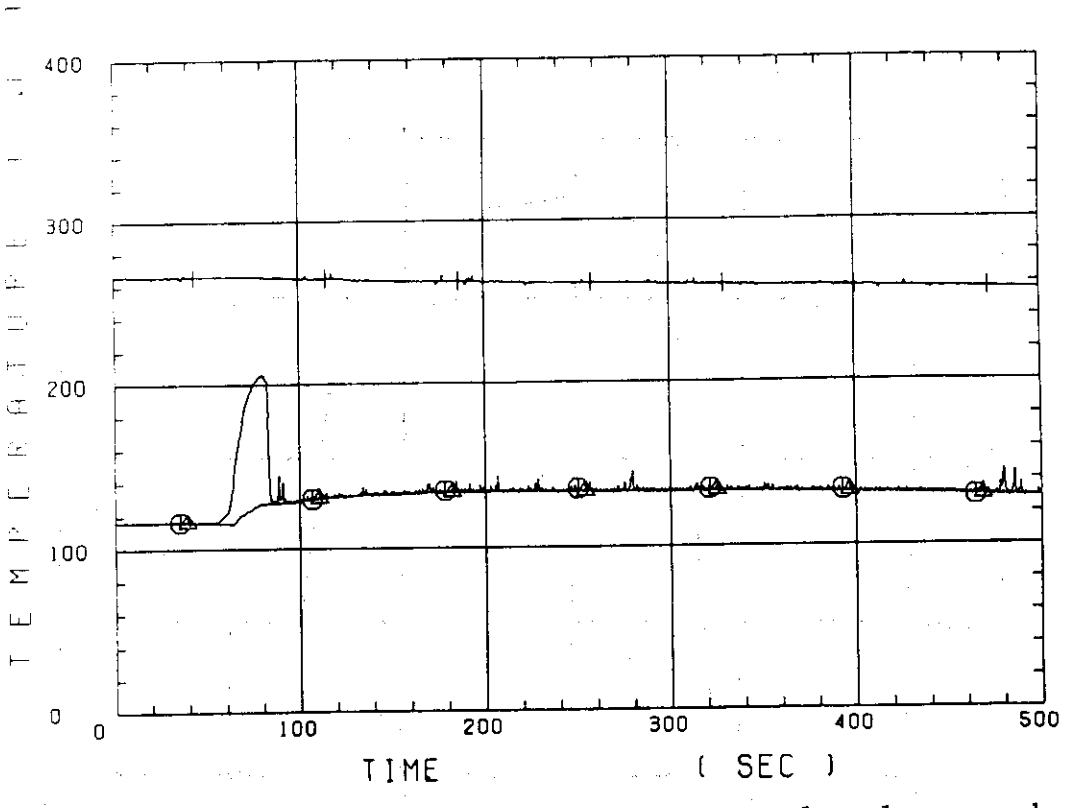

Fig. D-32 Fluid temperature in inlet plenum, outlet plenum, and secondary of steam generator 1

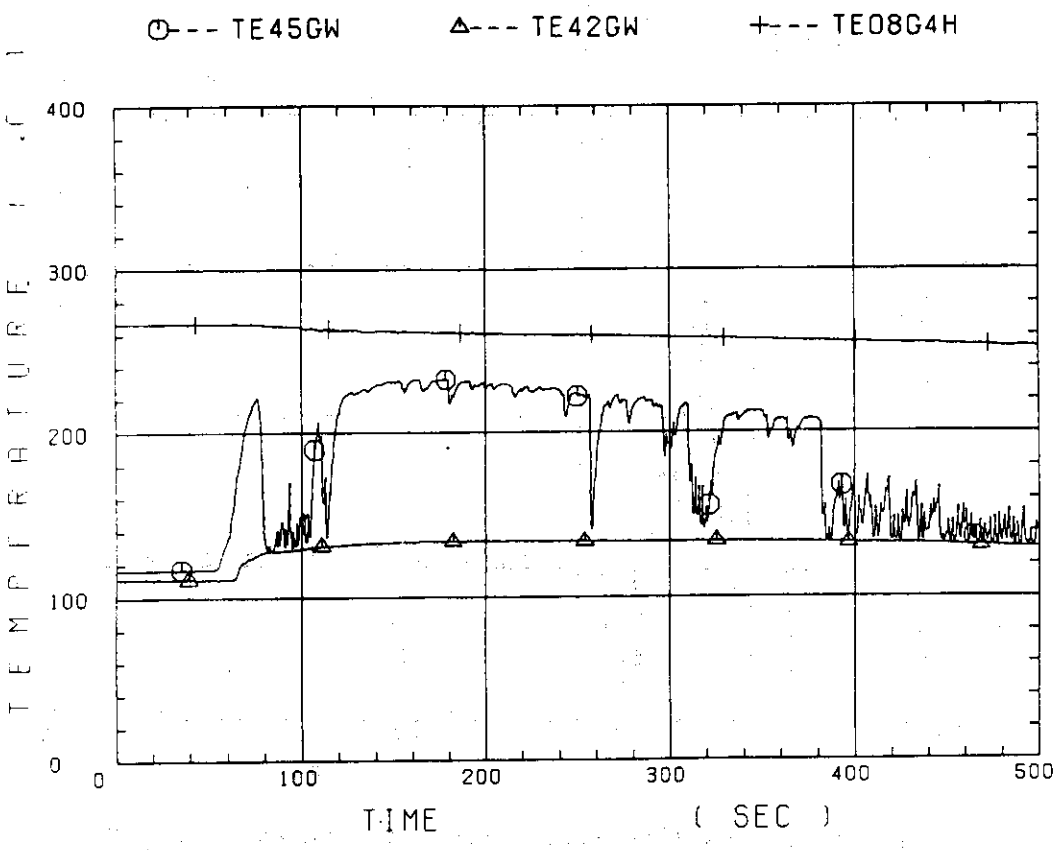

Fig. D-33 Fluid temperature in inlet plenum, outlet plenum, and secondary of steam generator 2

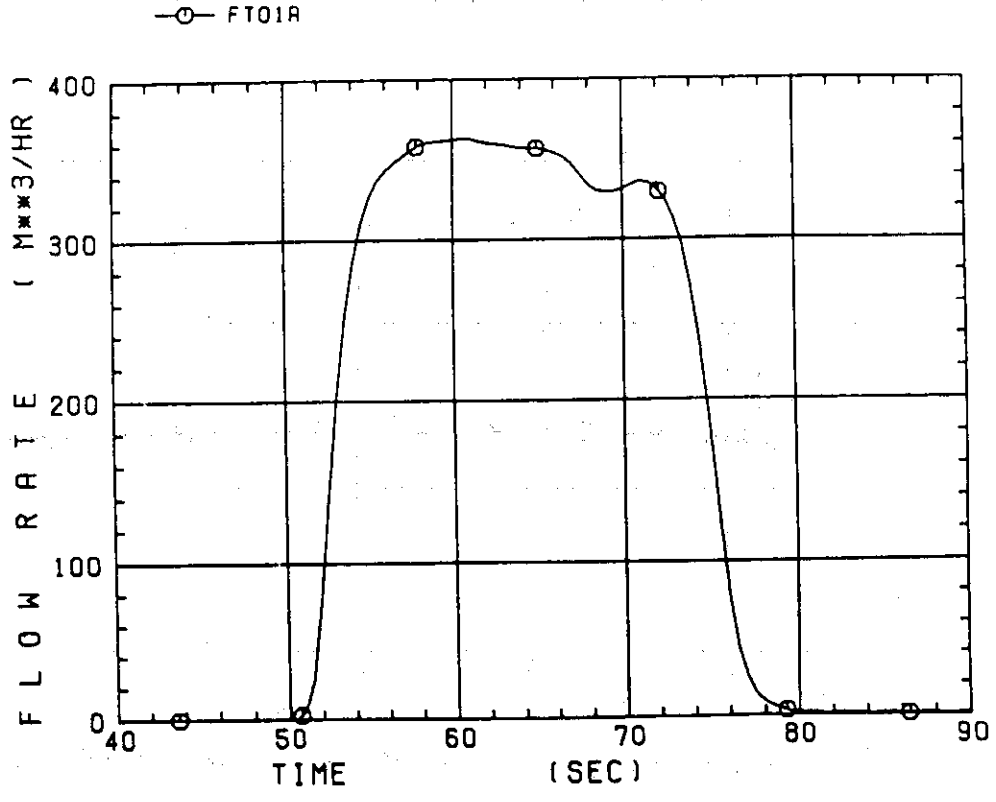

Fig. D-34 Total accumulator injection rate

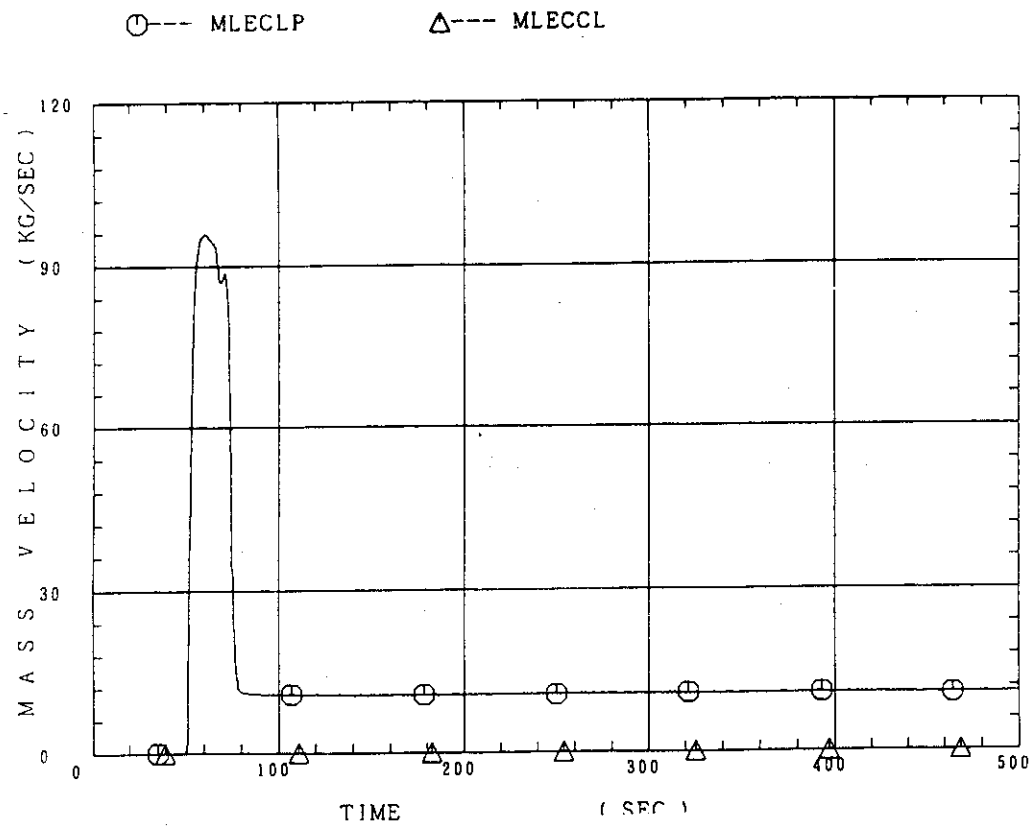

Fig. D-35 ECC water injection rates to lower plenum and to cold legs

Appendix E

Evaluation of core flooding mass flow rate

Figure list

Fig. E-1 Core flooding mass flow rates evaluated with Eqs.(1) and (2) for test C1-16 (Run 25)

Fig. E-2 Best estimate core flooding mass flow rates for test C1-16 (Run 25)

Fig. E-3 Integral masses flooded into core evaluated with Eqs.(1) and (2) and best - estimated for test C1-16 (Run 25)

Fig. E-4 Core flooding mass flow rates evaluated with Eqs.(1) and (2) for test C1-21 (Run 40)

Fig. E-5 Best estimate core flooding mass flow rates for Test C1-21 (Run 40)

Fig. E-6 Integral masses flooded into core evaluated with Eqs.(1) and (2) and best - estimated for test C1-21 (Run 40)

Fig. E-7 Core flooding mass flow rates evaluated with Eqs.(1) and (2) for test C1-22 (Run 41)

Fig. E-8 Best estimate core flooding mass flow rates for test C1-22 (Run 41)

Fig. E-9 Integral masses flooded into core evaluated with Eqs.(1) and (2) and best - estimated for test C1-22 (Run 41)

The reflood phenomena is a relatively slow transient and is assumed to be a steady state condition. In a stedy state condition, based on the mass balance relations of the system, the core flooding mass flow rates $\dot{m}_F$s can be written as follows:

By using the data measured at the downstream of the core inlet, $\dot{m}_F$ is derived as,

$$\dot{m}_F = \dot{m}_C + \dot{m}_U + \dot{m}_B + \Sigma\dot{m}_I \ , \tag{1}$$

where $\dot{m}_C$ and $\dot{m}_U$ are the mass accumulation rates in the core and the upper plenum respectively. The $\dot{m}_B$ and $\dot{m}_I$ are the mass flow rates in the broken loop and the intact loop, respectively.

By using the data measured at the upsteam of the core inlet, $\dot{m}_F$ is is derived as,

$$\dot{m}_F = \Delta\dot{m}_{DL} - \dot{m}_D - \dot{m}_O + \dot{m}_{ECC/LP}, \tag{2}$$

where $\dot{m}_{CL}$, $\dot{m}_O$ and $\dot{m}_{ECC/LP}$ are the mass flow rates of the water flowing into and overflowing from the downcomer and the mass flow rate of the ECC water injected into the lower plenum, respectively.

The $\dot{m}_I$s and $\dot{m}_B$ can be obtained from the pressure drops at the pump simulators with orifices by assuming the K-factor of the orifice is constant or from the data of Pitot tubes.

The values of $\dot{m}_C$, $\dot{m}_D$ and $\dot{m}_U$ can be evaluated with the differential pressure ΔP_C, ΔP_U and ΔP_U, respectively, as follows:

$$\dot{m}_n = d(\Delta P_n S_n/g)/dt \qquad (n : C,D,U) \ , \tag{3}$$

where g is the gravitational acceleration and S_n is the crossectional area. The value of $\dot{m}_O$ can be obtained from the liquid level X in the Containment tank 1 as,

$$\dot{m}_O = d(X\ \rho_\ell S_O)/dt \ , \tag{4}$$

where ρ_ℓ is the liquid density and S_O is the cross sectional area of the containment tank.

The value of $\dot{m}_{DL}$ is obtained from the following mass and energy balance relations at each ECC port under the assumption of thermal

equilibrium:

$$\dot{m}_{DV} + \dot{m}_{DL} = \dot{m}_{ECC} + \dot{m}_{I} \quad , \tag{5}$$

$$(\dot{m}_{DV} + \dot{m}_{DL})i = \dot{m}_{ECC} i_{ECC} + \dot{m}_{I} i_{I} \quad , \tag{6}$$

$$\text{if} \quad i_g \geq i \geq i_\ell \quad , \quad (\dot{m}_{DV} + \dot{m}_{LD})i = \dot{m}_{DV} i_g + \dot{m}_{DL} i_\ell$$

$$\text{if} \quad i \geq i_g \quad , \quad \dot{m}_{DL} = 0 \quad , \tag{7}$$

$$\text{if} \quad i \geq i_\ell \quad , \quad \dot{m}_{DV} = 0 \quad ,$$

where i is enthalpy of fluid and i_ℓ and i_g are enthalpies of liquid and steam at the saturation temperature, respectively.

The fluid temperatures can be measured with thermocouples immersed in the fluid and the enthalpies i_I, i_{ECC} can be estimated.

Mass balance calculations were performed with Eqs.(1) and (2), since it was found that the water entering the steam generator was completely evaporated. In the differentiation, higher frequency components of the data tends to be amplified more. Therefore, in the differentiation of the differential pressure data, the smoothing procedure was used to suppress the high frequency components of the data. Figures E-1, E-4 and E-7 show the flooding mass flow rates, $\dot{m}_F$s, calculated from Eqs.(1) and (2) by averaging data in 20 seconds for tests C1-16 (Run 25), C1-21 (Run 40) and C1-22 (Run 41), respectively.

In the ACC injection period, the calculated values, $\dot{m}_F$s, are slightly different from each other. This discrepancy may be caused by in accuracy of the mass flow rate injected into the system and by the unaccounting of the storage of water in the cold leg pipe. The former might be introduced from the slow time response (time constant 1 second) and the change of the gas volume in the injection line. In this period, specially before the steam generation from the core became noticable, the mass flow rate, $\dot{m}_F$, calculated with Eq.(1) is reasonable, since the calculation needs the increasing rates of the masses in the core and the upper plenum and their accuracy is enough for our estimation.

In the LPCI injection period, the calculated values, $\dot{m}_F$s, are almost identical with each other. The discrepancy was caused by the disregard of the steam generation in the downcomer due to the hot wall of the pressure

vessel in the calculation with Eq. (2). It was estimated that the disregard of the the downcomer steam generation was caused the error of 0.25 kg/s on predicted $\dot{m}_F$. The estimation was made by comparing the results of the tests with hot and cold downcomer conditions. In the LPCI injection period except for the early period, the mass flow rates, $\dot{m}_F$s, calculated with Eqs.(1) and (2) are reasonable, since the error from the injected ECC flow rate measurement is negligible under the quasi-steady state condition appeared in this period and the error caused by the steam generation in the downcomer is small.

In order to obtain the best estimate core inlet mass flow rate, the calculation with Eq.(1) were performed by reducing the averaging time. Figures E-2, E-5 and E-8 show the best estimate core inlet mass flow rate. In this calculation, the smoothing procedure was performed by averaging $\dot{m}_F$ in 10 seconds for tests C1-16 (Run 25), C1-21 (Run 40) and C1-22 (Run 41), respectively. Therefore the core inlet velocity at the reflood initiation was slightly lowered. The relation between the integral core-flooded water mass evaluated with Eqs.(1) and (2) and best-estimated are shown in Figs.E-3, E-6 and E-9 for tests C1-16 (Run 25), C1-21 (Run 40) and C1-22 (Run 41), respectively.

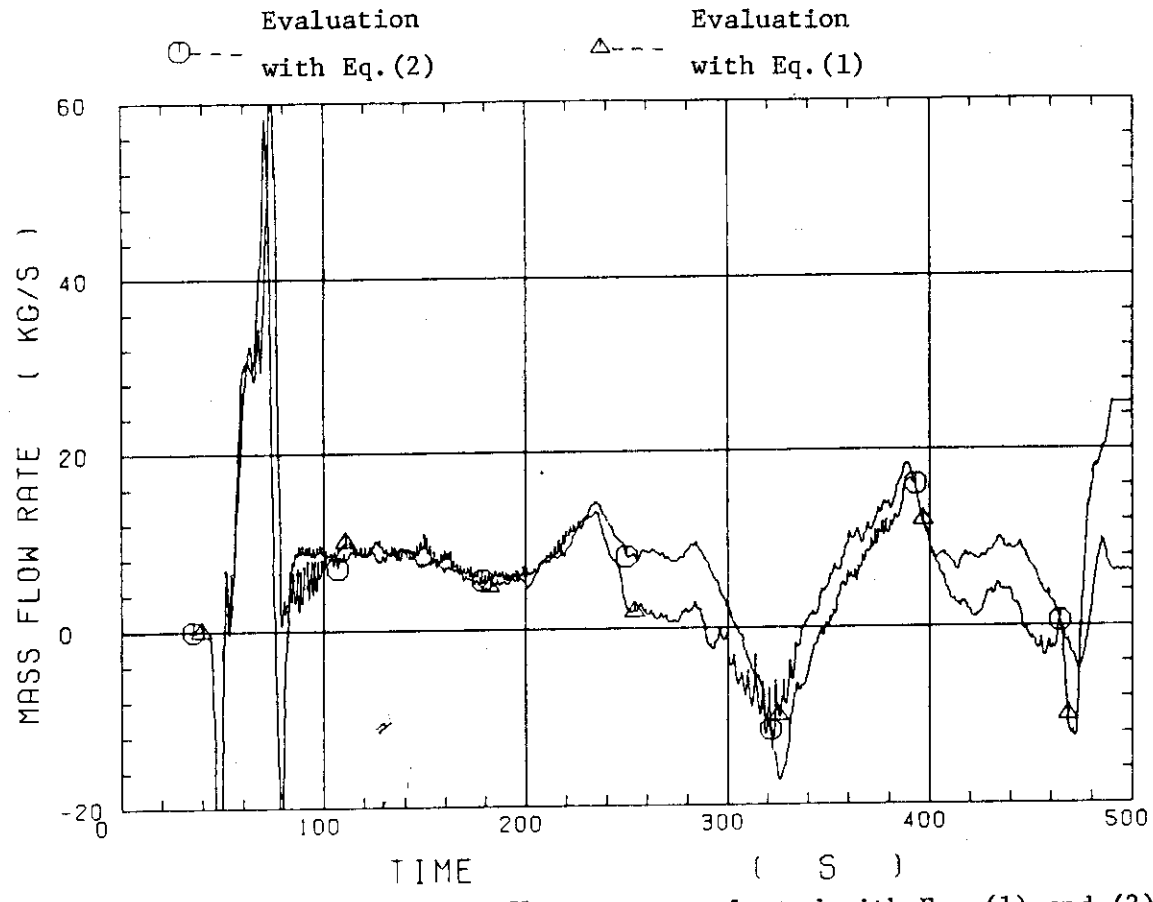

Fig. E-1 Core flooding mass flow rates evaluated with Eqs.(1) and (2) for test C1-16 (Run 25)

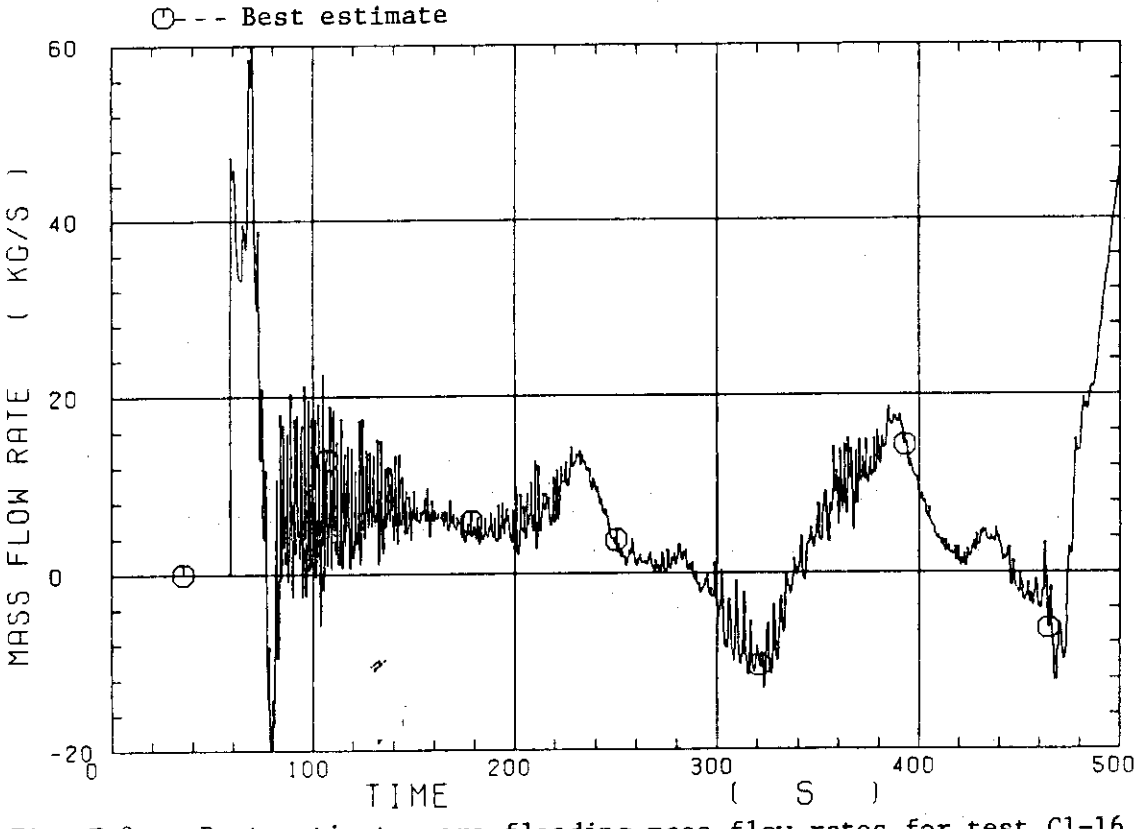

Fig. E-2 Best estimate core flooding mass flow rates for test C1-16 (Run 25)

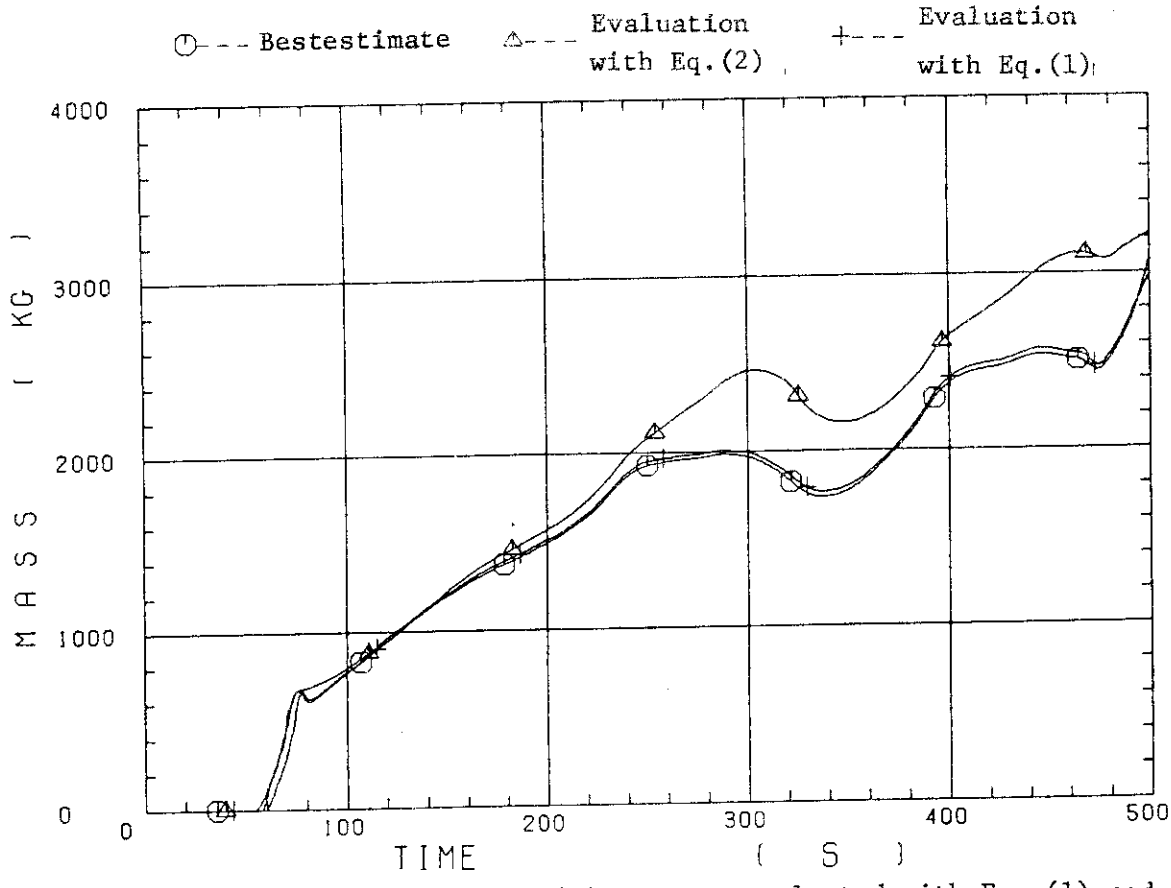

Fig. E-3 Integral masses flooded into core evaluated with Eqs.(1) and (2) and best - estimated for test C1-16 (Run 25)

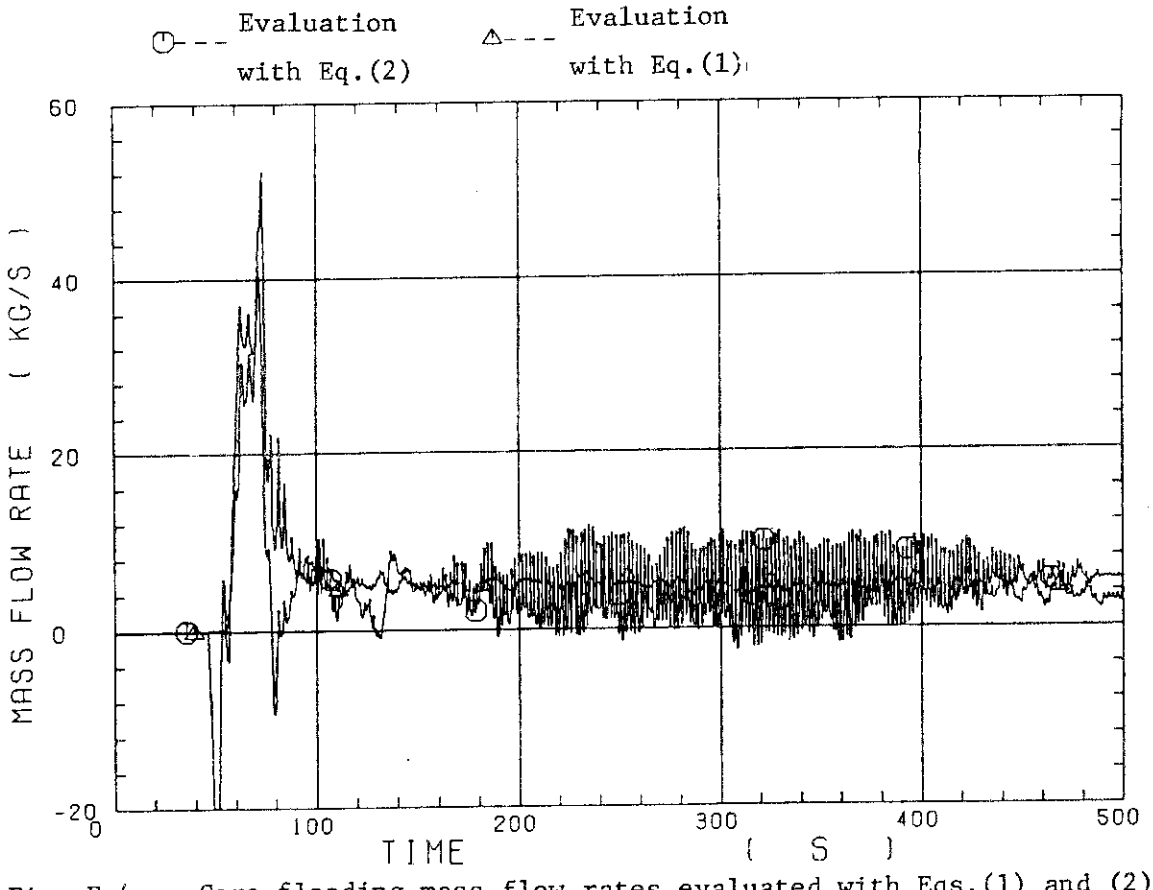

Fig. E-4 Core flooding mass flow rates evaluated with Eqs.(1) and (2) for test C1-21 (Run 40)

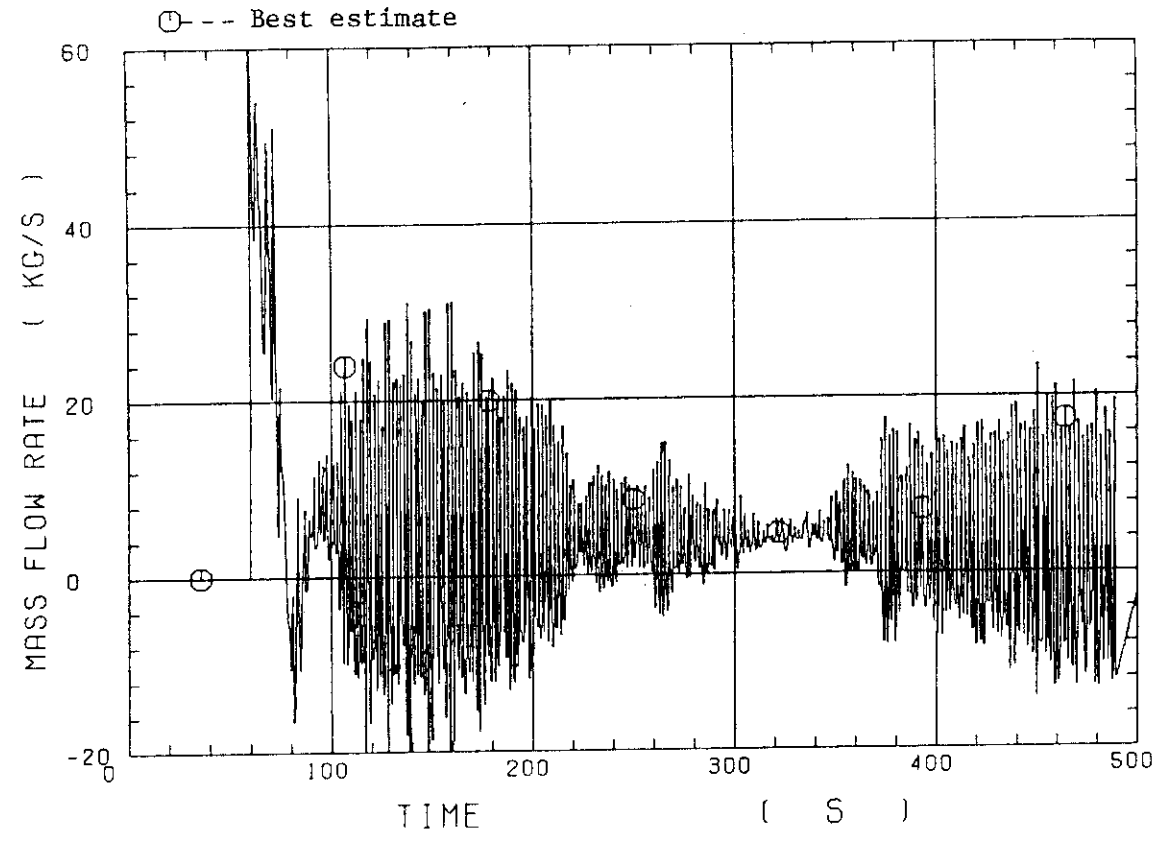

Fig. E-5 Best estimate core flooding mass flow rates for Test C1-21 (Run 40)

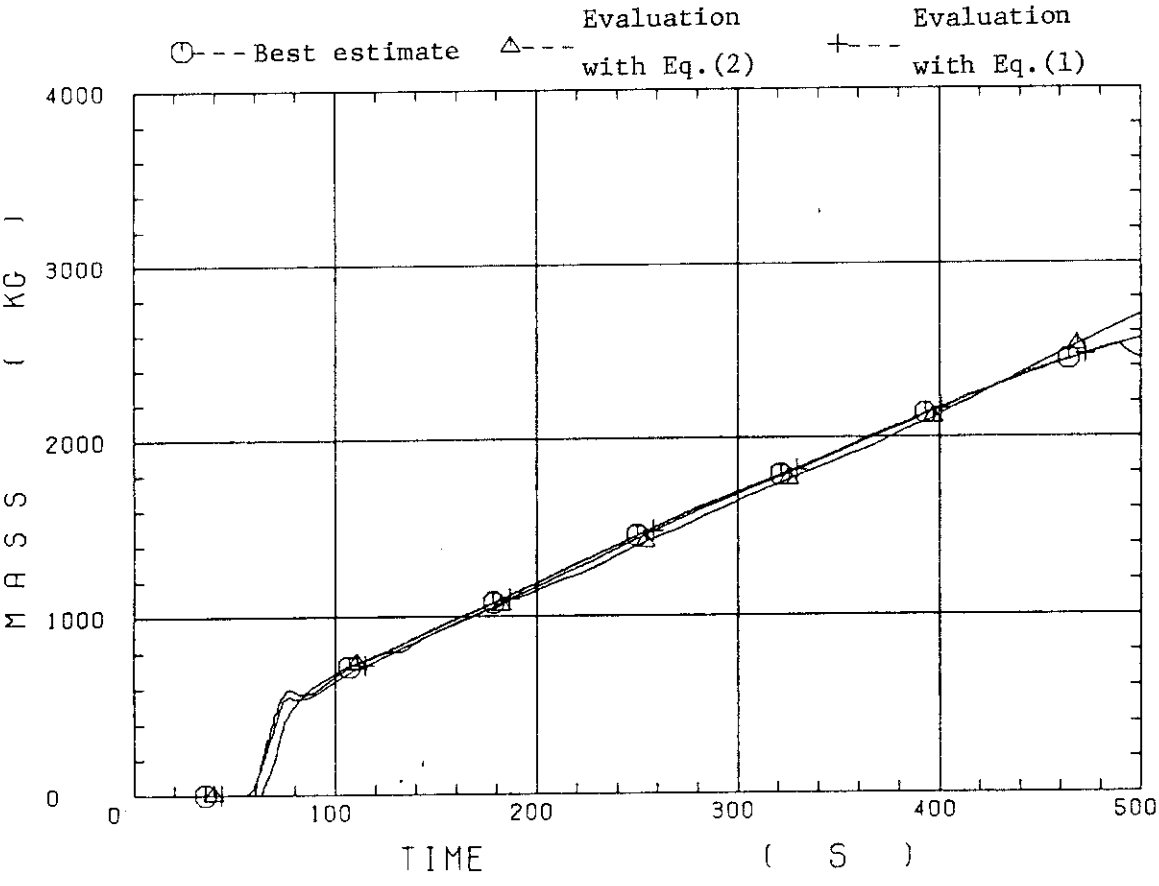

Fig. E-6 Integral masses flooded into core evaluated with Eqs.(1) and (2) and best - estimated for test C1-21 (Run 40)

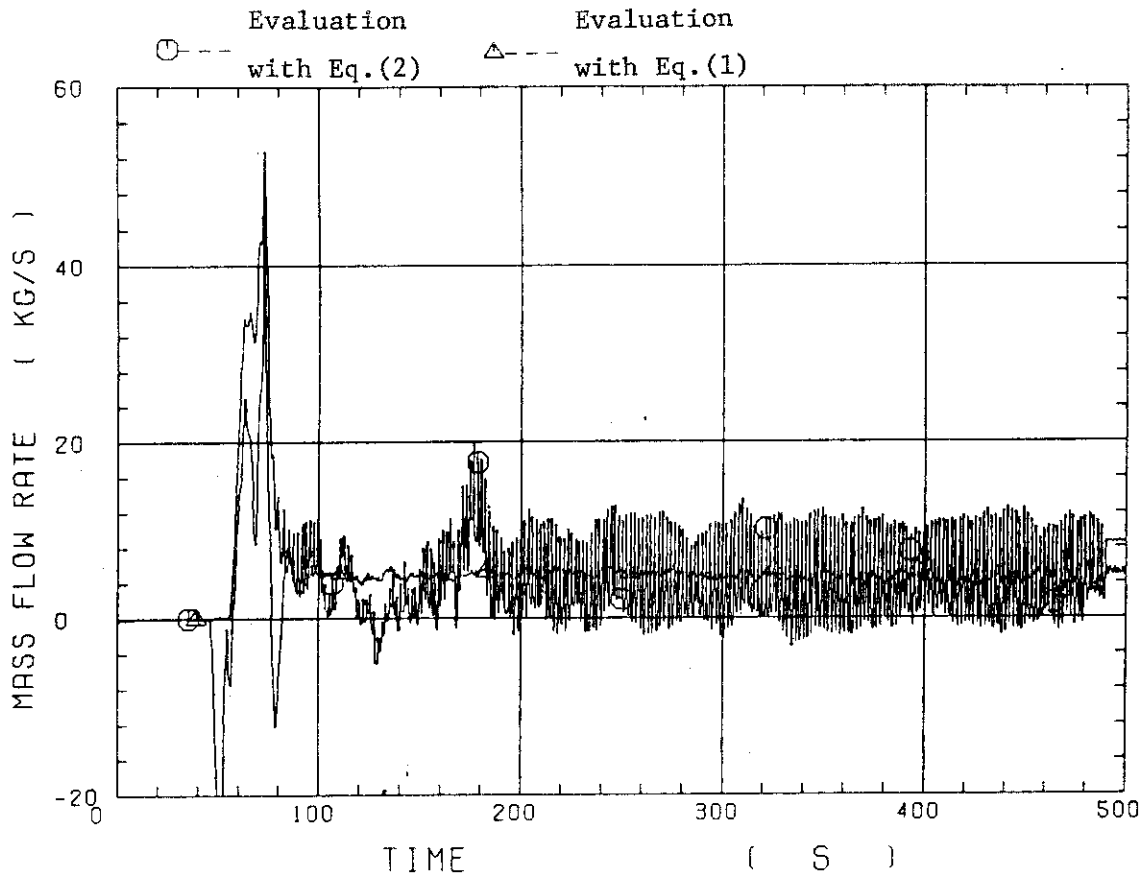

Fig. E-7 Core flooding mass flow rates evaluated with Eqs.(1) and (2) for test C1-22 (Run 41)

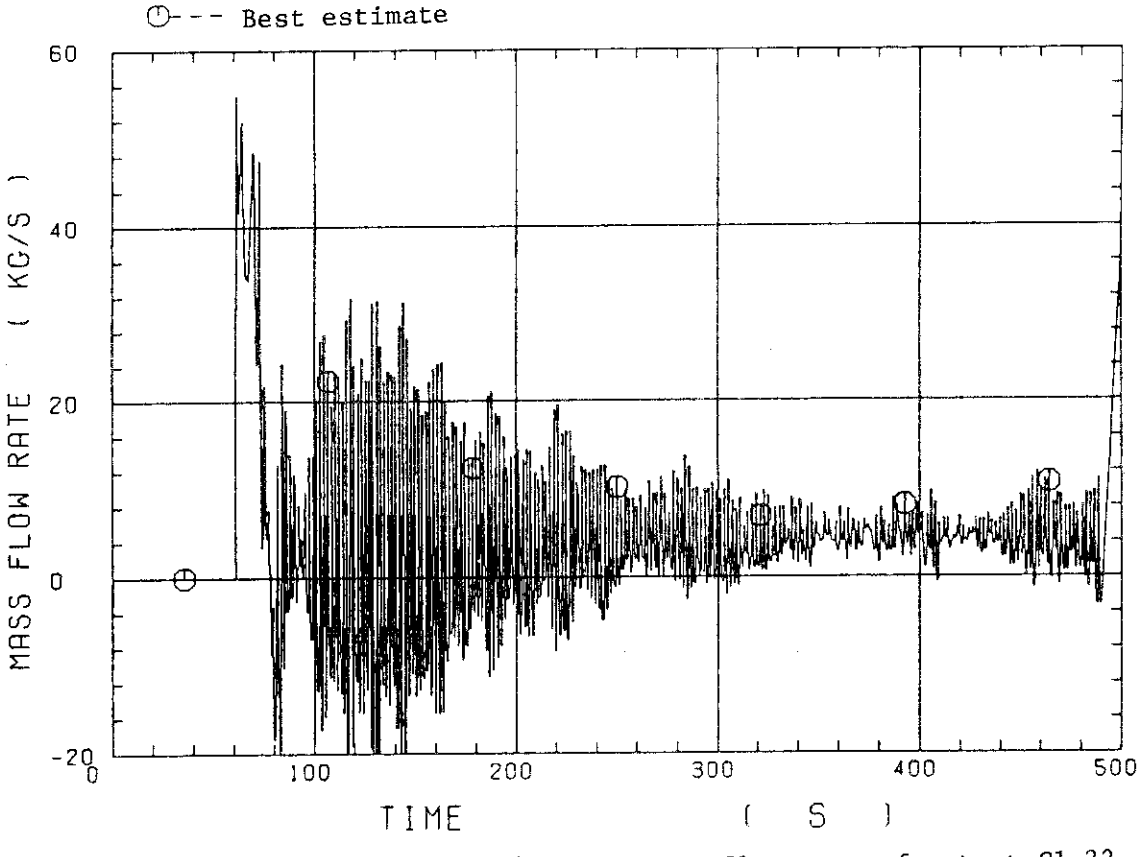

Fig. E-8 Best estimate core flooding mass flow rates for test C1-22 (Run 41)

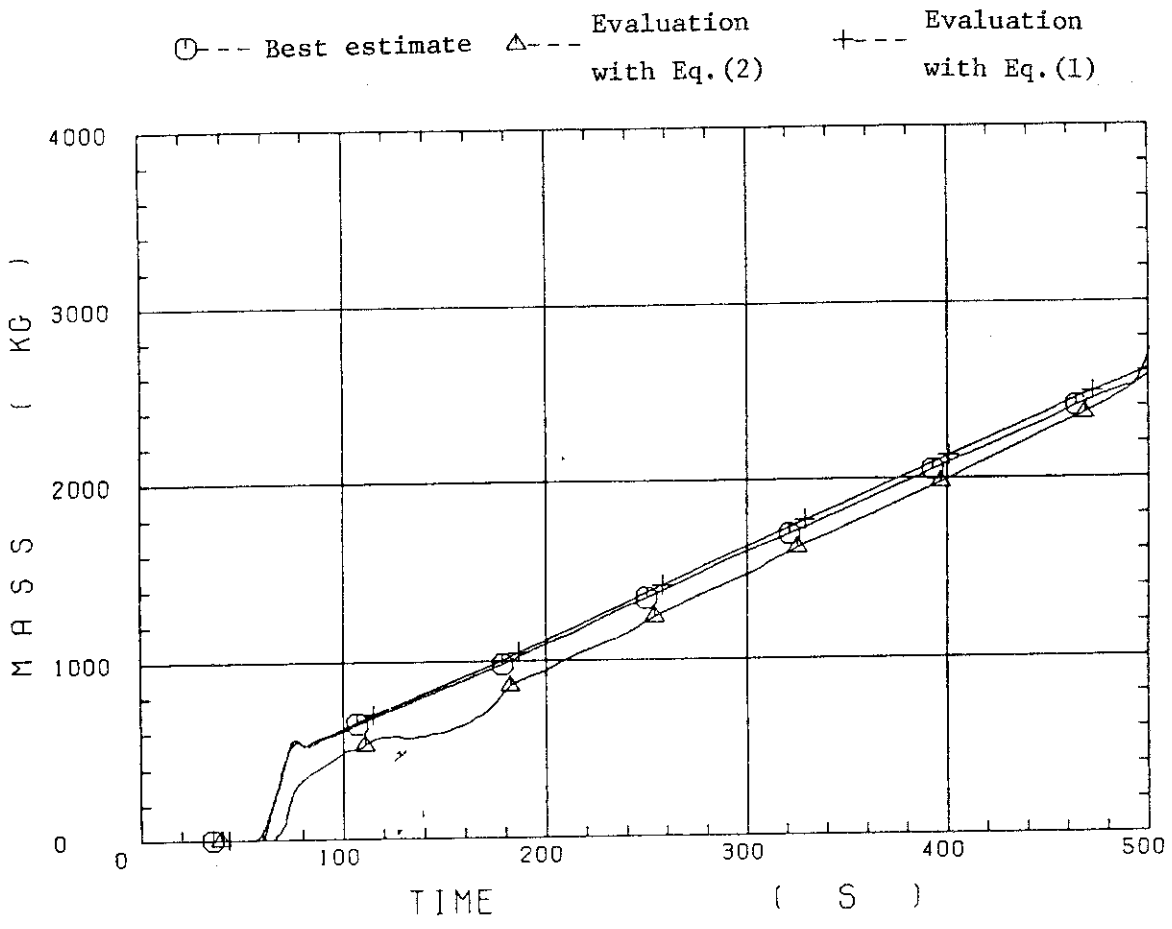

Fig. E-9 Integral masses flooded into core evaluated with Eqs.(1) and (2) and best - estimated for test C1-22 (Run 41)